

2008

Feasibility study of application of electrohydrodynamics to actuation and cooling systems

Kazim Mirza
University of Dayton

Follow this and additional works at: https://ecommons.udayton.edu/graduate_theses

Recommended Citation

Mirza, Kazim, "Feasibility study of application of electrohydrodynamics to actuation and cooling systems" (2008). *Graduate Theses and Dissertations*. 4461.
https://ecommons.udayton.edu/graduate_theses/4461

This Dissertation is brought to you for free and open access by the Theses and Dissertations at eCommons. It has been accepted for inclusion in Graduate Theses and Dissertations by an authorized administrator of eCommons. For more information, please contact mschlange1@udayton.edu, ecommons@udayton.edu.

**FEASIBILITY STUDY OF APPLICATION OF
ELECTROHYDRODYNAMICS TO ACTUATION AND COOLING
SYSTEMS**

Dissertation submitted to
School of Engineering

UNIVERSITY OF DAYTON

In partial fulfillment of the requirements for
the degree
Doctor of Philosophy in Mechanical Engineering

By

Kazim Mirza

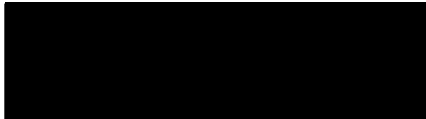
UNIVERSITY OF DAYTON

Dayton, Ohio

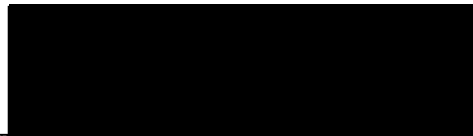
December, 2008

FEASIBILITY STUDY OF APPLICATION OF ELECTROHYDRODYNAMICS TO ACTUATION AND COOLING SYSTEMS

Approved By:



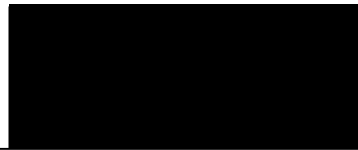
Kevin Hallinan, Ph.D.
Committee Member
Chairperson,
Mechanical and Aerospace
Engineering



Reza Kashani, Ph.D.
Advisory Committee Chairman
Associate Professor
Mechanical and Aerospace
Engineering



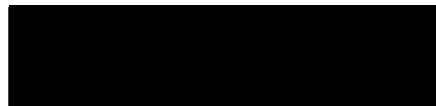
Robert A Brockman, Ph.D.
Committee Member
Professor,
Civil and Environmental Engineering &
Engineering Mechanics



Guru Subramanyam, Ph.D.
Committee Member
Associate Professor,
Electrical and Computer Engineering



Malcolm W Daniels, Ph.D.
Associate Dean
School of Engineering



Joseph E Saliba, Ph.D., P.E.
Dean, School of Engineering

© Copyright

**Kazim Mirza
All rights reserved
2008**

ABSTRACT

FEASIBILITY STUDY OF APPLICATION OF ELECTROHYDRODYNAMICS TO ACTUATION AND COOLING SYSTEMS

Name: Kazim Mirza

Advisor: Dr. Kevin Hallinan / Dr.Reza Kashani

A variety of actuation systems based on the hydraulic systems, piezoelectric and magnetostrictive systems have been developed. Various cooling systems with different technologies have been devised. Electrohydrodynamics has been an innovative as well as a creative field to develop momentum from the dielectric fluid medium by applying voltages to it. With the advent of the micro technologies, various problems have been solved by scaling to micro levels. The research aims at building a highly effective, miniaturized electrohydrodynamic pumped actuator to have a first hand knowledge of EHD phenomenon and a precursor to the development of EHD cooling systems. The actuator would provide greater performance in terms of higher force, higher displacement and equivalent bandwidth than the so-called smart material (piezoelectric and magnetostrictive) actuators of comparable size. The EHD actuators find applications in active structure-borne noise abatement, active vibration control, precision pointing, etc. The on-going research aims at parametrically understanding the actuator with respect to its geometry, contained dielectric fluid medium and electric fields. A multitude of prototypes have been designed in the commercial codes like ANSYS® and COMSOL®. Benchmarking of some of the models is done with the past researchers. We computationally calculated a velocity of 0.011m/sec by applying 150 volts to the emitter electrode and grounding the collector electrode. Various models involving electrostatic coupling with fluidics and also with the thermal fields have been devised computationally

and these results show the promising trends, which help us, understand electrohydrodynamic phenomenon.

ACKNOWLEDGEMENTS

I express my sincere appreciation and gratitude to my advisor, Dr Reza Kashani, for his constant support, guidance and encouragement through out my research. Dr Kevin Hallinan has instrumental in molding my career by giving invaluable assistance and support during my years at University Of Dayton. Dr. Andrew Sarangan and Dr. Guru Subramanyam were key professors in training me and giving me hands on skills in MEMS lab. I am indebted to Dr. Robert Brockman for knowledge in computational skills. I am truly thankful to Sergey Korpov of Boston based Cronos Air technologies, without whose help I would not progress further and build my computational model. I would also like to thank Mike Aulds of UDRI for his insight and help in setting up experimental model for induction EHD. I am honored to receive NSF funding through Dr Reza Kashani for my research, without whose help I wouldn't have done my PhD.

I am thankful to Dr. Kelly Kissock for providing me opportunities at UDIAC with whose help I cannot envision my future.

I am also thankful to Agha Ahmed and other friends for giving support and encouragement through my years in PhD. I am grateful to Robin Reeds for lending librarian books for longest periods of time ever imaginable.

Finally, a special mention of my deceased father, my mother, my brother and my nephews for allowing me to spend time for my PhD at University Of Dayton, without whose sacrifice and love, it wouldn't have been possible to realize my and their dreams.

Dedicated to my wonderful parents and my beautiful family

Table of Contents

ABSTRACT	iv
ACKNOWLEDGEMENTS	vi
CHAPTER I	1
1 Introduction	1
1.1 Background	1
1.2 Research Purpose/Aim	1
CHAPTER II	3
2 Study of EHD Physics	3
2.1 Introduction	3
2.2 Research Objectives	4
2.3 Literature Survey	5
2.4 Various Pumping Mechanisms	15
2.5 Electrohydrodynamic Pumping Background	16
2.6 Main types of EHD Pumping	17
2.6.1 Conduction EHD	17
2.6.2 Induction EHD	22
2.6.3 Ion Drag EHD	23
2.7 EHD Equations	24
2.8 Summary	29
CHAPTER III	30
3 Computational Efforts in EHD	30
3.1 Introduction	30
3.2 Numerical Studies using ANSYS®	30
3.2.1 Geometric Design Optimization	30
3.2.2 ANSYS® Sensitivity Analysis Results	35
3.3 COMSOL® Physics Environment	46
3.4 Numerical studies using COMSOL®	53
3.5 Ion drag EHD	56
3.6 Parametric evaluation of Micro-Ion Drag pump	63
3.7 Thermally Induced EHD Pumping	72
3.8 Summary	76
CHAPTER IV	78
4 Conclusion and future work	78
4.1 Computational Recommendations:	81
4.2 Experimentation Recommendations:	82
CHAPTER V	84
5 Appendix	84
A. Lessons Learnt (Micro pump Design and Fabrication)	84
5.1 Introduction	84
5.2 Setbacks and challenges	84
5.3 Fabrication of the EHD actuator	86
5.3.1 The Bottom part	87
5.3.2 The Top part	96
5.4 The EHD Device	97

5.5 Micro manufacturing Process Problems and Device packaging	98
of the thin film electrodes.....	98
5.6 Experimentation for the EHD pumping.....	100
B. References	105

LIST OF FIGURES

Figure 2.1 Schematic Representation of the EHD pumped Actuator.....	7
Figure 2.2 Ion drag Pumping Electrode configurations for a) Cartesian b) Cylindrical and c) Spherical coordinates.....	9
Figure 2.3 Thermal Induction Backward Pumping	11
Figure 2.5 Unequal Force distributions due to the unequal width of the electrodes.....	19
Figure 2.6 Unequal Force distributions due to the unequal width of the electrodes.....	19
Figure 2.7 Ring collector and central emitter electrode for the conduction EHD pumping.....	20
Figure 2.8 Induction EHD pumping from application of heat (Temperature induced Induction EHD).....	23
Figure 2.9 Induction EHD pumping for variation in the electrical conductivity of liquids.....	23
Figure 2.10 Ion Drag EHD pumping	24
Figure 3.1 The repeating unit of the electrode array	32
Figure 3.2 Schematic representation of the three dimensional actuator channel.....	33
Figure 3.3 Parametric variation of force/area with A and $D2$	35
Figure 3.4 Parametric variation of force with A and $D2$	35
Figure 3.5 Parametric Variation of force/area with B and $D2$	37
Figure 3.6 Parametric variation of force with B and $D2$	37
Figure 3.7 Parametric variation of force/area with A and B	38
Figure 3.8 Parametric variation of force with A and B	39
Figure 3.9 Parametric variation of force/volume with H and $D2$	41
Figure 3.10 Parametric variation of force with H and $D2$	41
Figure 3.11 Parametric variation of force/volume with H and $D1$	42
Figure 3.12 Parametric variation of force with H and $D1$	42
Figure 3.13 Parametric variation of force/volume with $D1$ and $D2$	43
Figure 3.14 Parametric variation of force with $D1$ and $D2$	44
Figure 3.15 Graphical user interface for COMSOL electrostatics physics solver	47
Figure 3.16 Graphical user interface for COMSOL electrostatics boundary conditions solver.....	48
Figure 3.17 Graphical user interface for COMSOL PDE coefficient form solver	49
Figure 3.18 Graphical user interface for COMSOL PDE coefficient form Boundary Conditions Interface.....	50
Figure 3.19 Graphical user interface for COMSOL Fluid physics solver	51
Figure 3.20 Graphical user interface for COMSOL Fluid physics boundary conditions.....	51
Figure 3.21 Graphical user interface for COMSOL Energy physics solver.....	52
Figure 3.22 Graphical user interface for COMSOL Energy physics solver.....	52
Figure 3.23 COMSOL integrated solver Manager.....	53
Figure 3.24 Progress bar cum convergence measure COMSOL integrated solver interface.....	53
Figure 3.25 Computational domain of the EHD pump	56
Figure 3.26 Close-up view of the Electric field distribution on the emitter electrode	57
Figure 3.27 Dimensions of the domain of the EHD pump.....	58
Figure 3.28 Meshed Ion Drag Model.....	60
Figure 3.29 Mesh statistics for the mesh model.....	60
Figure 3.30 COMSOL® screen shot of the electric potential distribution in the computational domain.....	61
Figure 3.31 Velocity, $u(y)$ in m/sec variation with height (meters) at the inlet.....	62
Figure 3.32 Pressure, $p(y)$ in m/sec variation with height (meters) at the outlet.....	62
Figure 3.33 .COMSOL® screen shot of the velocity variation in the domain.....	62
Figure 3.34 .COMSOL® screen shot of the velocity variation in the domain.....	62
Figure 3.35 Variation of the flow rates with emitter voltage in one stage EHD pump.....	64
Figure 3.36 Variation of the pressure with emitter voltage in one stage EHD pump.....	65
Figure 3.37 Variation of the Flow rates with the pressure developed for a computational single stage EHD pump.....	66
Figure 3.38 Electric field profiles for a single stage EHD pump at 100Volts.....	67

Figure 3.39 Electric field profiles for a single stage EHD pump at 80Volts.....	67
Figure 3.40 Variation of the velocity and pressure with the height of a single stage EHD pump.....	68
Figure 3.41 Variation of the velocity with the 110 microns of height of the pump.....	69
Figure 3.42 Variation of the outlet velocity with the 110 microns of height of the pump.....	69
Figure 3.43 Variation of the pressure with the 110 microns of height of the pump.....	69
Figure 3.44 Variation of the velocity with the 70 microns of height of the pump.....	70
Figure 3.45 Variation of the velocity at the outlet with the 70 microns of height of the pump.....	70
Figure 3.46 Variation of the pressure at the outlet with the 70 microns of height of the pump.....	70
Figure 3.47 Variation of the velocity with the 40 microns of height of the pump.....	71
Figure 3.48 Variation of the velocity with the 40 microns of height of the pump.....	71
Figure 3.49 Variation of the pressure with the 40 microns of height of the pump.....	71
Figure 3.50 Variation of the velocity with the distance between the electrodes.....	72
Figure 3.51 Schematic of the computational domain of the induced EHD pump with heat flux specified for temperature gradient.....	73
Figure 3.52 Velocity fields in COMSOL® for the voltage applied between the electrodes without the temperature fields.....	74
Figure 3.53 Velocity fields in COMSOL® for the voltage applied between the electrodes by applying temperature induced fields.....	74
Figure 3.54 Velocity fields in COMSOL® for the voltage applied between the electrodes by applying temperature induced fields.....	75
Figure 3.55 Velocity fields at the outlet in COMSOL® for by applying temperature of 50C and 70C at the top and bottom of the device.....	75
Figure 5.1 Laser machined electrodes on bottom substrate.....	85
Figure 5.2 Ultrasonic machined glass top.....	85
Figure 5.3 A picture of the top part connected to the pipettes along with the broken part.....	86
Figure 5.4 Schematic representation of the three dimensional actuator channels.....	90
Figure 5.5 Schematic representation of the first set of design of electrodes on the top part.....	91
Figure 5.6 Schematic representation of the alternative set of design of electrodes on the top part of the actuator.....	92
Figure 5.7 An AUTOCAD® drawing of the electrodes of characteristic length of 5 microns.....	93
Figure 5.8 A zoomed area of top left corner of the figure 5.7 , depicting the electrodes with the.....	94
Figure 5.9 An image of the electrodes, jumpers and the insulator block with alignment marks on the mask.....	94
Figure 5.10 A picture of the jumpers along with electrodes.....	95
Figure 5.11 Alignment marks on the silicon.....	95
Figure 5.12 Picture of the bus lines along with the alignment marks.....	95
Figure 5.13 Jumpers along with the electrodes.....	95
Figure 5.14 Schematic representation of the electrodes with the Glass cavity as seen from.....	97
Figure 5.15 EHD pump along with the two pipettes attached with four wires.....	98
Figure 5.16 Close up view of EHD pump.....	98
Figure 5.17 A picture of the completely damaged electrodes.....	95
Figure 5.18 A picture of the near undamaged electrodes.....	99
Figure 5.19 A picture of the top part connected to the pipettes.....	96
Figure 5.20 A picture of the top part connected pipettes along with the broken part.....	99
Figure 5.21 Picture of the Experimental setup.....	98
Figure 5.22 Picture of the High.....	101
Figure 5.23 Picture of the scale signifying the level in meniscus.....	101
Figure 5.24 A photo of the zero millimetres for comparison.....	101
Figure 5.25 Picture of the electrical supply in the tupperware shown in the figure 5.24.....	102
Figure 5.26 Schematic of the Circuit diagram for the one of the drivers for the Supply three phase supply in the tupperware shown in the figure 5.25.....	102

LIST OF TABLES

Table 2.1: Comparison of different actuation methods (1)

Table 2.2: Comparison of different characteristics of actuation methods (2)

Table 5.1 Physical properties of corn oil

Table 5.2 Experimental values of Voltages applied and Height registered.

CHAPTER I

1 Introduction

1.1 Background

Electrohydrodynamics (EHD) has been the focal point of research for two to three decades. Initially, the technology relied on the high voltages and heavy insulation. With the advent of the micromechanical (MEMS) fabrication techniques, the high voltages can be scaled down to the smaller voltages due to the scaling of the dimensions. The benefits derived from EHD are numerous: noiseless and no moving parts, simple electrode structures and pump, precise control of the flow rates and pressure generated with applied voltages.

1.2 Research Purpose/Aim

The research primarily investigates electrohydrodynamics (EHD) augmented with scaling benefits derived from micro technologies, for solving industry related problems. This research looks at the prospects of proving feasibility of using the electrohydrodynamics as one of the effective solutions in the active damping for building an EHD actuator in a broader vision, while also looking tangentially at the application of electrohydrodynamics in heat transfer for enhancing the heat transfer in chilling applications. In the field of active dampening, this research entails building a highly effective, miniaturized electrohydrodynamic pumped actuator. The actuator would provide greater performance in terms of higher force, higher displacement and equivalent bandwidth than the so-called smart materials (piezoelectric and magnetostrictive) actuators of comparable size. The

EHD actuators find applications in active structure-borne noise abatement, active vibration control, precision pointing. The research aims at parametrically understanding the actuator with respect to its geometry, contained dielectric fluid medium and electric fields. A multitude of prototypes were designed, fabricated and tested to provide experimental benchmarking of the model predictions. At the same time, this experimental bench-marking will provide practical expertise in both fabricating the concept and incorporating it into smart structures.

CHAPTER II

2 Study of EHD Physics

2.1 Introduction

Industrial revolution began with the boom of inventing big machines and as time went by; larger and smaller machines and products began to inundate the world. The other name for such smaller machines was meso machines. These machines offered the comfort of using them where the previous big machines couldn't be employed and with them came, lots of functionality with in a very compact design. This translated to more efficiency and lesser material for building those machines. The smaller the machines became, there were more challenges faced in designing products with immense and value added functionality in a very small space. Mechanisms, which work cumulatively at the mega level, become individualistic at the micro level. In the modern era, the micromechanical technologies are the theme of the future. Among these technologies, EHD (electrohydrodynamic pumping) is being pursued as a very innovative and effective technology among macro system and mesosystem technologies. Some of the advantages of EHD are morphable and changeable simple electrodes and system design, absence of moving parts, performance based on the control of the input variables like electric fields and electric voltages, low power consumption and applicability to microgravity and terrestrial environments.

2.2 Research Objectives

Two scenarios of electrohydrodynamic pumping have been considered. The first is ion drag pumping where the charges are induced in the fluid due to corona discharge. This produces the charges and produces the momentum within the dielectric fluid. This application can be used for building an electrohydrodynamic actuator for active dampening applications. The second scenario is the temperature-induced electrohydrodynamic pumping, where the charges are produced due to the variation in the electrical conductivity via the application of temperature fluxes or fields and the pumping is induced in the fluid. This application can find use in the thermal management aspects of electronic cooling and even in the heat transfer augmentation of the chillers. The research study of electrohydrodynamics is done in the following sequence:

1. The conceptual fundamental aspects and the physics behind the phenomenon of electrohydrodynamics is studied for the microfluidic applications.
2. The fields of electrohydrodynamics in the ion drag pumping and temperature induced induction pumping were simulated using COMSOL®, a commercial finite element program.
3. Design and fabricate the devices demonstrating electrohydrodynamics as the basis of the ion drag pumping and temperature induced electrohydrodynamic pumping, thereby forming a basis for the actuation and cooling systems.

2.3 Literature Survey

Low damping leads to free vibration problems during operation of many structures. The use of lightweight, advanced materials in the construction of such structures and elements has made the vibration problems even more severe. In addition to free vibrations, these systems are sometimes subject to single and multiple frequency excitations leading to forced vibration. Abatement of forced vibration is normally achieved by cancellation through the introduction of a secondary (control), out-of-phase vibration. Although damping can be added to a system both passively and actively (each having their own advantages and disadvantages), active control is used almost exclusively for vibration cancellation. Some systems are subject to both free and forced vibration where both damping and cancellation remedies are necessary to address the vibration control problem. Vibration in helicopter rotor blades, transmitted vibration from engine to the chassis of a ground vehicle, and 'high cycle fatigue' in gas turbine engine blades fall into this category.

Active response to vibration (through damping and/or cancellation) is an effective and adaptable approach to lowering the deleterious effects of vibration on a system. The success of active vibration control in most applications hinges on the capability of the actuator(s) used in those applications.

Much progress has been made in recent years using both piezoelectric and magnetostrictive, high-bandwidth actuators for active vibration control of structures and micro-positioning of mechanical systems. Shape memory alloys have also been used for actuation purposes but their use for applications such as vibration control has been limited due to their lack of agility, i.e., low bandwidth. Successful utilization of these actuators depends on their bandwidth,

effectiveness—force/displacement generation. A typical piezoelectric stack or magnetostrictive actuator with the diameter of 25 mm and length of 100 mm has the block force capability of around 400 N and the maximum displacement of about 40 to 50 micrometers. Increasing the cross-sectional area and length will increase the force and displacement, within limits, respectively but with the weight and cost penalty. High displacement could be generated through proper leveraging, but at the expense of losing the force and increasing the size and weight. These actuators, with physical dimensions on the order of centimeters, are not capable of providing the needed actuation in most real-life structures.

This research deals with a newly envisioned, hydraulic actuator employing an array of electrohydrodynamically (EHD) driven pumps to pump liquid between two reservoirs and to generate pumping head that can be used to provide actuation, as shown in the figure 2.1. Previous research has demonstrated the feasibility in generating improved force, displacement and bandwidth relative to piezoelectric and magnetostrictive devices, but with significantly reduced volume requirements.

The concept relies on the micro scale electrohydrodynamic pumping of a dielectric fluid medium through small channels. Configured as an actuator, the EHD pumps would be used to move fluid between two reservoirs, each having a compliant membrane that provides interface with the outside world for micro actuation. The pumping is achieved by imposing two or three phase electric fields, depending upon the amount of actuation needed, on the electrodes. The electrohydrodynamic action is produced in a fluid medium due to the presence of free electric charges. These electric charges can be established in fluid medium either by injection of ions (ion drag EHD and conduction EHD pumping) or by

induction due to fields (Induction pumping). The first is by corona discharge, where a highly localized electric field strips the electrons from the atoms and the second is by permittivity gradient in the fluid, which is achieved by placing differential heating and cooling systems on the channel(induction EHD pumping). The second type of pumping is attained by constant influx of charges into fluid. The applied electric fields exert force on the free charges in the fluid medium and the momentum of the charges is transferred to the fluid, due to which the fluid moves. The electric fields and electric potentials produced in the fluid are intimately dependent upon the geometrical contour of the electrodes. The electrode design therefore is one of the key factors defining the physics of the electrohydrodynamics of the fluid. Various types of electrodes have been considered for finalizing the shape of the electrodes to achieve the highest electrohydrodynamic force and maximum pressure. The electrode/fluid interfaces is also the most important region to lucidly understand the electrohydrodynamics occurring in the bulk of the fluid medium.

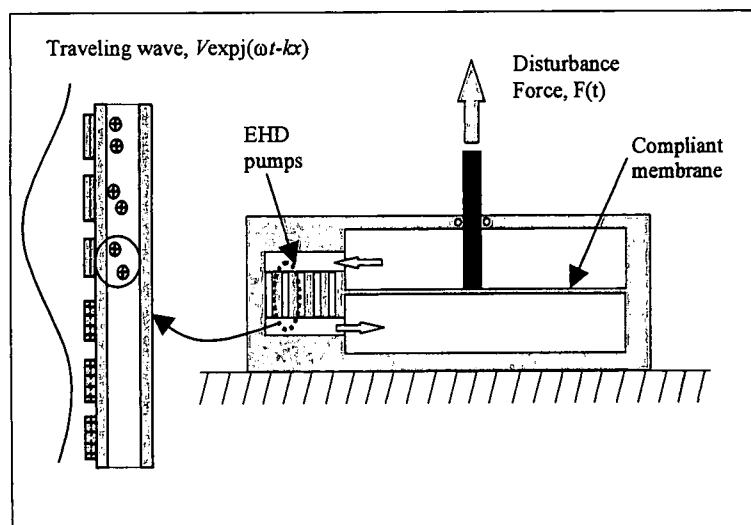


Figure 2.1 Schematic Representation of the EHD pumped Actuator.

EHD pumping is made possible by the generation of electrohydrodynamic forces within a dielectric fluid due to the application of electrostatic fields. The following section seeks to review the evolution of EHD pumps. Two types of EHD pumps have evolved. The ion drag work has been attributed to Stuetzer [1] and the thermal induction type to Melcher [6-8].

Stuetzer [1] studied the ion-drag pressure generation theoretically and experimentally. He presented an approximate theory for ion-drag pressure generation applicable to unipolar conduction in gases and insulating liquids. In his experiments, the ions were induced by the field due to the generation of corona discharges. His theory gave good agreement with the experiments but was limited to the static case, i.e., a non-moving fluid. His experimental model was shown capable of generating pressures of up to 0.2 atm in liquid using single electrode pairs. Later, Stuetzer [1] presented a theoretical model with supporting measurements which described the dynamic behavior of an ion-drag pumping arrangement for unipolar ion conduction.

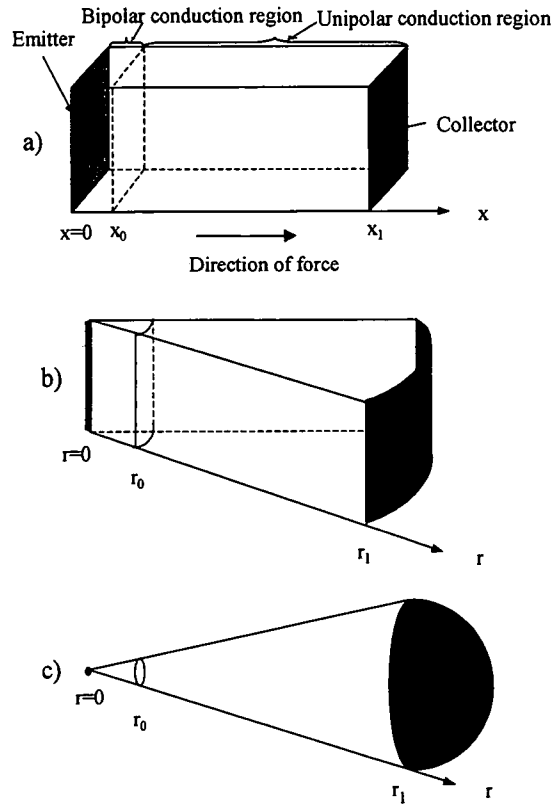


Figure 2.2 Ion drag Pumping Electrode configurations for a) Cartesian b) Cylindrical and c) Spherical coordinates.

Stuetzer's theoretical model considered an idealized electrode such as those shown in Figure 2.2a-c. The emitter electrode is shown at $x=0$ or $r=0$. The ionization occurs in the region from $x=0$ to x_0 for the Cartesian system and $r=0$ to r_0 for the cylindrical and spherical arrangements. In this region, the negative ions formed or the electrons that are released move to the emitter electrode where their charge is negated. The positive ions move toward the collector electrode. There is a columbic force imposed upon these ions. The non-charged molecules are 'dragged' along. He showed that the pressure difference between the electrode pairs was $\frac{9}{8}\epsilon\left(\frac{\Delta V}{x_1}\right)^2$, $\epsilon\left(\frac{\Delta V}{r_1}\right)^2 \log \frac{r_1}{r_0}$, and $\frac{3}{8}\epsilon\left(\frac{\Delta V}{r_1}\right)^2\left(\frac{r_1}{r_0}-1\right)$ for the planar, cylindrical, and spherical electrodes, respectively, where ΔV is the emitter-collector voltage.

With large r_1/r_0 ratios, the pressure exerted on the electrodes for cylindrical and spherical electrodes can be substantially larger than for planar electrodes. In terms relevant to micro-sized pumps, these pressure jumps are equal to: $\frac{9}{8}\epsilon E^2$, $\epsilon E^2 \log \frac{L}{a}$, and $\frac{3}{8}\epsilon E^2 \left(\frac{L}{a} - 1 \right)$ for planar, cylindrical, and spherical electrodes, where L is the electrode spacing and r_0 can be no greater than the pore size, a .

Pickard [3, 4] re-examined Stuetzer's ion drag pumping theory. In particular, he analyzed the phenomena of the "cut-in" voltage. The cut-in voltage is the voltage level below which the pump is inoperative and above which a pressure is generated. Sharbaugh and Walker [5] experimentally investigated the pumping of transformer oil by an ion-drag pump. They were able to achieve a velocity close to 5 cm/s in a 6-cm diameter pipe.

Melcher et al. [6-8] developed the basic theory for thermal induction pumping and demonstrated a small working model. They showed that an EHD traveling-wave induction interaction could pump slightly conducting liquids without electrical contact with the flow. Since the induction process required no electrical contact with the fluid, they viewed EHD pumping as not only a means for pumping liquids but also a means to study electrical properties of fluids.

The physics of a thermally induced EHD pump in the more effective backward pumping mode of operation is depicted in Figure 2.3. Heat is added at the top and removed at the bottom. The electric field produced between the emitter and collector electrodes is responsible for ionizing molecules in the fluid (frees some electrons in the fluid).

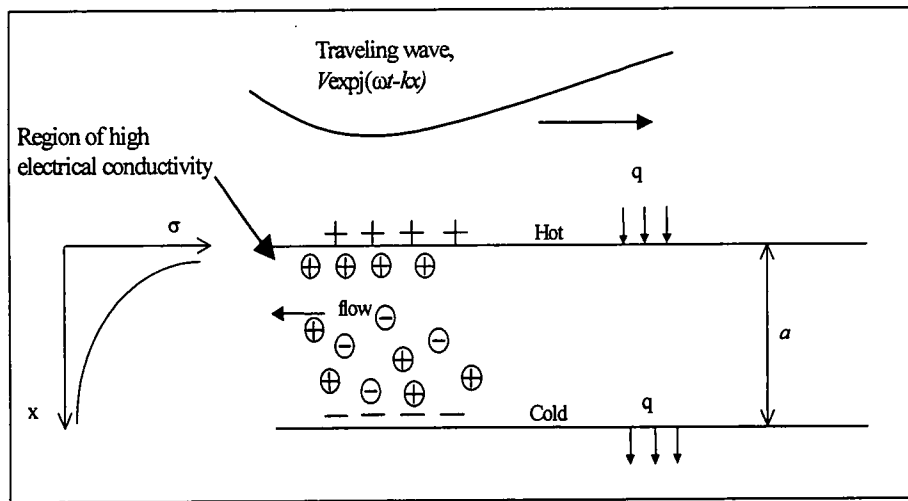


Figure 2.3 Thermal Induction Backward Pumping

Locally, opposite charges are induced on the cooler bottom surface. Because the fluid conductivity increases dramatically with temperature increase, the freed electrons near the heated wall in proximity to the emitter electrode are able to conduct rapidly toward the hot wall. The positively charged ions remain and are repulsed by the emitter electrode. A backward flow results. Ultimately, it is the temperature difference that generates the free charges (ions) in the fluid. Without a conductivity gradient in the fluid, there would be no free charge build-up and no flow (or pressure head generation)

Okapal [9] examined the generation of a traveling wave by using a single-phase voltage excitation. He demonstrated EHD pumping with a single-phase voltage supply using discrete circuitry composed of resistors and capacitors only. Results were sporadic, but a peak flow velocity of 0.5 cm/s was achieved. Krein [12] continued the work performed by Okapal and was able to achieve reproducible velocities on the order of four cm/s using a single-phase voltage supply.

To better understand the behavior of an EHD pump, Crowley [11] obtained analytical solutions for the forward pumping of an EHD pump by using a two-layer model. The basic idea was to break the region under consideration into two layers, each with constant electrical conductivity and permittivity. Since each layer has its own characteristic properties, the induction EHD pump in this case did not need a heat input, which was required in a thermal induction EHD pump to induce electric charges by producing an electrical conductivity gradient. The properties change only at the interface between the two layers; therefore all of the change is concentrated at the interface between the two layers.

Kervin [12] carried out numerous measurements of an EHD pump velocity under different operating conditions. The traveling wave was produced by a three-phase power supply. These measurements enabled him to determine which of various parameters were most important in the design of a practical pump. The maximum velocity achieved was ten cm/s within a 2.2-cm diameter pipe. His work indicated that poly-phase EHD pumping was more productive than single-phase

Kuo [13] performed a numerical study of an EHD pump in a horizontal configuration for underground electric cable systems with temperature dependent properties, particularly viscosity. He found that the temperature-dependent properties had only a minor effect on the axial velocity and on the friction.

Seyed-Yagoobi [14] performed a theoretical, numerical, and experimental study of EHD pumping in a vertical configuration with steady-state flow and temperature dependent variables. He studied the controlling factors of an operating an EHD pump by varying thermal, electrical, and physical properties. His parametric study of EHD pump operation improved the understanding of thermal induction pumps. Seyed-Yagoobi and Bohinsky

developed a theoretical model of a thermal induction EHD pump. From their model they were able to establish optimal fluid characteristics for such pumps [15]. Crowley et al. [16] theoretically studied the effects of various dielectric fluid properties on the efficiency and flow rates of an EHD pump. Their theoretical analysis of the physics of the EHD pump revealed insight into the conditions that could produce maximum flow rate and efficiency for given volumes. From their research, they were able to establish criteria for selecting a working fluid to increase the efficiency and flow rate of an EHD pump. They concluded that high dielectric constant and low viscosity lead to high flow velocities, while low conductivity and mobility promote high efficiency. Later, Bryan and Seyed-Yagoobi [17] performed an experiment with an ion-drag pump in a vertical axisymmetric configuration, having two pumping sections with one and ten electrode pairs. They achieved a pumping velocity of 33.4 cm/s at 25 kV within a seven-cm diameter pipe. They also studied the effect of electrical conductivity level of dodecylbenzine on the performance. Their study showed that increasing the electrical conductivity level reduced the pumping velocity. Additional work by Seyed-Yagoobi, Margo, and Bryan [18] and Bryan and Seyed-Yagoobi [17] has respectively revealed determination of the optimal frequency of three-phase thermal induced pumps and provided an analytical model of an ion-drag pump that has successfully matched experimental data.

The work led by Barbini of the University of Genova has also contributed to an improved understanding of ion-drag pumping. Barbini and Coletti [20] studied the influence of electrode geometry on ion-drag pump static pressure development. Their experiments were compared with two different theoretical pressures versus voltage relations, due to Stuetzer and to Pickard, for several dielectrics. The general validity of such of the predictions of Stuetzer and

Pickard are discussed and questioned. Coletti et al. [21] showed that the assumption of a stationary fluid used in the models predicting the pressure rise across the pump when static conditions exist is incorrect. Electroconvective flows are shown to dissipate significant energy.

At small scales, Bart et al. [22] and Richter et al. [23] were the first to demonstrate the feasibility of generating fluid motion in a microfabricated structure as a result of application of an electric field Fuhr et al. [24] examined the feasibility of using travelling wave-driven microfabricated electrohydrodynamic pumps for liquids. They concluded that the best opportunity for achieving electrostatic pumping was to use the thermal induction pumping approach of Melcher. They suggested that the minimal required temperature gradients in the fluid could be easily tolerated by microscale devices. Recently, Choi et al. [25] designed, constructed, and tested a micro EHD pump (3 mm long, 40 microns wide, and 50 microns of channel depth). They were able to produce a pressure differential of nearly 100 Pa between inlet and outlet without any heat addition, using only a 120-Volt source. Finally, also at the microscale, Fracais et al. [26] and Bourouina et al. [27] have developed micropumps that are electrostatically actuated, but rely upon the use of an electric field to deform a membrane to displace fluid. In summary there has been significant progress in the development of both thermally induced and ion drag EHD pumps. But outside of the work by Bart et al., Richter et al., Fuhr et al., Choi et al., the work has focused on macroscopically large sizes. They showed that generating head was possible for a micro-sized EHD pump but were far from pushing the envelope of possibility for generating head with their micro EHD pump system. None have considered taking advantage of this head generation for the purpose of actuation. In an on-going research, we aim at parametric understanding of

micro-sized EHD pump actuator with respect to its geometry, contained dielectric fluid medium and electric fields. To do so, an extensive two and three dimensional finite element analysis with the goal of designing the geometry, including the electrode arrangement, have been performed in ANSYS®. Due to the lack of minima within the acceptable geometry of the pump, our first attempt to design the geometry using optimization routines failed. Sensitivity analysis was used, instead of rigorous optimization, to accomplish the task.

2.4 Various Pumping Mechanisms

A wide array of pumping systems is available in the market for every specialized application. Tables 2.1 and 2.2 gives a close up and a good summary of the different pumping applications and their individual advantages and disadvantages.

Table 2.2.4: Comparison of different actuation methods (1)

Actuator Method	Voltage Volts	Work per unit volume, J/cm ³	Typical Response, milliseconds	Temperature sensitive	Power Use	Reference
Electromagnetic	100	0.9	<<1	No	Very low	[34]
electrostatics	100	0.4	<<1	No	Very Low	[35]
Thermo mechanical	12	0.02	100	Yes	Medium	[36]
Phase Change	15	4	300	Yes	Medium	[37]
Piezoelectric	90	0.02	20	No	Low	[38]
Piezoelectric	2	0.01	1	No	Low	[39]
Shape Memory	5	6	30	Yes	Medium	[40]

Table 2.2: Comparison of different characteristics of actuation methods (Contd.)

Method	Efficiency	Speed	Power Density
Electromagnetic	high	fast	high
Electrostatic	Very high	fast	low
Thermomechanical	very high	medium	medium
Phase change	very high	medium	high
Piezoelectric	very high	fast	high
Shape memory	low	medium	very high
Magnetostrictive	medium	fast	very high
Electrorheological	medium	medium	medium
electrohydrodynamic	medium	medium	very low
Diamagnetism	fast	high	fast

2.5 Electrohydrodynamic Pumping Background

The electrohydrodynamic pumping is a complex multiphysics phenomenon. The pumping is the result of the application of the electric fields on the dielectric charged fluids. The columbic force on charges induces momentum and as a result, exerts force on the liquid. This results in the movement of the liquid and develops pressure. There has been endless search for the better pumps, which could ideally convert all the input energy into the pumping fluids. Friction between the moving parts constituted an important part of the inefficiencies. This resulted in investigating different propulsion mechanisms like electric fields, magnetic fields, which could charge the suitable fluids to induce pumping. The drawback rested on finding the right type of fluid with appropriate electrical fluids to induce pumping. The drawback rested on finding the right type of fluid with appropriate electrical properties like electrical conductivity and mechanical properties like viscosity and density only as opposed to design an optional design of the impeller, which is a major source of inefficiencies. Important components of the EHD Pump / actuator constituted electrodes,

electrode design, appropriate type of insulating fluid, the type of voltage, and the temperature field imposed on the pump in some cases. All / some of the above factors interplay to produce velocity and pressure fields in the pump. Over the years, researchers have categorized these pumps into majority three types of pumps.

- Conduction EHD Pumps
- Induction EHD Pumps
- Ion-drag EHD Pumps

2.6 Main types of EHD Pumping

2.6.1 Conduction EHD

The conduction type of EHD pumping is a type of the EHD pumping which is based on the impurities in the dielectric liquid. The power supplied is the small DC supply of usually in range of 100V to 500V. The nature of the power supply is DC supply. The DC supply is just a static case of the application of the voltaic fields to the electrodes. It is reasoned that the DC field should drive the opposite charges to their respective electrodes and end the process, but the continuous dissociation and association of the impurity charges in the fluid is responsible for the generation for the columbic forces in the liquid, which in turns produces momentum in the dielectric and produces the pressure and velocity in the fluids. The conduction EHD can be devoted to work in an isothermal environment, where there is no thermal gradient. It is not the dielectric fluid, which actually dissociates and re-associates in this type of EHD pumping. The geometry of electrodes also plays a very important role in the conduction pumping. The number of the positive and negative pairs also accelerates

pumping. Impurities are weak electrolytes which are capable of undergoing reversible reactions. The bulk fluid doesn't because it is a dielectric. Either a single phase or two phase dielectric medium could be employed in Conduction EHD. When it is a single phase flow, the flow is obtained by the unequal force distribution in the pump obtained through the designing of the electrodes. If a two phase flow is used in Conduction EHD pumping, then electric forces due to the drastic change in the conductivity of the liquids across the interface also develop the free charges and are responsible for the interfacial electric forces in the liquid. These forces are negligible in comparison to the actual large columbic forces in the association-disassociation reaction of the weak electrolytic impurities.

The design of the electrodes is a major player in the Conduction EHD pump. The design has taken into consideration that there should be unequal columbic forces in the pump for the getting a cumulative force in one direction. The ring and mesh electrode in Yagoobi et al [58] design is one such example, a cross section of which is shown in the Figures 2.4. The circumferential forces cancel each other and the axial forces cumulate in one direction, provide the motion. The other designs in the EHD conduction are given in the Figures 2.5 and 2.6.

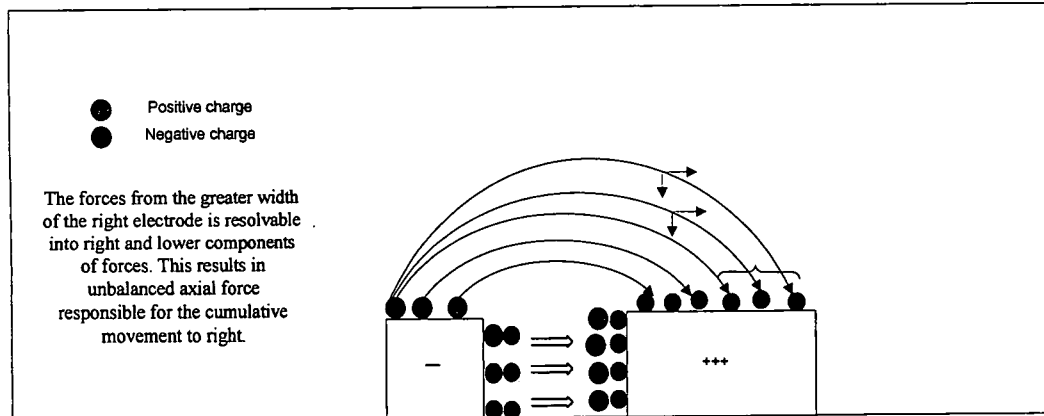


Figure 2.5 Unequal Force distributions due to the unequal width of the electrodes.

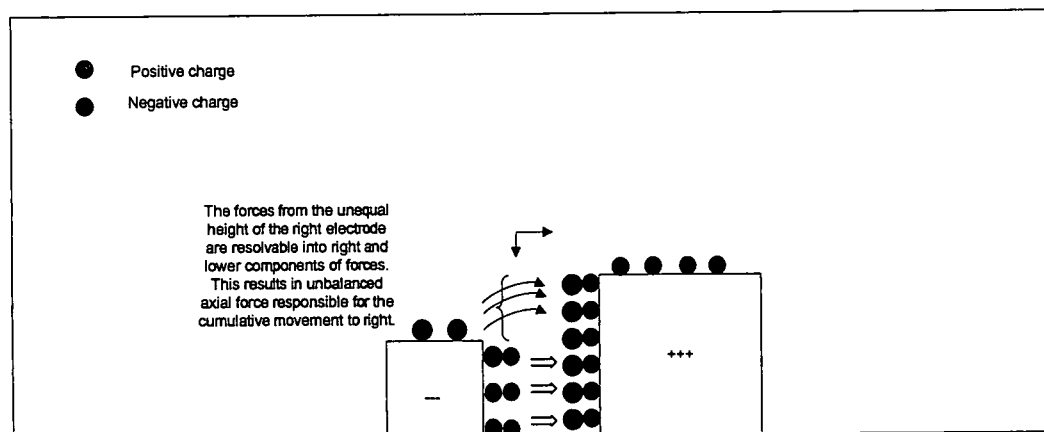
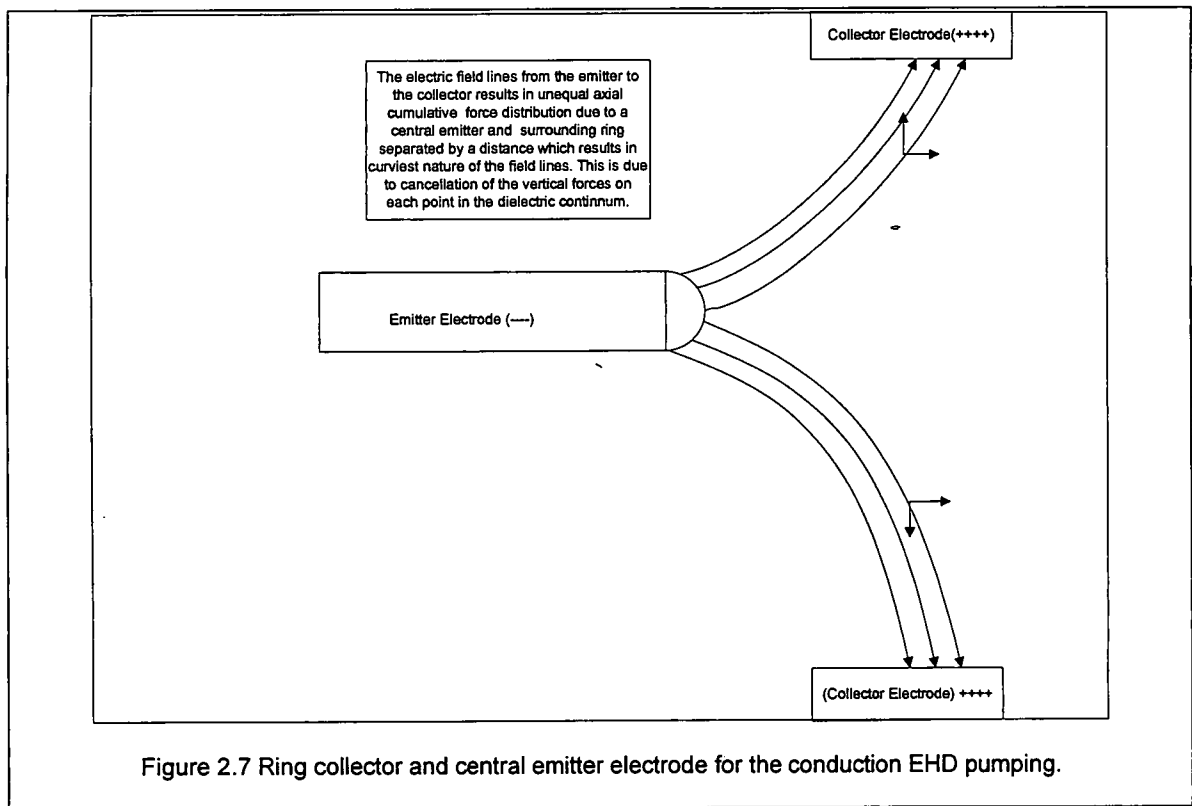


Figure 2.6 Unequal Force distributions due to the unequal width of the electrodes.



In Figure 2.4, the extra height of the second electrode produces a double layer which is uncanceled from the forces of the height of the first electrode. This induces the net cumulative axial force in the horizontal direction in the dielectric medium. In the Figure 2.5, the width of the electrode produces the axial forces on the surface of the second electrode which are uncanceled from the first electrode and produces the net axial force in the horizontal direction. A combination of unequal height and unequal widths of the electrodes can also produce a doubling effect of the net horizontal axial force required for the electrohydrodynamic action. Fluid momentum can be suppressed or developed due to the placement of the electrodes. Instead of fabricating the first electrode and placing at the same height as the second electrode, it behooves to place the first electrode in a central position where it can produce the fields in the core of

the pump, which is not possible in the earlier designs. These fields induce larger horizontal and axial forces and there are net horizontal and axial forces which drive the fluid. In this design, uncanceled vertical force is present, which is unnecessary as the fluids need to propel in the horizontal direction, but instead it can decrease the overall production of the cumulative axial force. If another electrode is also present at the bottom, then it establishes fields with the central emitter electrode as well and produces similar horizontal and vertical forces as the top horizontal electrode. The vertical forces from the top electrode cancel the vertical forces from the bottom electrode and leave the horizontal forces uncanceled, as in Figure 2.6 and in fact cumulatively doubles up the axial forces and produces more electrohydrodynamic action in the pump. This can be fabricated in a rectangular cross section pumps and the second electrode can be a ring structure in circular cross section pumps, where the axial forces are produced all along the periphery of the pump. Hence the circular pumps are more effective electrohydrodynamically than the rectangular pumps. In the central placement of the electrode design, the central electrode should have larger diameter as compared with the sharp tips of the electrodes in the ion drag pumping. The dielectric medium is supposed to have impurities which dissociate and associate within the heterocharge layers of the electrodes. The electric charges are produced from the dissociation and association of the fluid medium and not that from the electrodes as in ion drag pumping in Yagoobi et al [58]). The weak electrolytes in the dielectric medium follow the reactions $A+B \rightarrow AB$ and $AB \rightarrow A+B$, with a certain forward and backward reaction rates, where the A, B and AB are impurities and resultant products in the electrolytes.

2.6.2 Induction EHD

The induction type of the EHD pumping is a novel type of EHD pumping where the electrohydrodynamics is heavily dependent upon the electrical properties of the fluids. Since the electrical conductivity of the fluids is a strong function of the temperature, application of the temperature becomes a core issue in a single phase liquid. Melcher [7] and Seyed Yagoobi [15] have indicated that, for the backward movement of the fluids, heat application at the top and heat removal at the bottom is required. For forward movement of the fluids, heat is applied at the bottom and is removed at the top. The design of the electrodes is regular and can be symmetric. The electrodes are only responsible for the generation of the electric fields and support the movement of the dielectric fluids and don't actually take part in the electrohydrodynamics. Induction type of EHD is best suited for the regular or symmetric set of the electrodes. For the so used with the liquids of mildly conducting dielectrics with the weak electrolytes (impurities). Although there is association and dissociation of the ions, the axial columbic forces cancel and there is no set motion of the liquids. There are equal numbers of positive and negative charges generated in an Induction EHD pump, which is same in the case of conduction EHD. For driving these liquids, the **electrical conductivity dependence** of the temperature is used, as in Figure 2.7. The variation of the electric forces with the height, perpendicular to the flow is derived from the application of the temperature gradient. The two phase flow is another way of having an electrical conductivity change and the interfacial charges, along the height give the forces which actually make the flow, as in Figure 2.8. The AC supply is used for traveling these interfacial charges. A DC supply would actually stall the charges and does not result in movement.

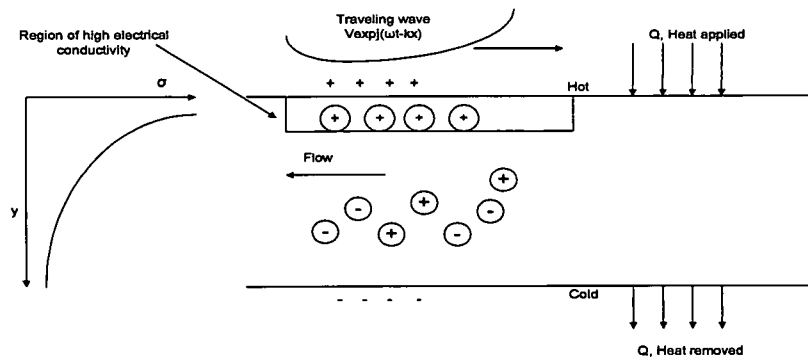


Figure 2.8 Induction EHD pumping from application of heat (Temperature induced Induction EHD)

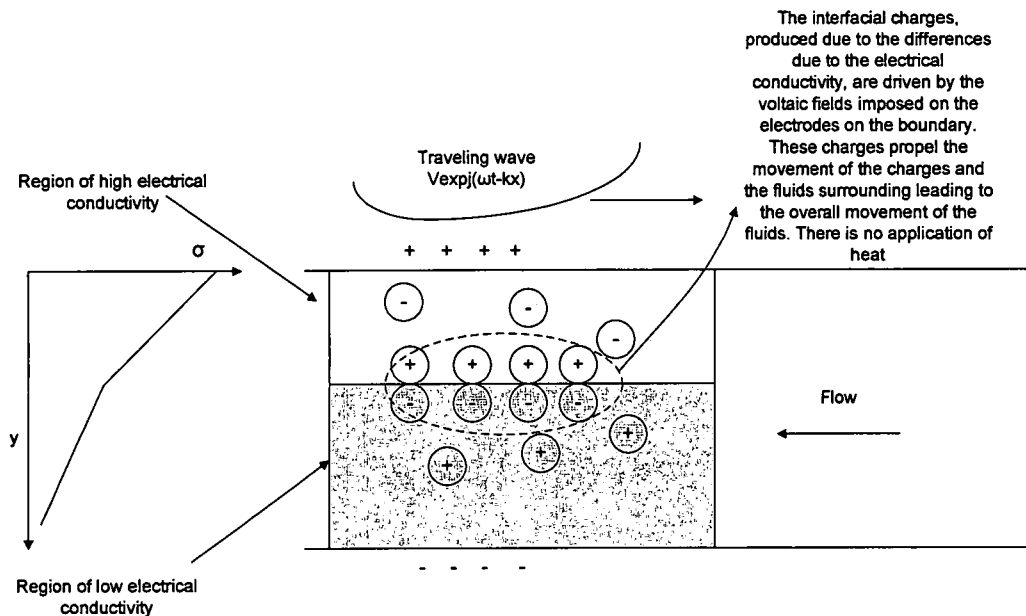


Figure 2.9 Induction EHD pumping for variation in the electrical conductivity of liquids (Phase change induced Induction EHD pumping).

2.6.3 Ion Drag EHD

In Ion drag EHD, electrons are pulled away from the electrode towards liquid. The ions are made from the impurities as well as the liquids. There is huge corona discharge from the emitter towards the collector, which is responsible for derogating the properties of the fluid, particularly electrical properties. The ion drag pumping is the extreme limit of the breaking down the dielectric strength of the liquids. In a conduction pumping, the voltage applied is low and below the

dielectric strength of the fluids, relies on the dissociation and recombination of the ions and is therefore a function of the heterocharge layer and the movement of the fluids from the emitter towards the collector. In an ion drag pump, since there is dependency on the corona charge, the flow is from the collector to the emitter, as shown in Figure 2.9. A high voltage *non-travelling* DC supply is made use for Ion Drag pumps.

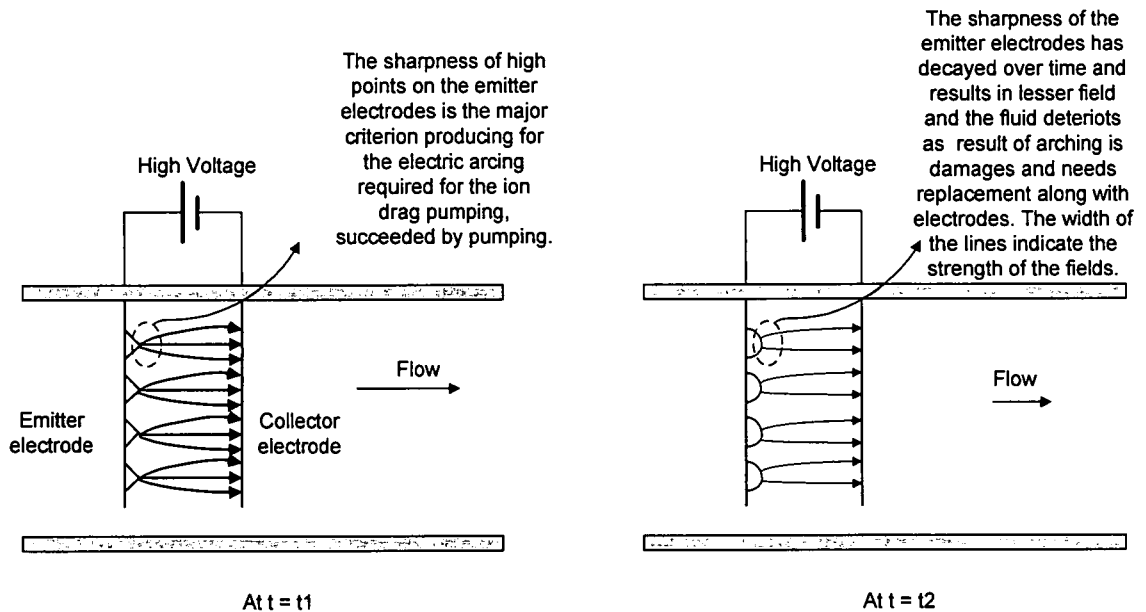


Figure 2.10 Ion Drag EHD pumping

2.7 EHD Equations

For any neutral electrical system, charges are conserved. For an ionized system, there is a net flow flux of charges into or out of the system. The conservation of charge equation is given by Equation (1)

$$\frac{\partial \rho}{\partial t} + \nabla \cdot \vec{J} = 0 \quad (1)$$

where ρ is the free charge

J is the current density

Due to the presence of charges, either free or bounded, electric fields develop and create voltage fields. Both the voltage and electric fields are orthonormal to each other. The relationship between the electric field \vec{E} or \vec{D} flux and free charge is given by Gaussian law, Equation (2) and reformatted as Equation (3)

$$\nabla \cdot \vec{D} = \rho_{free} \quad (2)$$

$$\nabla \cdot \epsilon_0 \vec{E} = q \quad (3)$$

The voltage field developed due to an arbitrary electric field is given by Equation (4)

$$\vec{E} = -\nabla V \quad (4)$$

Substituting equation (3) in Equation (4) yields,

$$\nabla^2 V = -q / \epsilon_0 \quad (5)$$

The current density J is defined as the sum of three components

1. Conduction of ion, given by $\mu_e \vec{E} q$, where

\vec{E} is the electric field

μ_e is the mobility of ions

q is the charge of ions.

This gives the motion of ions, \vec{U} under electric field, \vec{E} relative to entire flow.

2. convection of ions, given by $\vec{U} q$, where

\vec{U} is the velocity of entire flow.

q is the charge of flow.

3. Diffusion of charges, given by $\vec{D} \nabla q$, where

\vec{D} is the diffusivity coefficient of ions and

∇q is the charge gradient density with in a space.

Hence, J is given by Equation (6) as:

$$J = \mu_e E q + U q - D \nabla q \quad (6)$$

For a steady electrical system, $\frac{\partial q}{\partial t} = 0$ and $\nabla \cdot \vec{J} = 0$ which defines the current

continuity of the system. Since the mass entering and exiting the system is conserved, the conservation of mass is given by Equation (7)

$$\nabla \cdot \vec{U} = 0 \quad (7)$$

The moment of fluid given by Navier's stokes equation for incompressible steady state flow is given by Equation (8):

$$\left[\rho \vec{U} \cdot \nabla \cdot \vec{U} = -\nabla P + \mu \nabla^2 U - q \nabla V \right] \quad (8)$$

Substituting Equation (6) in $\nabla \cdot \vec{J} = 0$ results in Equation (9) as:

$$\nabla \cdot \left(\mu_e \vec{E} q + \vec{U} q - D \nabla q \right) = 0 \quad (9)$$

which is equal to the following equation:

$$\begin{aligned} \nabla \cdot (-D \nabla q - \mu_e \nabla V q) + \nabla \cdot (\vec{U} q) &= 0 \\ \Rightarrow \nabla \cdot (-D \nabla q - \mu_e \nabla V q) + q \left(\nabla \cdot \vec{U} \right) + U \cdot \nabla q &= 0 \end{aligned}$$

taking $\nabla \cdot \vec{U} = 0$ results in Equation (10)

$$\nabla \cdot (-D \nabla q - \mu_e \nabla V q) + q \left(\nabla \cdot \vec{U} \right) = 0 \quad (10)$$

For an electrical system, \vec{E} , electric field and V , voltage field is solved from the given EHD charge configuration. Knowing the mobility and diffusivity of charges, equation 10 is solved to give velocity fields and charge distribution. The charge distribution and velocity field is solved from the Navier Stokes Equation (8). Equations (5), (8) and (10) form a coupled system, which when solved, reaches the equilibrium.

For induction EHD pumping, thermal fields in form of temperature or heat flux is applied to maintain the electrical conductivity variation in the liquid. In addition to the equations,

Equations (5) (8) and (10), equation of conservation of energy, which is equation (11) is also solved. The conservation of energy yields the first law of thermodynamics and leads to:

$$\frac{\partial E_i}{\partial t} + \nabla \cdot E_i V = \partial Q \text{ on a domain } i. \quad (11)$$

The first law of thermodynamics / Energy equation is

$$\dot{Q} - \dot{W}_s - \dot{W}_{shear} - \dot{W}_{other} = \frac{\partial}{\partial t} \int_{CV} e \rho dV + \int_{CS} (e + pv) \rho \vec{V} \cdot d\vec{A} \quad (12)$$

where $e = u + \frac{V^2}{2} + gz$ and

e is the specific total energy.

u is the specific internal energy

v is the velocity of fluid

z is the elevation of the fluid

The steady state macroscopic electrostatic behavior, described by James Q Feng [57] due to the corona discharge from small emitter is given by Equations

(14), (15) and (16) and can be deduced from the set of equations (2) to (10). The Navier Stokes equation along with conversation of mass can be described as Equation (14), in Feng's paper [57] as:

$$\text{Re } u \cdot \nabla u = \nabla \cdot [-pI + \nabla u + (\nabla u)^T] - St_e q \nabla V, \text{ along with } \nabla \cdot u = 0 \quad (14)$$

Poisson's equation for electric potential is given by Equation (15)

$$\nabla^2 V = -q \quad (15)$$

The charge transport Equation is given by Equation (16) as

$$(\text{Re}_E u - \nabla V) \cdot \nabla q + q^2 - \frac{1}{Pe_E} \nabla^2 q = 0, \quad (16)$$

where the Reynolds number is given $\text{Re} = \frac{\rho LU}{\mu}$, Stokes number is

$$St_E = \frac{\varepsilon_0 V_0^2}{\mu UL} \text{ and Peclet number is } Pe_E = \frac{\mu_e V_0}{D}$$

The boundary conditions on the emitter S_w and on the collector electrode, S_c dirichlet boundary conditions as Equation (17) can be applied as the no-slip and no-penetration conditions. Typically, we have

$$u = 0, V = V_w \text{ on } S_w \text{ and } u = 0, V = 0 \text{ on } S_s \quad (17)$$

It is desirable to specify a value for charge density on the emitter in terms of the dirichlet condition as $q = q_w$ on S_w . The value of q_w has been inadequately described throughout the literature and is specified as the Kaptsov's assumption and it is specified in terms of the E_{onset} and is given by:

$$n \cdot \nabla V = E_{\text{onset}} \text{ on } S_w \quad (18)$$

Where the E_{onset} is the breakdown strength of the medium for corona onset or local air breakdown at the surface, with n denoting the local unit normal vector

that points into the wire. According to the literature, a reasonably accurate value of E_{onset} can be obtained from the nondimensional peek's formula as

$$E_{onset} = \frac{L}{V_0} (A\delta + B\sqrt{\frac{\delta}{R_w}}) \quad (19)$$

Where $A = 32.3 \times 10^5$, $B = 8.46 \times 10^4$ and $\delta = 1$ are assumed in the present work.

2.8 Summary

In summary, it is intended to present the theoretical aspects of the research work. Effort is made to understand the physics behind the electrohydrodynamics of ion drag pumping and thermally induced electrohydrodynamic pumping, the inter-coupling of physics of fluidic and electric fields, impact of the material media and the classification of the equations in the interdisciplinary fields and boundary conditions.

CHAPTER III

3 Computational Efforts in EHD

3.1 Introduction

The non-linear problem of electrohydrodynamics is a very complex one. Many authors have carried out extensive computational efforts to stimulate the problem using variety of numerical techniques, sometimes with the imposition of the primary fluid flows [49, 50, 51, 52, 53, 54, and 55]. When the primary flows were imposed, electrohydrodynamics became secondary flows and serious studies of the actual electrohydrodynamics induced flows were not carried out. ANSYS® has limited capabilities of solving electrostatics problems with limited one way coupling with fluids. COMSOL® serves as a perfect platform to solve different physics with the flexibility and adaptability of solving PDE equations as well.

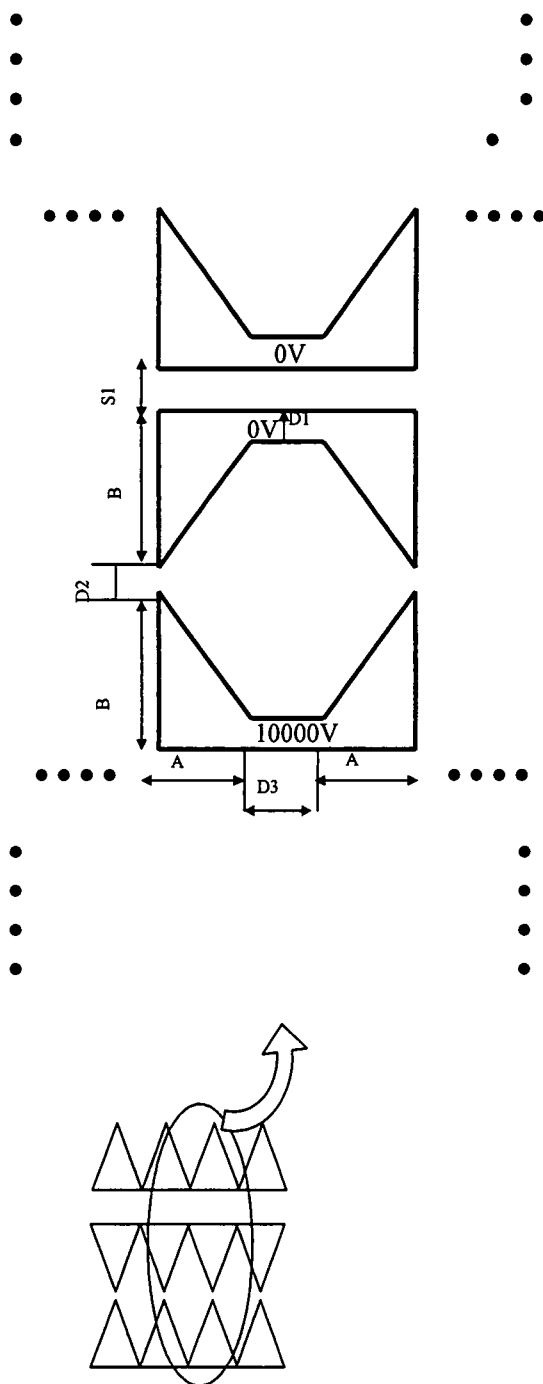
3.2 Numerical Studies using ANSYS®

3.2.1 Geometric Design Optimization

A two dimensional pointed electrodes model is modeled in ANSYS® environment under the constraints of the geometric, temperature, electric field and fluidic constraints. Figure 3.2 depicts the repeating pattern of the electrodes modeled in ANSYS®. The following assumptions are employed in the model.

1. There are no resident free charges in the medium.
2. The electrical permittivity of the medium is taken as constant in all directions.
3. The medium is assumed pristine i.e., there are no impurities and hence there are no electric field sinks. Therefore there is homogeneous variation in the electric field lines in the medium.
4. The fluid is assumed to mimic the flow at a particular instant between the electrodes and all the calculations are done at that particular instant of time. Therefore the forces in the medium are due to the applied voltages.
5. The voltages applied on the electrodes are static in nature.

The constraint put on the maximum electric field between the electrodes is that it should be lower than the dielectric breakdown strength of the fluid medium. The dimensions of the geometry are constrained below a certain value ($4\text{e-}6\text{ m}$). The resultant ANSYS® data is fed into the MATLAB® and the variations of the force/area and force were plotted against various dimensions of the geometry of the electrodes.



1.1.1 Nomenclature of electrodes:

- A = Width of an electrode, m
- B = Height of an electrode, m
- $D1$ = Distance between the two horizontal planar surfaces of the same electrode set
- $D2$ = Distance between the upper and the lower electrodes of the repeating unit
- $D3$ = Distance between the adjacent electrodes in the same row
- $S1$ = Distance between the lower electrode of the upper array and the upper electrode of the lower array
- H = Height of the channel
- L = Breadth of the channel
- $T1$ = Thickness of the electrodes

The sensitivity analysis of a two dimensional pointed electrodes is done and the graphs of the force/area and force were plotted as shown in the Figures 3.2-3.8. As the parameters B , $D2$, $S1$ decreased and A increased, the force/area and force increased and the pointed electrode configuration, where B became equal to $D1$ and $D2$ became equal to $S1$ gave way to the planar parallel electrode configuration. This guaranteed that the maximum force was obtained for minimum area, which is most important requirement for making of an EHD induced actuator.

Figure 3.1 The repeating unit of the electrode array

Force/volume was represented as force/area for a two dimensional model as the third dimension (height) has been taken as unity. Maximum ratio of Force/area is representative of the fact that maximum force is to be obtained for minimum area. Various iterations were made where the area and force differed according to the defined constraints on the geometry of the electrodes. As the height of the electrodes was reduced and distance between the electrodes was lessened, the force and force/area increased. This led to the conclusion that *the parallel electrodes are the best set of the electrodes*. These electrodes should be separated by a distance, which would provide the highest electric field. This also gave the highest force/area and force between the electrodes at an instant. The best electrode design determined from the two dimensional analysis, possess rectangular shape for maximum force/area, while satisfying the given dimensional, electric and fluidic constraints.

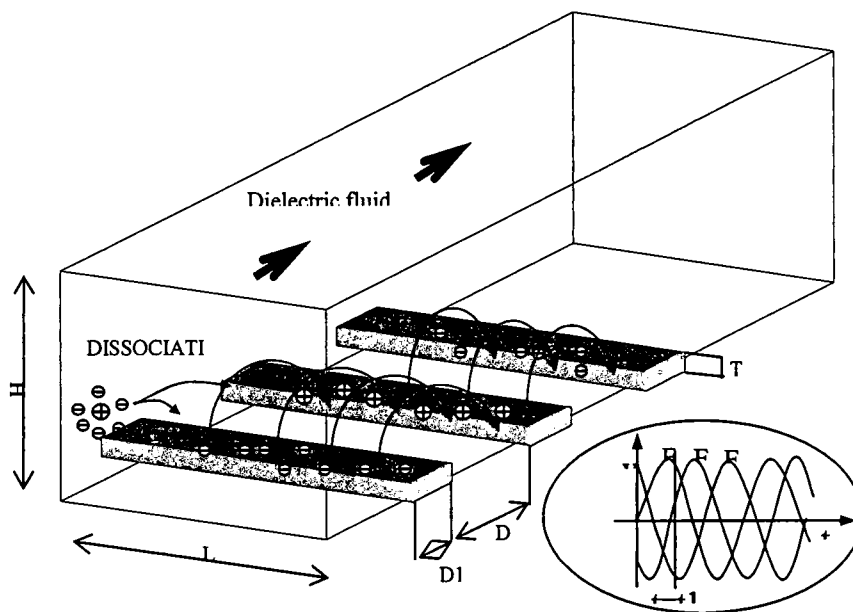


Figure 3.2 Schematic representation of the three dimensional actuator channel

The parallel plate configuration obtained from the sensitivity analysis of the two

dimensional model, is considered in the development and design of the three dimensional model, as shown in Figure 3.1. The parameter B is taken as equal to $D1$ and the total length of the electrodes ($2A+D3$) is taken as L . The height of the channel is taken as H and the thickness of the electrode as $T1$.

The resultant two-dimensional parallel electrode designs are incorporated in the three dimensional channel (actuator) model. These electrodes are placed at the bottom of the channel and are excited by the application of a *three phase, traveling* electric field. The excitation of the electrodes is dependent upon the various parameters like relaxation time of the charged species, which are generated by the dissociation of the fluid dielectric medium, distance between the electrodes and the ability of the electric field to dissociate the fluid molecules.

The three dimensional configuration, shown in Figure 3.1, is again modeled in ANSYS® and the results depicted for force and force/volume for various geometric parameters of the model at a given instant of the excitation as shown in the same figure. The variation of the force/volume and the force with respect to the height of the channel were approximately parabolic. The force/volume and the force both obtained were maximum for the minimum height, H and the distance between the electrodes, $D2$. *This variation promises that the actuator can be further scaled down to give maximum force and maximum force/volume*

3.2.2 ANSYS® Sensitivity Analysis Results

3.2.2.1 Two-Dimensional Parametric analysis of geometry with respect to force and force/volume

1) Varying A and D2

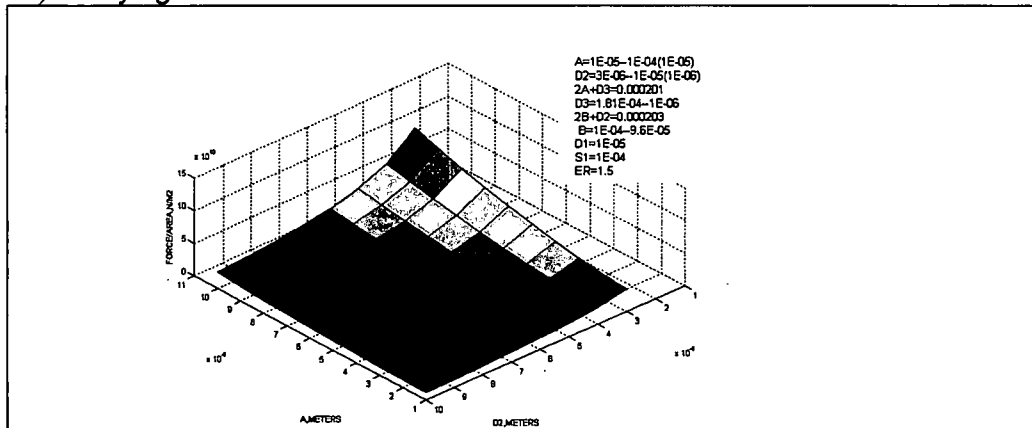


Figure 3.3 Parametric variation of force/area with A and D2

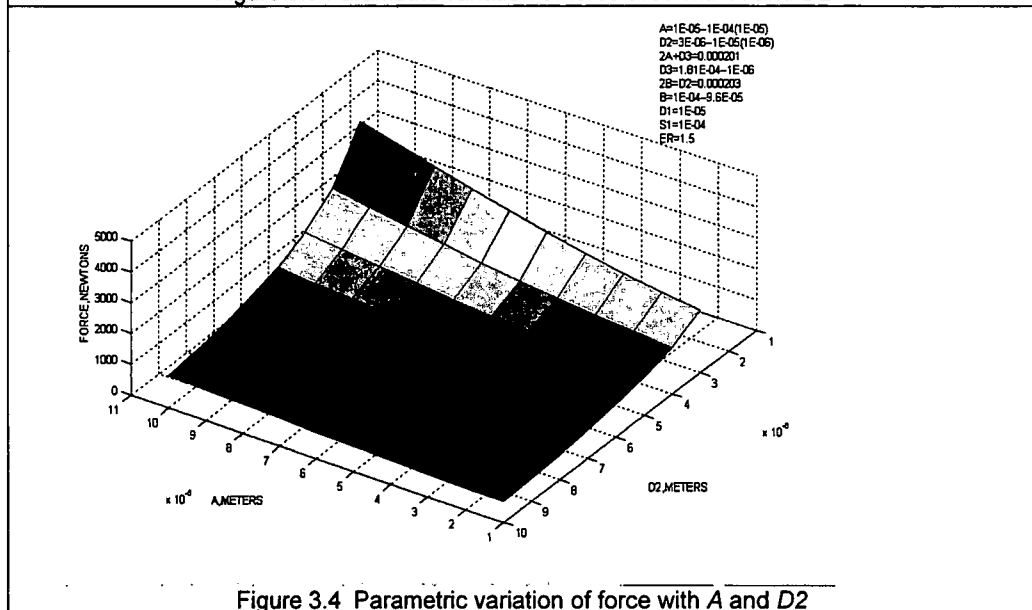


Figure 3.4 Parametric variation of force with A and D2

For Constant B, D1 and S1

- i) For a given A, force/area and force, shown in Figures 3.3 and 3.4 respectively, increase with decreasing D2. This is because the electric field increases with decreasing D2.
- ii) For a given D2, as A increases, area decreases, therefore force/area increases. The force also increases as A increases because the

electrodes become increasingly parallel and there is more interaction between the adjacent electrodes in the same row.

- iii) Since the width of the electrodes remains constant, increasing A would amount to decreasing the area. When $D2$ decreases simultaneously with increasing A , the electrostatic interaction between the upper and lower electrodes as well as that between the adjacent electrode boundaries increases. Hence there will be greater force over a reduced area. For a variation of $D2$ ¹ more than 0.15×10^{-5} m, there is almost no variation in force/area with variation in A .
- iv) The maximum point of force/area ($1.09\text{E}+11\text{N/m}^2$) is at $A=1 \times 10^{-4}$ m and $D2=3 \times 10^{-6}$ m. The maximum force (4463.2N) is obtained at $A=1 \times 10^{-4}$ m and $D2=3 \times 10^{-6}$ m.
- v) The variation between force/area and $D2$ for lower values of A is approximately parabolic. The force also varies in a similar way, as shown in Figure 3.4.

II) Varying B and $D2$

¹ The lower limit on $D2$ has been taken as 3×10^{-6} m to ensure that the electric field in the medium stays below than the breakdown electric field of the medium (3×10^9 V/m)

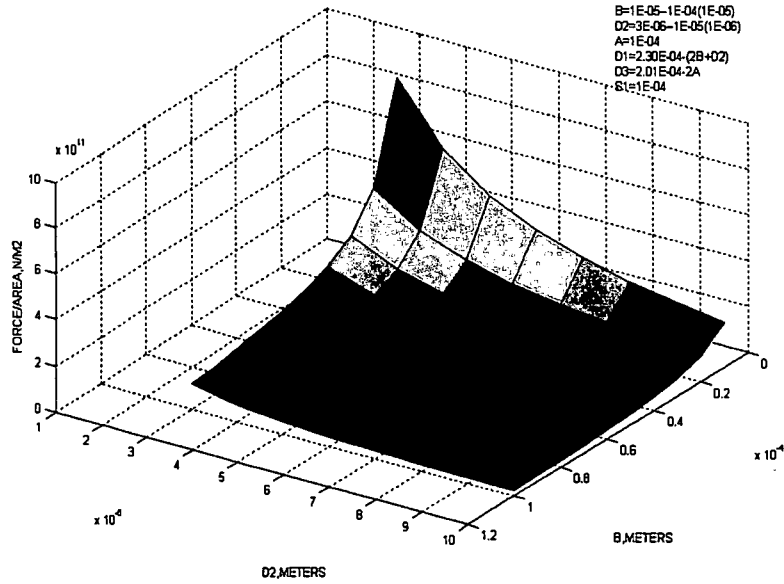


Figure 3.5 Parametric Variation of force/area with B and $D2$

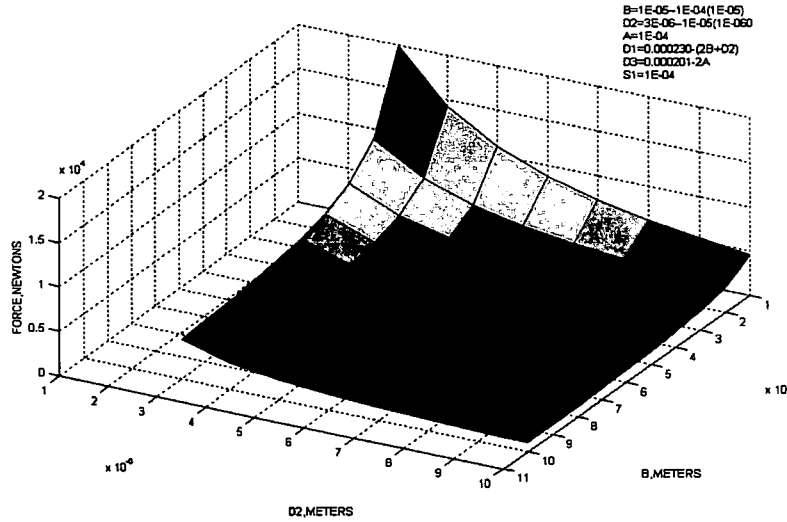


Figure 3.6 Parametric variation of force with B and $D2$

For Constant A , $D3$ and $S1$

- i) As B decreases for a given $D2$, the force/area, shown in Figure 3.5 increases as area decreases. As the interaction between the upper and lower electrodes increases, the electric field increases, this in turn

increases the force. The variation of the force is vividly depicted in Figure 3.6.

- ii) For a given B , force/area increases as $D2$ decreases, as the electric field between the pointed edges of the upper and lower electrode increases. This also results in increase in force.
- iii) For B greater than 4×10^{-5} m for any given $D2$, there is absolutely no variation in the force/area².
- iv) The maximum force/area ($8.77\text{E}+11\text{N/m}^2$) is at $B=1 \times 10^{-5}$ m and $D2=3 \times 10^{-6}$ m. The maximum force (19929.72N) is obtained at $B=1 \times 10^{-5}$ m and $D2=3 \times 10^{-6}$ m.

III) Varying A and B

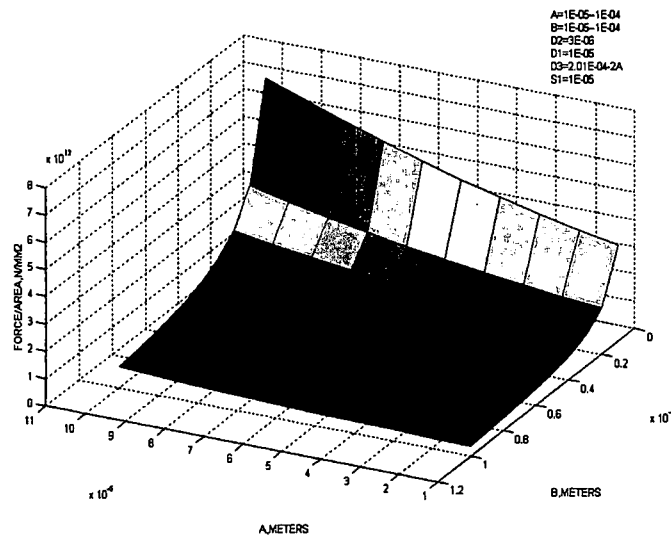


Figure 3.7 Parametric variation of force/area with A and B

² The lower limit on $D2$ has been taken as 3×10^{-6} m to ensure that the electric field in the medium stays below than the breakdown electric field of the medium (3×10^6 V/m)

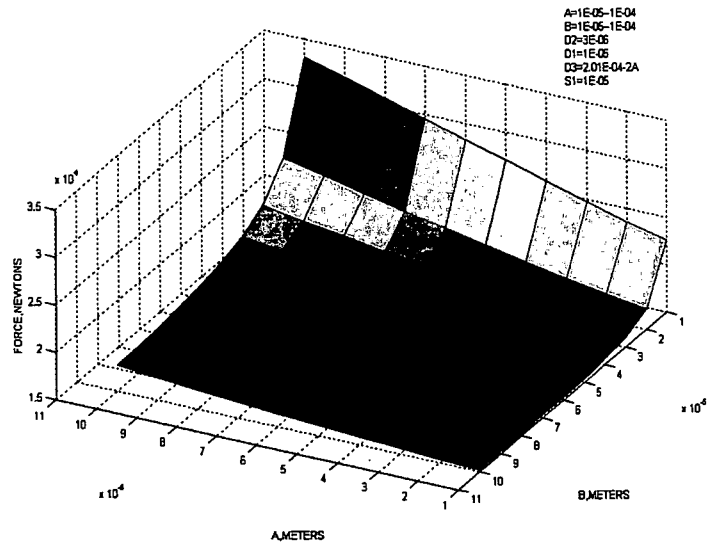


Figure 3.8 Parametric variation of force with A and B

For Constant $D1$, $D2$ and $S1$

- i) For a given B , the force/area increases with increasing A . Since the width of the electrodes is constant, increasing A would be tantamount to decreasing the area. At the same time the electric field interaction between the upper and lower electrodes increases which implies that the force on the medium also increases. The force on the medium increases but the volume decreases, thereby the ratio force/area also increases. The variation of force/area and force are depicted in the Figure 3.7 and Figure 3.8 respectively.
- ii) For a given A , the force/area increases with decreasing B . For a constant $D2$, decreasing B would be equivalent to decreasing the area and the interaction between the upper and lower electrodes increases. The electric force on the medium increases. The ratio force/area increases.

- iii) In general, the force/area increases sharply with increasing A and decreasing B , for a constant $D1, D2, D3, S1$. It has maximum at $7.15 \times 10^{+12} \text{ N/m}^2$ for $A=1 \times 10^{-4} \text{ m}$ and $B=1 \times 10^{-5} \text{ m}$. The force is maximum at 33143.65 N for $A=1 \times 10^{-4} \text{ m}$ and $B=1 \times 10^{-5} \text{ m}$.

3.2.2.2 Three Dimensional Parametric analysis of the geometry with the force and force/volume of the rectangular channel

I) Varying H and $D2$

For Constant L and $D1$,

- (i) For a given height of the channel, H , the force/volume as shown in the Figure 3.9, increases with decreasing distance between the electrodes, $D2$, as the electric force increases inversely with the distance between the electrodes and also the volume decreases at the same time. The force as shown in the Figure 3.10 also follows similar pattern.
- (ii) For a given distance between the electrodes, $D2$, the force/volume increases for the decreasing height of the channel, H . More force is obtainable as the H decreases, since the fluid experiencing the intense electric field near the electrodes would be increasing.
- (iii) The maximum force/volume obtainable is given by $4.54 \times 10^2 \text{ N/m}^3$ at $D2=3 \times 10^{-6} \text{ m}$ and $H=1 \times 10^{-6} \text{ m}$, while the maximum force is obtainable at $H=1 \times 10^{-6} \text{ m}$ and $D2=1 \times 10^{-6} \text{ m}$.

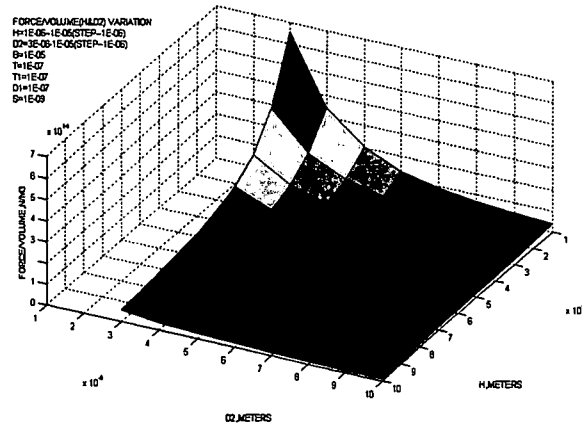


Figure 3.9 Parametric variation of force/volume with H and $D2$

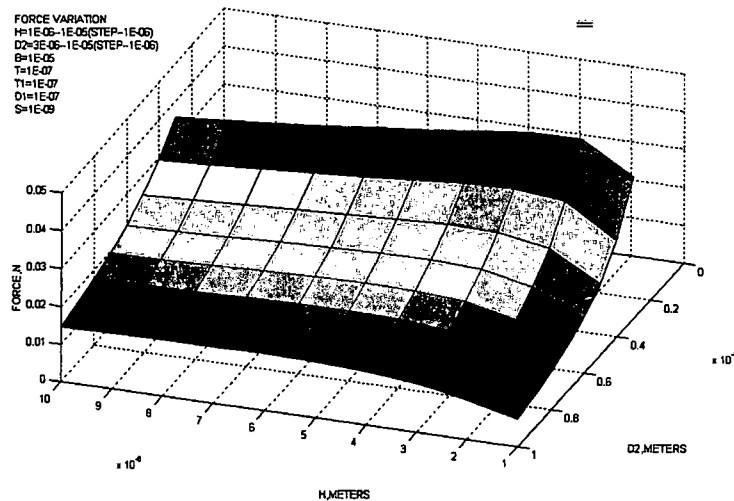


Figure 3.10 Parametric variation of force with H and $D2$

II) Varying H and $D1$

- (i) For a given height of the channel, H , the force/volume, as shown in the Figure 3.11 increases as the width of the electrodes $D1$, decreases for the given distance between the electrodes, $D2$. The force, as shown in the Figure 3.12 almost remains constant and rises a little with decreasing width of the electrodes; $D1$.

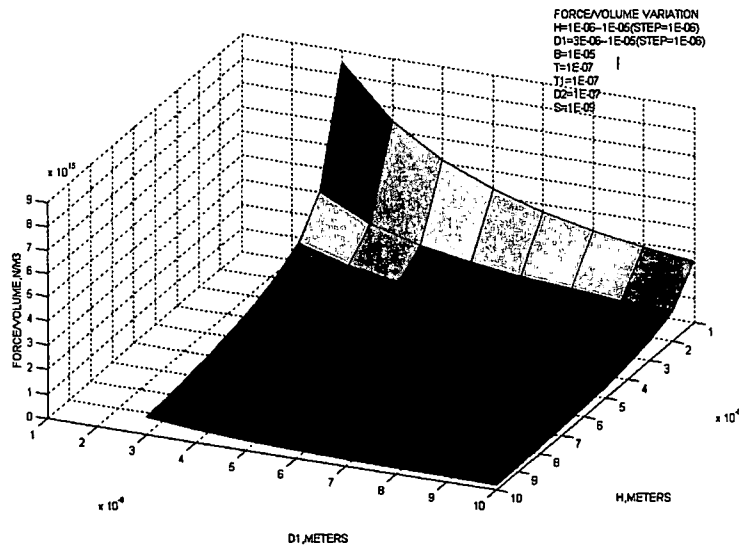


Figure 3.11 Parametric variation of force/volume with H and $D1$

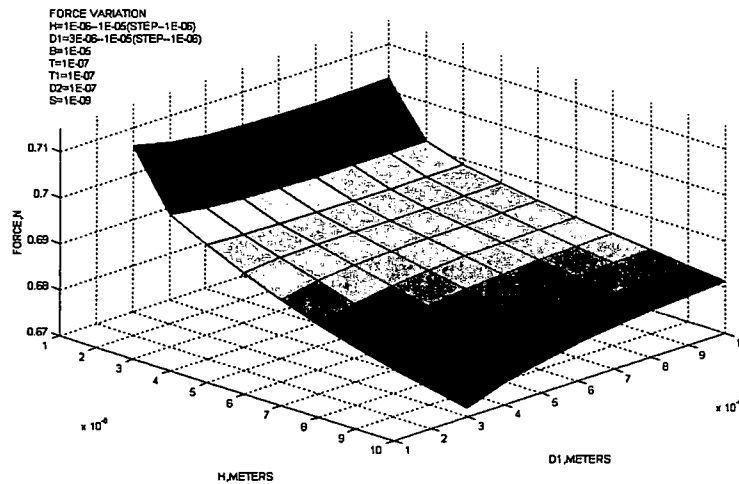


Figure 3.12 Parametric variation of force with H and $D1$

The force in any electrical system is derived from the potential difference between the electrodes and is not depended only upon the absolute potential of the electrodes.

- (ii) For a given width of the electrodes, $D1$, the force/volume increases as the height of the channel, H decreases for a constant distance between the electrodes, and $D2$. The force increases as the height of the channel decreases.

- (iii) The maximum value of the force/volume ($1.8\text{e}+15 \text{ N/m}^3$) is obtainable at the $H=1\text{e}-06\text{m}$ and $D1=3\text{e}-06\text{m}$ and the maximum force (0.69N) is obtainable at the same point .

III) Varying $D1$ and $D2$

For Constant L and H

- (i) The force/volume, as shown in the Figure 3.13 increases with decreasing width of the electrodes, $D1$ and the spacing between the electrodes, $D2$. The force, as shown in the Figure 3.14, varies almost parabolically with distance between the electrodes, $D2$ for the given $D1$.

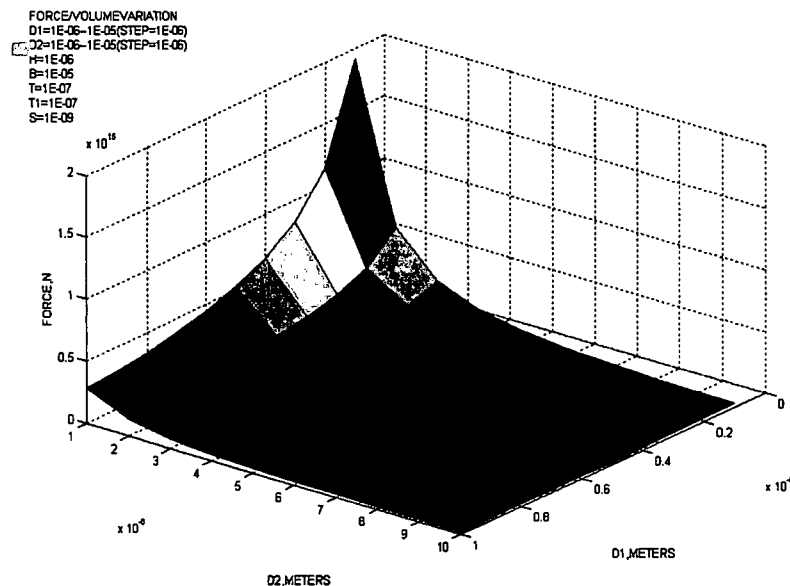


Figure 3.13 Parametric variation of force/volume with $D1$ and $D2$

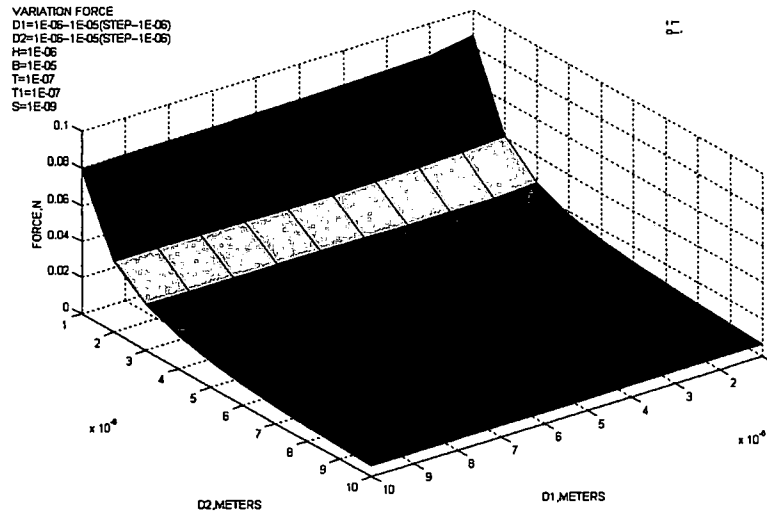


Figure 3.14 Parametric variation of force with $D1$ and $D2$

For Constant L and H

The force, as shown in the Figure 3.14 remains constant for a given $D2$ as the force is derived in an electromagnetic system from the potential difference between the electrodes.

- (ii) The maximum value of the force/volume at $D1=1e-06$ and $D2=3e-06$ is $6e+14N/m^3$. The maximum force (0.08N) is obtainable at minimum $D2=3e-06m$ and $D1=1e-06m$.

3.2.2.3 Conclusion from the design of the electrodes:

The two dimensional sensitivity analyses prove that pointed electrode design gives highest force/volume and force when it is optimized to a set of parallel plate configuration. This resultant design is incorporated in the three dimensional model of the actuator. Three phase electric fields are imposed on the electrodes and force/volume and force are computed. Force/volume and force increase as the distance between the electrodes as well as the height of the channel decrease. Constraints are imposed on the dimensions of the

channel, dielectric breakdown strength of the medium and maximum electric field between the electrodes. This translates to highest force being obtained for the smallest dimensions for the geometric parameters of the channel. This two and three dimensional analysis is near to simulating the pseudo-fluidic electrohydrodynamic (EHD) environment in ANSYS®. ANSYS® is an excellent multiphysics package capable of simulating complex multiphysics problems. For every type of analysis, ANSYS® has its own generic element which is specially built for simulating the concerned physics environment. For instance, to simulate a piezoelectric analysis, there are specific 2-D and 3-D piezoelectric elements. For cases where there are no generic elements for certain types of physics, there is a possibility of establishing either one-way or two-way coupling between different elements to simulate the physics. Fluid analysis can be done in ANSYS using Flotran®. The above analysis is done as a purely electrostatics analysis, which solved for the electrostatic voltage and electric fields. The above model is a valid representative EHD model the standpoint of solving an electrohydrodynamic problem, without involving the fluidics. *There was no strong one-way or a two-way coupling involved in ANSYS® between the electrostatics and the fluidics module. It was determined that solving an electrostatics model without full blown EHD analysis is a good, if not an accurate representative way for solving. An efficient electrode design as the basis of EHD totally rests on the peak electric and voltage fields between the electrodes and not on the induced fluid flows. As these fields are determined by the geometry and proximity of the electrode, optimizing the shapes and distance between the electrodes coupled with the acute difficulty of simulating a very weak one-way electrostatics–fluidics coupling led to the determination of using the above parallel design as suitable first design iteration.* The first and subsequent electrodes designs were also

fabricated using the parallel electrode design concept. Since the feasibility of applying high voltages on the electrodes was also restricted by the material of the electrodes and dielectric constraints of the fluids, the focus of the EHD mechanism and the corresponding analysis changed from *ion-drag EHD* to *induction EHD*. The problem of multi physics coupling is solved using by using COMSOL[®] suite, where both the electrostatics and fluidics physics can be solved in either one-way or two-way coupling by incorporating the Coulomb force term in the Navier Stokes equation. The inputs can be fed into the physics either through the PDE mode as actual equations or in physics mode, where the PDE coefficients are provided. In essence, COMSOL[®] has the capability for the coupling of electric fields and charges from the Gaussian law and the velocity fields from the Navier Stokes equation and is suitable platform is to create a model.

3.3 COMSOL[®] Physics Environment

COMSOL[®] is a multipurpose multiphysics commercial finite element program. It offers the advantages of formulating complex physics equations, which are not cast in a traditional standard version in the commercial finite element software and solved as part of the multiphysics equation set. The electrostatics solver solves for the Gaussian equation (2) and a graphical user interface for inputs for this solver is shown in Figure 3.15

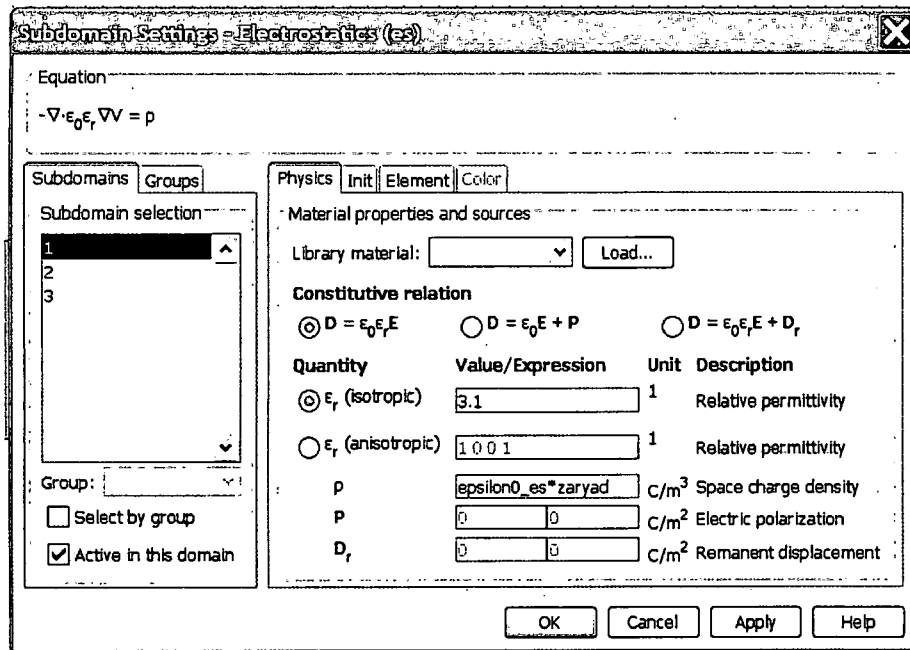


Figure 3.15 Graphical user interface for COMSOL electrostatics physics solver

This solver solves for the equation at the top left. The dielectric constant and the space charge density are the required inputs in this domain. The displacement field constitutive law is checked according to the mode of the analysis required to be done. The boundary conditions are defined in this domain as shown in the Figure 3.16. The boundary condition mentions zero charge/symmetry, electric potential, ground, surface charge condition and electric displacement and the left click and roll section "Boundary selection", is shown in this Figure 3.16. The term "zaryad" is taken as $-\nabla^2 V$ (personal communication, Sergey Korpov)

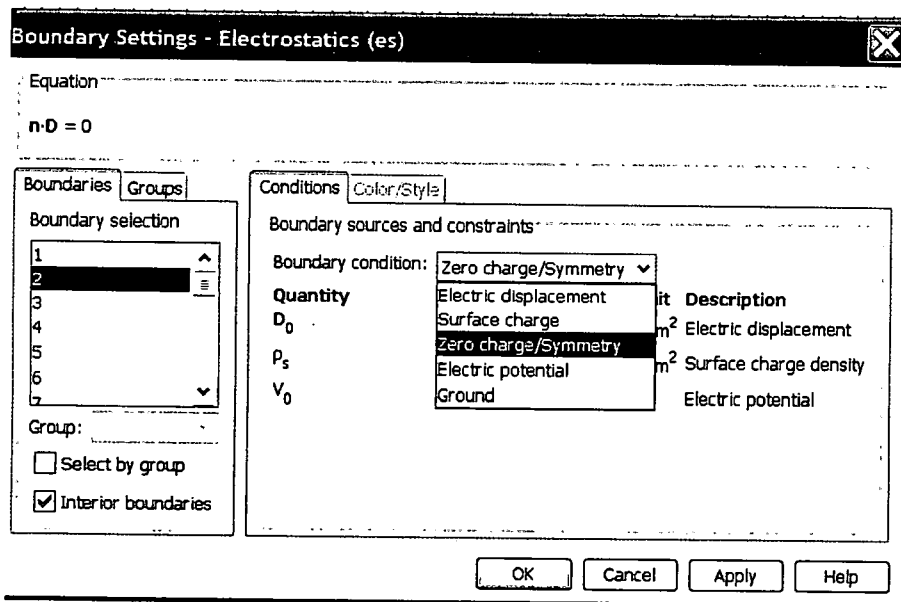


Figure 3.16 Graphical user interface for COMSOL electrostatics boundary conditions solver

The general form of the PDE coefficient form in COMSOL is given by the Equation (20). Charge density Equation (10) is formulated in terms of the PDE Equation (20). The PDE solver solves for the PDE equation (10) and a graphical user interface for inputs for this solver is shown in Figure 3.17. The coefficient form PDE mode is a specialty PDE solver interface and can be used to solve several PDE equations not solvable by the traditional modes.

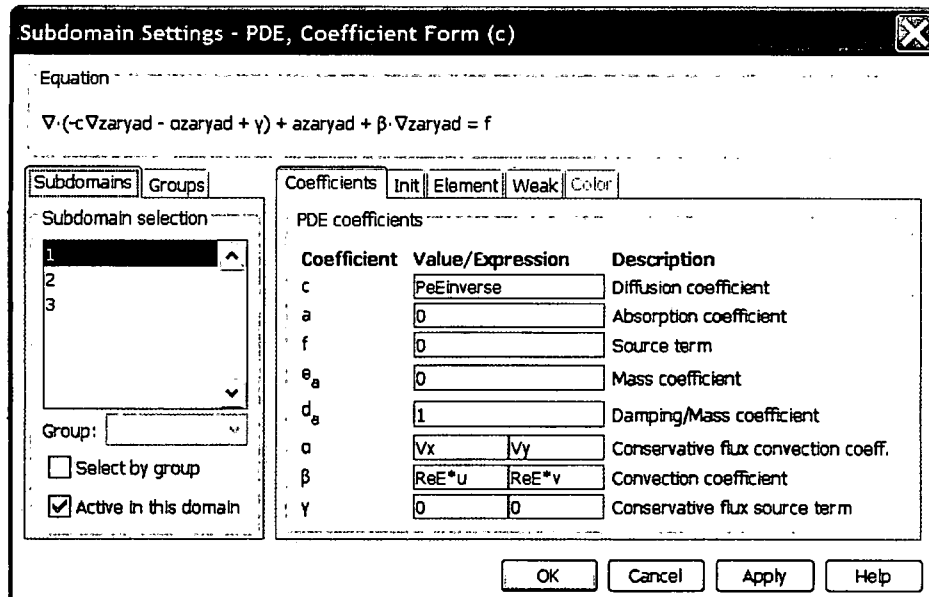


Figure 3.17 Graphical user interface for COMSOL PDE coefficient form solver

The general form of PDE Equation (20) is given by:

$$C_a \frac{\partial^2 u}{\partial t^2} + d_a \frac{\partial u}{\partial t} + \nabla \cdot (-c \nabla u - \alpha u + \gamma) + \beta \cdot \nabla u + \alpha u = f \quad \text{in } \Omega \quad (20)$$

$$n \cdot (c \nabla u + \alpha u - \gamma) + q u = g - h^T \mu \quad \text{in } \partial \Omega$$

$$h u = r \quad \text{in } \partial \Omega$$

where, the Ω is the computational domain and is the sub union of all the domains. $\partial \Omega$ is the domain boundary and n is the outward unit normal vector on $\partial \Omega$. According to COMSOL[®] documentation [60], the first equation in the system of equations (20) is the PDE equation to be satisfied in Ω , the second equation is the generalized Neumann's condition, also called as the natural boundary conditions. These conditions occur implicitly in the weak form of the PDE equation. This condition also represents as a flux or derivative of another variable. The third equation is the Dirichlet condition is also called as the essential boundary condition, as they confine the domain solution space. The values are functions of coefficients C_a , α , γ , a , q and h and the terms f , g and r should be determined according to a particular physics environment.

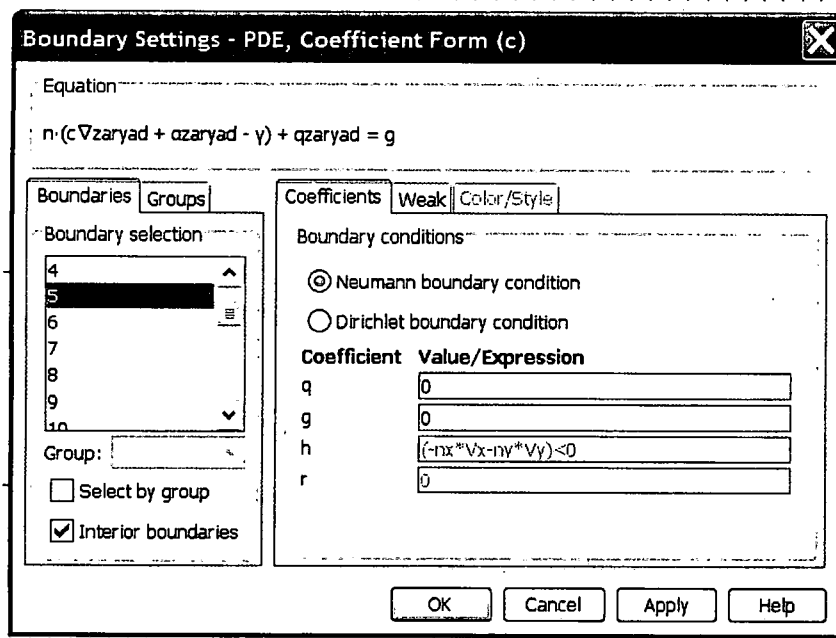


Figure 3.18 Graphical user interface for COMSOL PDE coefficient form Boundary Conditions Interface.

The boundary conditions are inputted in the graphical user interfaces much like that shown in Figure 0.18. The Neumann's boundary condition and the Dirichlet boundary condition can be specified by highlighting any individual box.

Appropriate values of q , g , h and d are inputs to customize boundary conditions to define a given problem domain. The fluid solver in COMSOL® is shown in the Figure 3.19. It solves the Navier stroke's Equation (8) and also conservation of mass Equation (9). Boundary conditions on the domain are given by the Figure 3.20 and acts as an input consol for assigning boundary conditions on the finite element computational domain according to the boundary conditions of the problem definition.

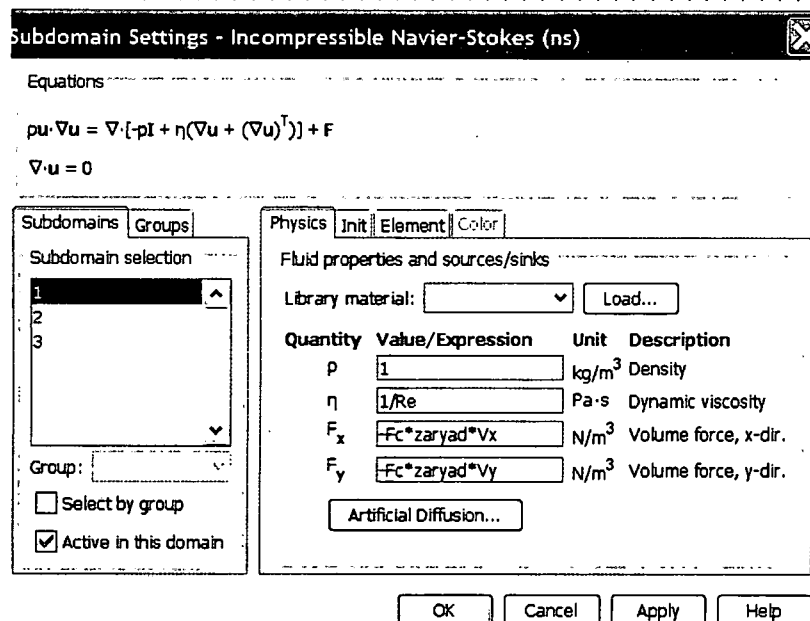


Figure 3.19 Graphical user interface for COMSOL Fluid physics solver

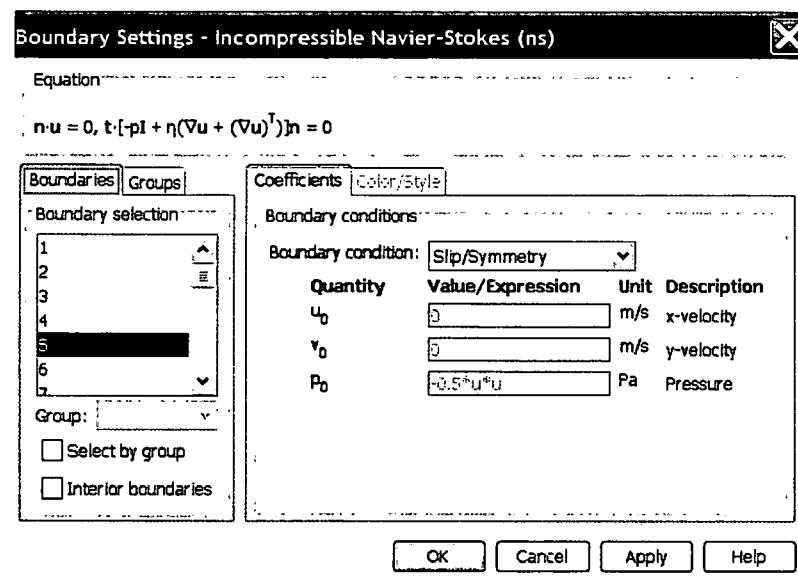


Figure 3.20 Graphical user interface for COMSOL Fluid physics boundary conditions

The energy equation graphical interface is shown in Figure 3.21, where the density, heat capacity, thermal conductivity can be substituted and modeled for the model. The boundary condition for the energy equation is shown in Figure 3.22 and shows different boundary conditions like thermal insulation, temperature and heat flux.

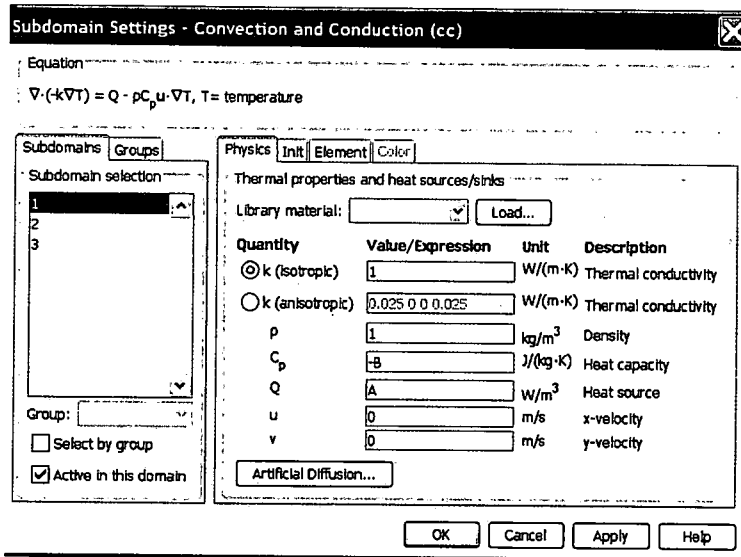


Figure 3.21 Graphical user interface for COMSOL Energy physics solver

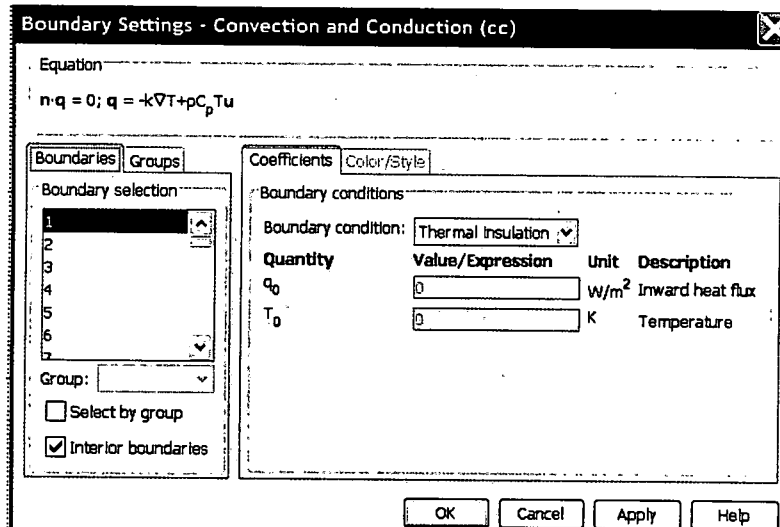


Figure 3.22 Graphical user interface for COMSOL Energy physics solver

All the above solvers are used for simultaneously of solving the thermally induced problem of EHD. They have to be solved in two-way coupling, as shown in Figure 3.23. A convergence window is shown in Figure 3.24.

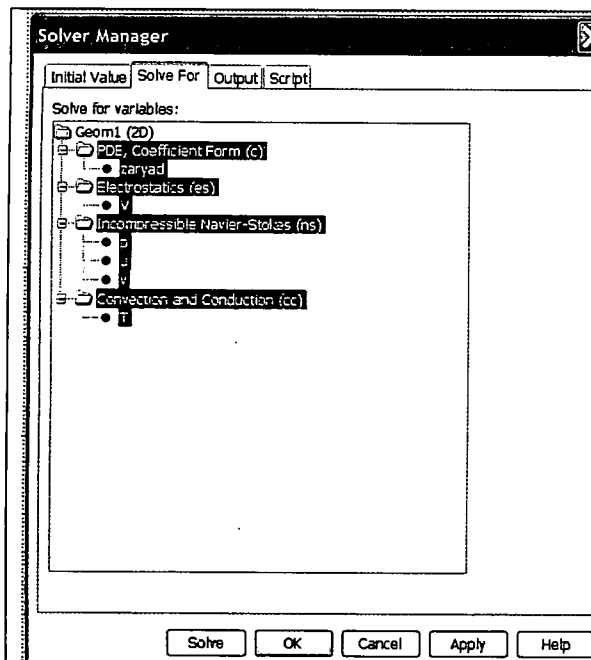


Figure 3.23 COMSOL integrated solver Manager

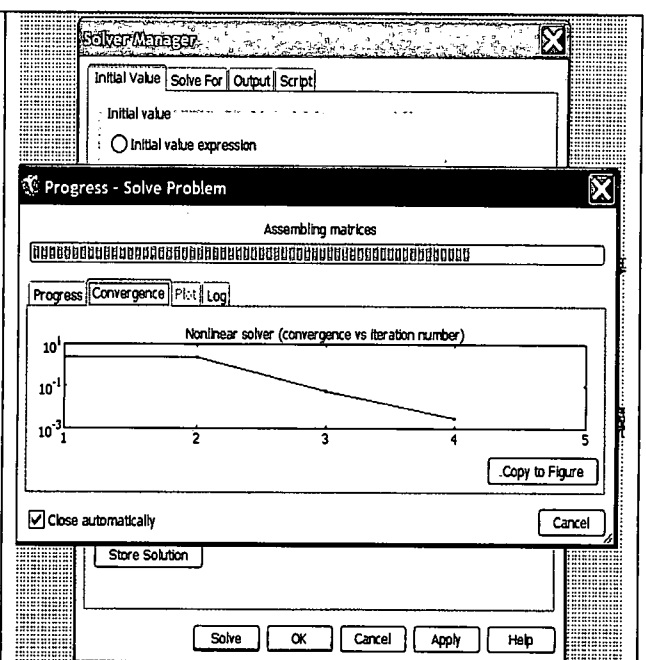


Figure 3.24 Progress bar cum convergence measure COMSOL integrated solver interface.

3.4 Numerical studies using COMSOL®

For fundamental understanding of the nonlinear interactions among the space charge density, electric field and the electrohydrodynamic flow, the terms of the current density as in the equation (6), has to be defined and coupled properly, as a part of the coupled equation set. In COMSOL®, the electrostatic Gaussian Equation (2) solves for the voltage in the finite element domain, assuming zero charge for given voltaic conditions. PDE from the COMSOL Equation (6), solves for current density, for given electric fields and voltage fields from Equation (2). The PDE equation and the electrostatic Gaussian equation are solved simultaneously in a two-way coupling, to yield charge and the velocity fields in the finite element domain. Subsequently, the Navier strokes equation is solved in a two way coupling with PDE equation, for the velocities and pressures fields from the velocity input provided from solving the PDE equation. All the

three physics are solved interactively with a two way coupling for the whole finite element domain yielding optimized values for the voltages, charges, velocities and pressure fields in the domain.

Need to simulate and benchmark Sergey Korpov's model:

The physics of electrohydrodynamics presents several challenges and is really tough to model the nonlinearity of the Navier strokes equation along with the Gaussian equation. The *parallel design electrode* from 2D/3D ANSYS analysis is fabricated using MEMS lift-off techniques, while simultaneously computationally analyzing the electrodes, using ANSYS® and FIDAP® (Fluent). This fabrication method of electrodes is mentioned in the next chapter of "Micro pump Design and Fabrication". Experimentally, this parallel design of electrodes yielded little head and wasn't consistent with pressure heads noticed by different researchers [6, 7, 8, 13, 14]. For instance, Chio et al [25] observed corn oil velocity of 4.75 $\mu\text{lit}/\text{min}$ and pressure of 10 pascals at six phase AC voltage of 310V and 0.5 Hz. They had 60 electrodes having width and distances between them as 100 microns. *In order to investigate the influence of the electrode design on the overall electrohydrodynamics, it was **decided to embark on a different strategy to analyze the ion drag pumping with a central emitter and the peripheral collector electrode--different from original induction EHD pumping with parallel design of electrodes.*** For a while, the analysis was simulated in Fidap®, as the software had an EHD section. The model was unsuccessfully aborted due to the convergence problems in spite of refining meshes, lower time steps, changing the parameter variables and no computational help. Search for a proper software which could simulate EHD phenomena led to COMSOL®. The quest for a finding an example problem and/or computational help in COMSOL® led to an example analysis in Sergey Korpov's paper [56].

Korpov [56] presented the results of simulating an air based ion drag pump with in a computational domain of 20cms x 4cms produced air velocity of 1.8 m/sec by applying 9kV between the central emitter and the collector electrode. This design was the best and only design available in the literature review in COMSOL®, partially because it has been verified experimentally by Korpov. This design is copyright of Cronos Air technologies and Sergey Korpov [personal communication and email dated September 6th 2007]. As a first step in modeling the EHD physics for a given electrode arrangement, it is often better to benchmark an already simulated EHD problem, which has been verified experimentally. Hence, Korpov's electrode model is first modeled in COMSOL® and subsequently, induction EHD analysis with and without temperature is extended to include the *actual parallel electrode design configuration* from ANSYS® analysis. Hence the overall goal of analyzing an ion drag model with a different design was reasoned from a mix of the computational and experimental decisions.

3.5 Ion drag EHD

A two dimensional working Ion drag EHD model of the electrodes along with a semi insulating dielectric corn oil is modeled in COMSOL®. Only a small part of the repetitive pattern of the electrodes is considered for analysis, with symmetric boundaries at right, left and the bottom sides. The inlet is considered far enough such that there is no voltage variation in this region due to the electrodes. A schematic of the ion-drag pump (Courtesy: Sergey Korpov, personal communication), is shown below in Figure 3.25:

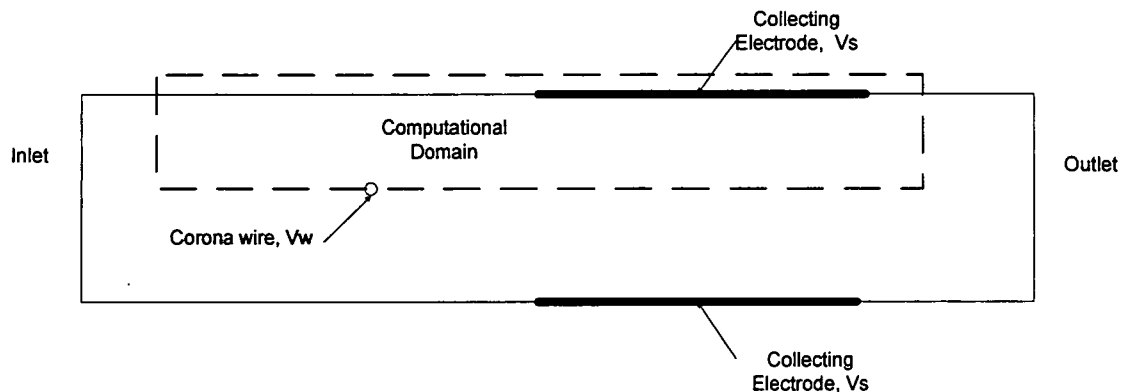


Figure 3.25 Computational domain of the EHD pump

For solving the voltage configuration in the domain of the Ion Drag EHD pump, the Gaussian law is solved for a given set of boundary voltage conditions on the electrodes. A DC voltage of 150 V is applied at the central emitter corona wire electrode and the ring low curvature collector is grounded.

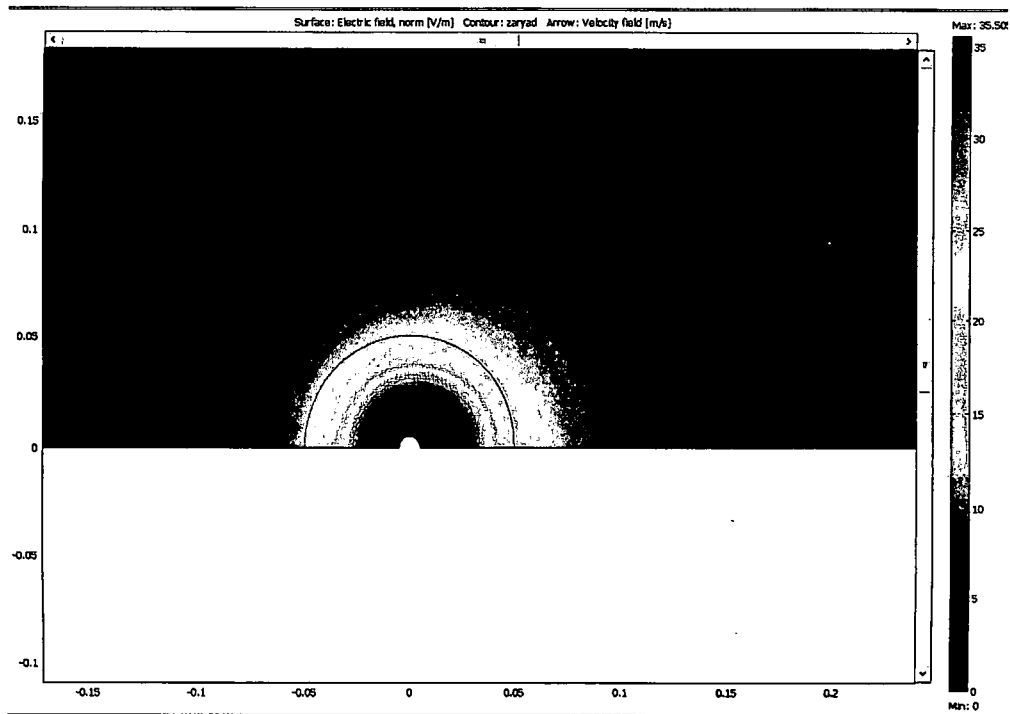


Figure 3.26 Close-up view of the Electric field distribution on the emitter electrode

The potential distribution from the emitter electrode varies from the electrode in a parabolic way and settling down to 100 volts in the major inner domain of the pump, as shown in Figure 3.26. This voltage generates the maximum electric fields strength of the 7.5×10^4 V/m, which is less than the dielectric breakdown strength of the corn oil which is 2×10^6 V/m. The velocities imposed at the inlet are such that it results in the pressure differential of $-\rho u^2/2$ between the inlet and the outlet. The vertical velocities at both the inlet and outlet are set zero. No slip boundary conditions are used on all boundary surfaces (wire and the collectors): $u = v = 0$. The pressure at the outlet is set as zero. The voltage specified at the inlet is V_{inlet} and the voltage specified at the outlet is V_{outlet} . The straight edge at the top left is specified zero surface charge as it is insulated. A zero charge condition at the right side corner beyond the collector electrode is specified as $n \cdot D = 0$ by using zero charge/symmetry condition in COMSOL® electrostatics module. The properties of corn oil are: density (ρ) = 900 kg/m^3 ,

Viscosity (μ) = $60\text{e-}3 \text{ N/m}^2\text{-sec}$, Mobility (μ_e) = $3.3\text{e-}10 \text{ m}^2/\text{Vsec}$, Diffusivity (D) = $5.3\text{e-}3 \text{ m}^2/\text{sec}$, Electrical conductivity (σ) = $5\text{e-}7 \text{ (Ohm m)}^{-1}$. The total length of the domain is 800 microns. The corona radius of the wire is 5 microns. The external radius of ionization used is $R_0 = 10$ microns. The distance between the center of the wire and the collecting electrode is 200 microns. The length of the collector electrode is 300 microns. The dimension so of the pump is shown in figure 3.27.

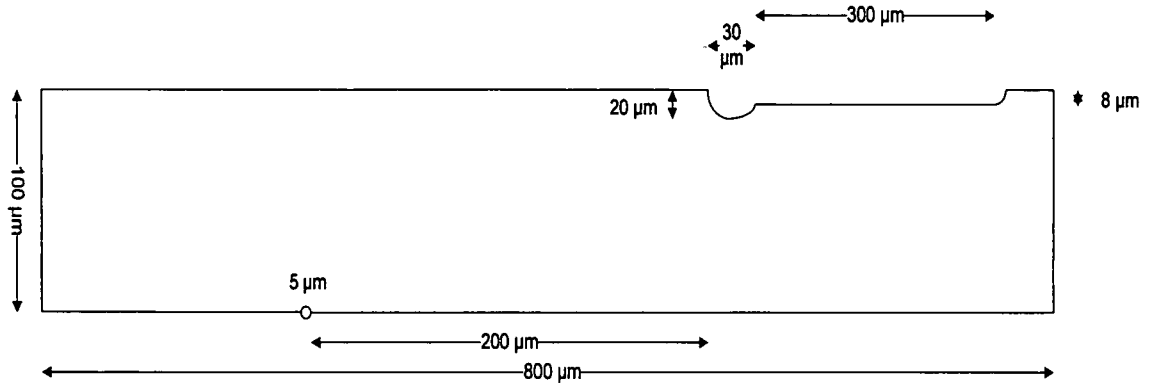


Figure 3.27 Dimensions of the domain of the EHD pump

The $n \cdot D = 0$ condition is also the symmetry condition on the left side, bottom side and right side of the computational domain. The voltage and charge output from the Gaussian law is fed into the PDE Equation (20) which is cast as Equation (10), which solves for velocity for a given charge. The velocity output from PDE is, then fed into the Navier Stokes equation, which is augmented to possess columbic force as source term and solved for the velocity and pressure fields. This result has resulted in only one-way coupling of the voltage, charge and velocity fields. To get a better optimized values of the voltage, charge and velocity fields, i.e., solving in a two way coupling- a combination of all the three equations – electrostatics, PDE and the Navier Stokes equations is solved simultaneously to give the velocity and pressure fields in the domain, as the output in the semi insulating fluids, due to the input voltage distribution on the

electrodes. Free meshing is used and convergence studies are done to confirm the velocity output of the NS solver. Finer meshing is done near the electrodes to enhance the resolution of the electric field and electric voltage lines. The emitter electrode region consists of two regions (James Q Feng; Sergey Korpov [57]). A zero charge diffusive flux $\frac{dq}{dn} = 0$ is imposed on all boundaries except the ionization surface of the wire. Kaptsov's assumption was also used on the wire, stated as equation (18), given in the second chapter. There is highly intense region of ionized high voltage region between the wire and the ground. Corona discharge occurs between these two, when the voltage difference between them exceeds the breakdown strength of the medium. There can be positive corona or a negative corona, depending upon the voltage of the emitter, where it is positive or negative. This region of ionization is localized mainly near the emitter and in case of positive corona, negative ions are attracted to the emitter and the positive ions are repelled from the emitter into the drifting region, which is the region between the high curvature emitter and the low curvature collector electrode. The positive ions in the drifting zone collide with the electrically neutral molecules of the semi insulating dielectric fluid like corn oil and transfer the momentum to them. This results in the flow of dielectric fluid. Grid sensitivity is performed to ensure that the numbers of the elements are adequate for accurate results. A aspect ratio of the model is 40 with the smallest dimension being 5 microns and the largest dimension is 800 microns. Different aspects ratios were performed as the parametric analysis was changed to investigate the performance of the pump. The model with aspect ratio of 40 is meshed using 14,670 elements using 125,099 degrees of freedom, shown below in Figure 3.28:

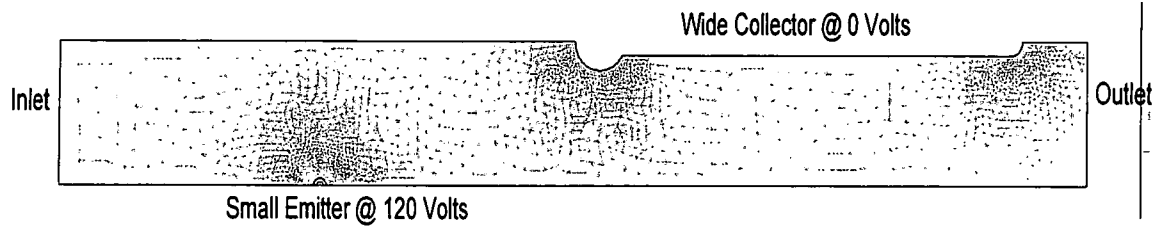


Figure 3.28 Meshed Ion Drag Model

Screen shot of the mesh statistics is shown below, in Figure 3.29:

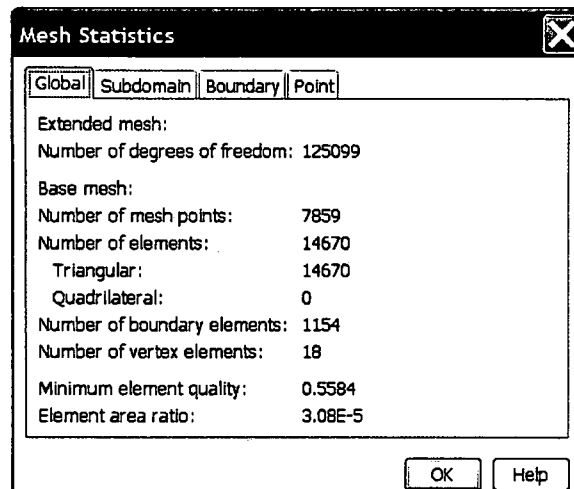


Figure 3.29 Mesh statistics for the mesh model.

Figure 3.30 shows the variation of the electric potential. There is intense variation of the electric potential lines near the emitter and gradually decreases between the emitter and the collector. The electric field straightens up near the collector. The variation between the electric potential lines is responsible for the developing the momentum with in the fluid. Almost whole of the variation comes from the intense electric fields near the emitter. The flow accelerates. The flow fields morph from plug flow of negligible magnitude to the almost parabolic flow.

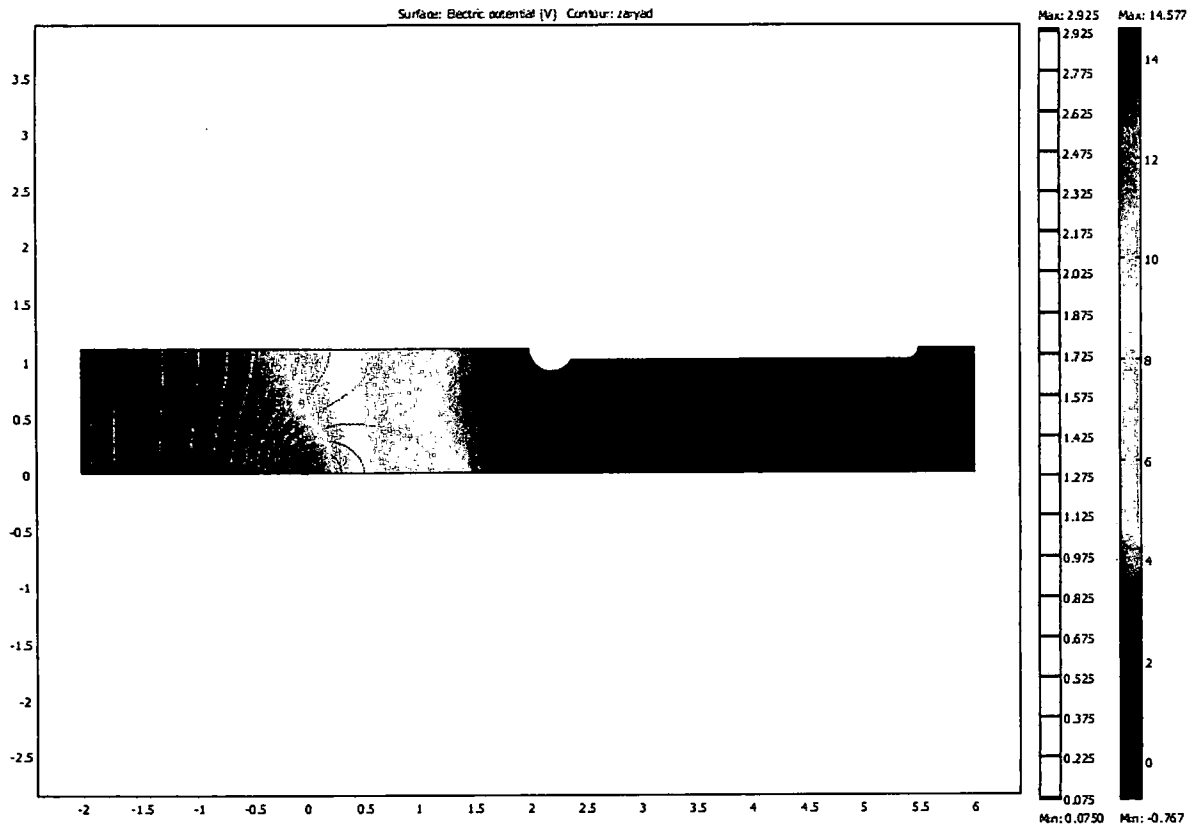


Figure 3.30 COMSOL® screen shot of the electric potential distribution in the computational domain.

The velocity and pressure profile at the inlet is given by the Figures 3.31 and 3.32 below. The velocity at the inlet is negligible and is 0.018m/sec at the outlet. The pressure variation (P/P_0) at the inlet is of the order of 50 pascals. The Figure 3.35 shows the COMSOL screen shot velocity arrows from the inlet to the outlet along with the charge distribution inside the domain. A close-up of the velocities in Figure 3.35 is shown in Figure 3.36.

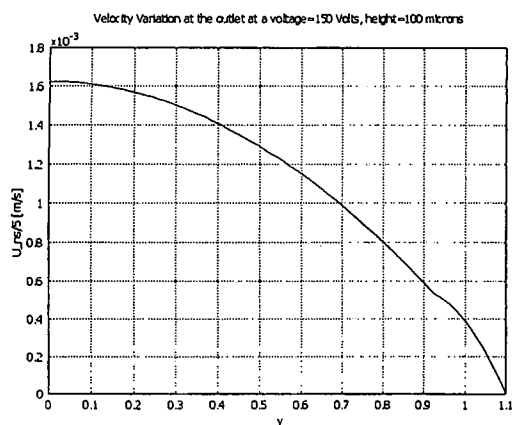


Figure 3.31 Velocity, $u(y)$ in m/sec variation with height (meters) at the inlet

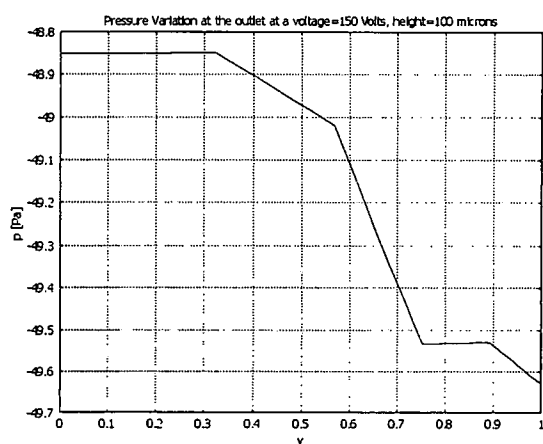


Figure 3.32 Pressure, $p(y)$ in m/sec variation with height (meters) at the outlet



Figure 3.33 .COMSOL® screen shot of the velocity variation in the domain

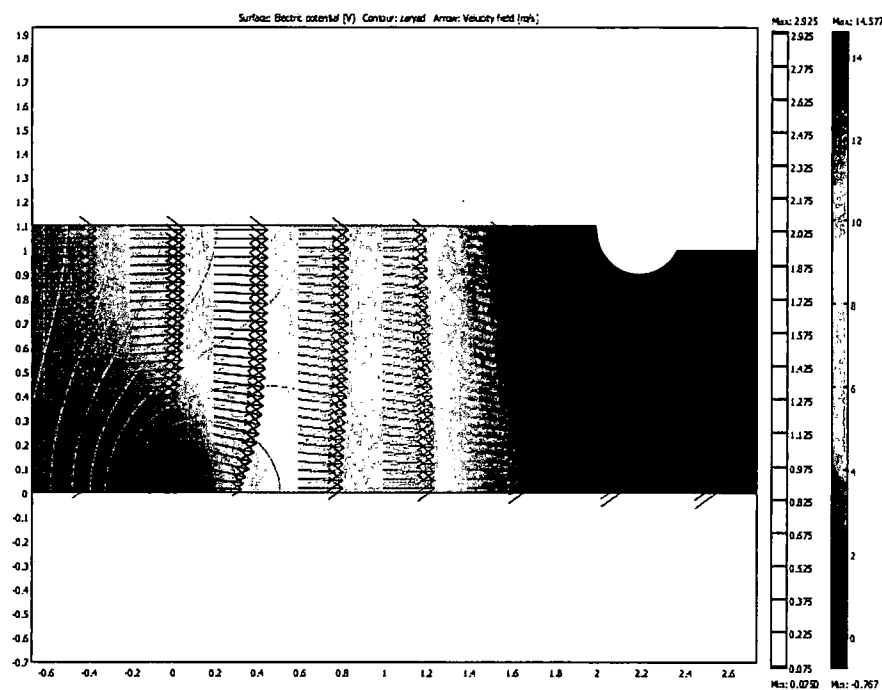


Figure 3.34 .COMSOL® screen shot of the velocity variation in the domain

3.6 Parametric evaluation of Micro-Ion Drag pump

A semi-parametric analysis in COMSOL® wasn't converging and sometimes not running at all, where COMSOL personnel acceded that a full blown parametric analysis was not in realm of COMSOL software package. According to COMSOL Inc, the optimization module could be included in future. It was decided to perform a semi-parametric analysis on the ion drag pump and perform characterization of the ion drag pump to analyze the flow rates and electric field trends. The analysis was performed on critical parameters such as height of the pump, distance between the electrodes, voltage applied on the electrodes and thermal conductivity of the liquid. All three physics involving the electrostatics solver, PDE solver and the navier strokes equation was solved simultaneously in a two-way coupling.

1) Voltage applied to the electrodes:

The electrode voltage is a critical component of the electrohydrodynamic process. The voltage applied should not be higher than the dielectric electric strength of the liquid. The voltage applied on the electrodes should not be too low that it results in no flow. After literature survey, an arbitrary value of about 150 volts was applied. The voltage was increased from 40 volts to 10^7 volts and flow rates and pressure profiles were simulated. The electric fields were varied from $2e4$ to $5e9$ V/m and the flow rates and pressures were registered as shown in Figure 3.35 and 3.37.

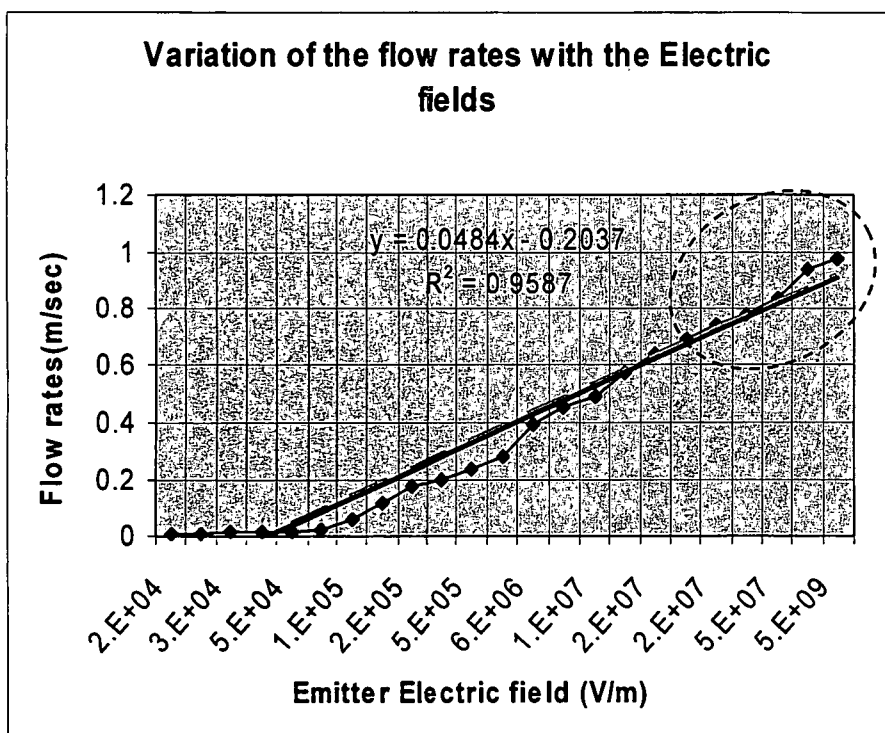


Figure 3.35 Variation of the flow rates with emitter voltage in one stage EHD pump.

The flow rates increase with the voltage applied to the emitter, suggesting that the kinetic energy imparted to the fluid increases with applied voltages, as shown in the above Figure 3.35. The flow rates almost follow a linear variation with the applied voltages. Dimensional scaling achieved from microfabrication technique of manufacturing can dramatically lower the voltages that can be applied on the electrodes.

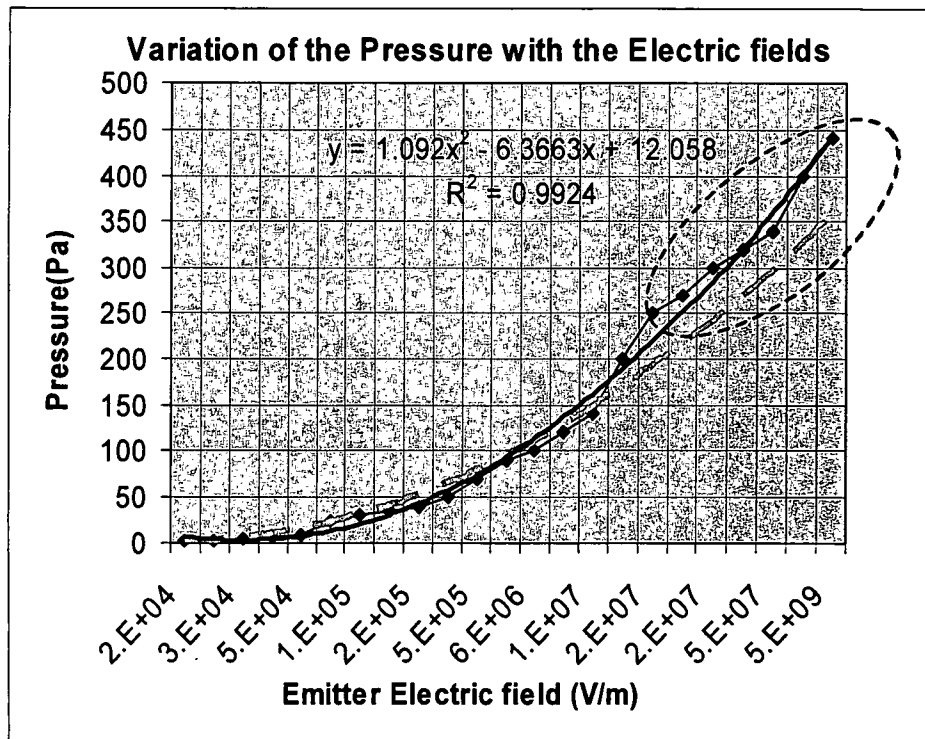


Figure 3.36 Variation of the pressure with emitter voltage in one stage EHD pump.

Voltages are applied to the emitter over a range, from 40 volts to 150 volts, resulting in variation of electric fields from $2e4$ V/m to $5e9$ V/m. The resulting pressure variation with the applied electric fields is shown in the Figure 3.36. Various types of degradation occur when the applied electric fields are nearing the dielectric breakdown strength of the dielectric fluids, such as the inception of the pre-dielectric breakdown of the insulating fluids culminating in sudden drop of the thermal, electric and physical properties of the liquid itself. The pressure profiles and data obtained from the simulations disregard the electric double layer (EDL), association and dissociation of ions in the fluid and various breakdown phenomenons. The dotted line along the curve, in Figure 3.36, shows a domain over which the above mentioned phenomenon develops and to get an accurate picture, the simulation should also include above mechanisms as well. The pressure varies quadratically with the applied electric field. The flow rates vary with different pressures at different voltages and are given by the

characteristic curves, as shown in Figure 3.37. These characteristic curves show that the performance of the pump is enhanced by increasing the magnitude of the voltages on the electrodes. These characteristics portray the ability to overcome the frictional pressure drop in the pump.

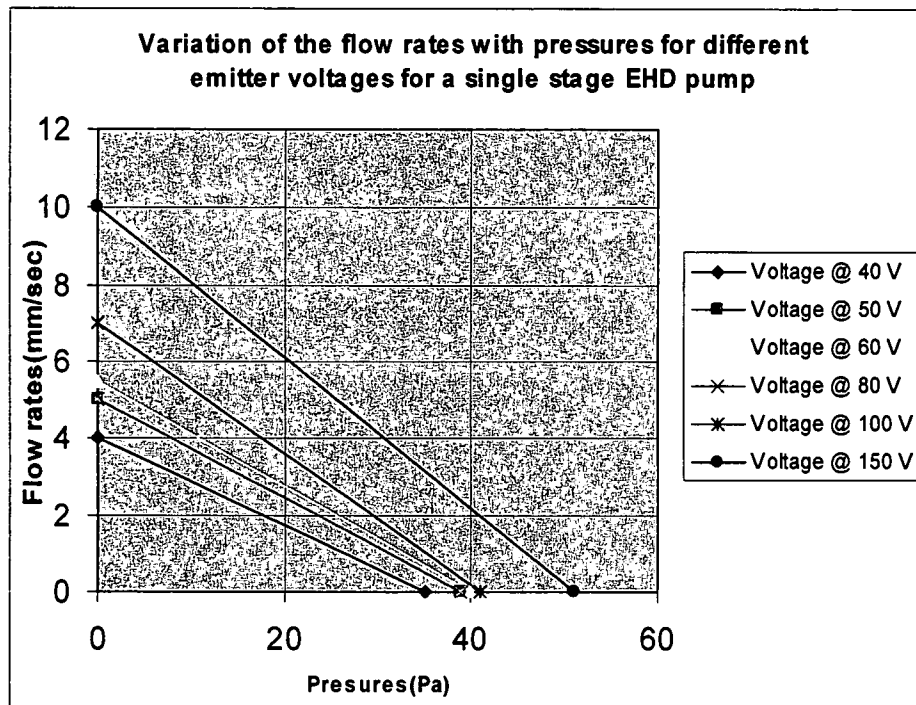


Figure 3.37 Variation of the Flow rates with the pressure developed for a computational single stage EHD pump.

The electric fields and the velocity variation along the length of the device at 100 Volts and 80 Volts is shown below.

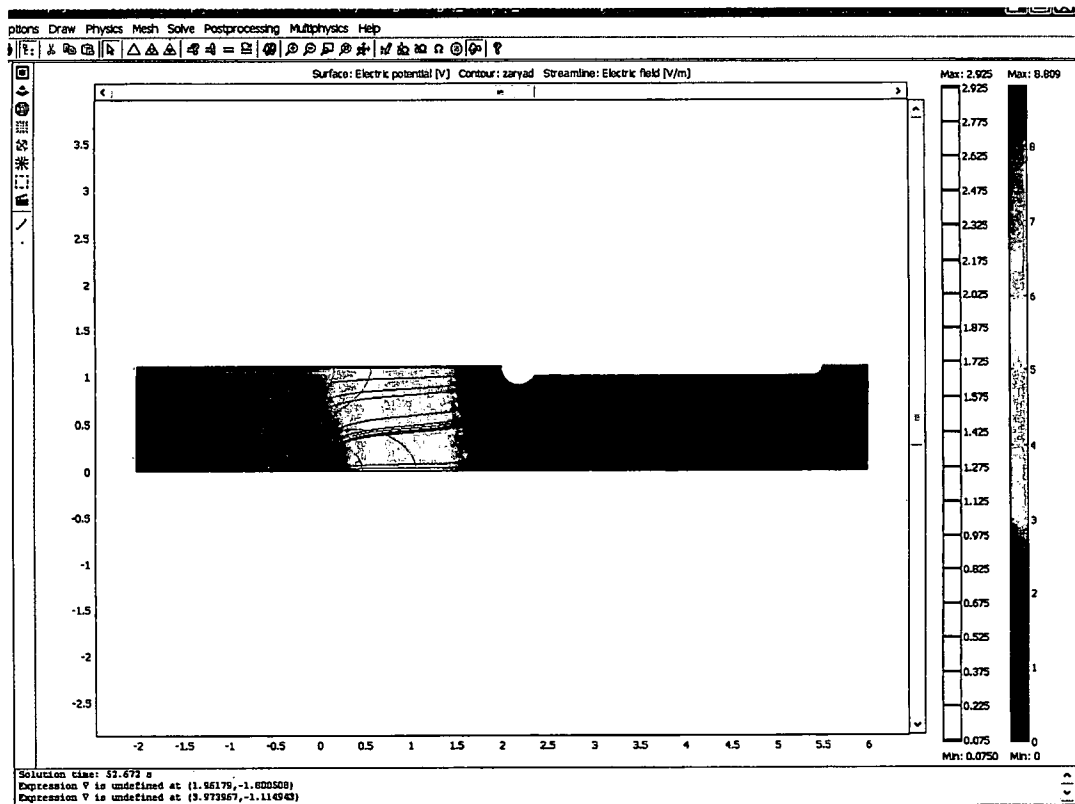


Figure 3.38 Electric field profiles for a single stage EHD pump at 100Volts.

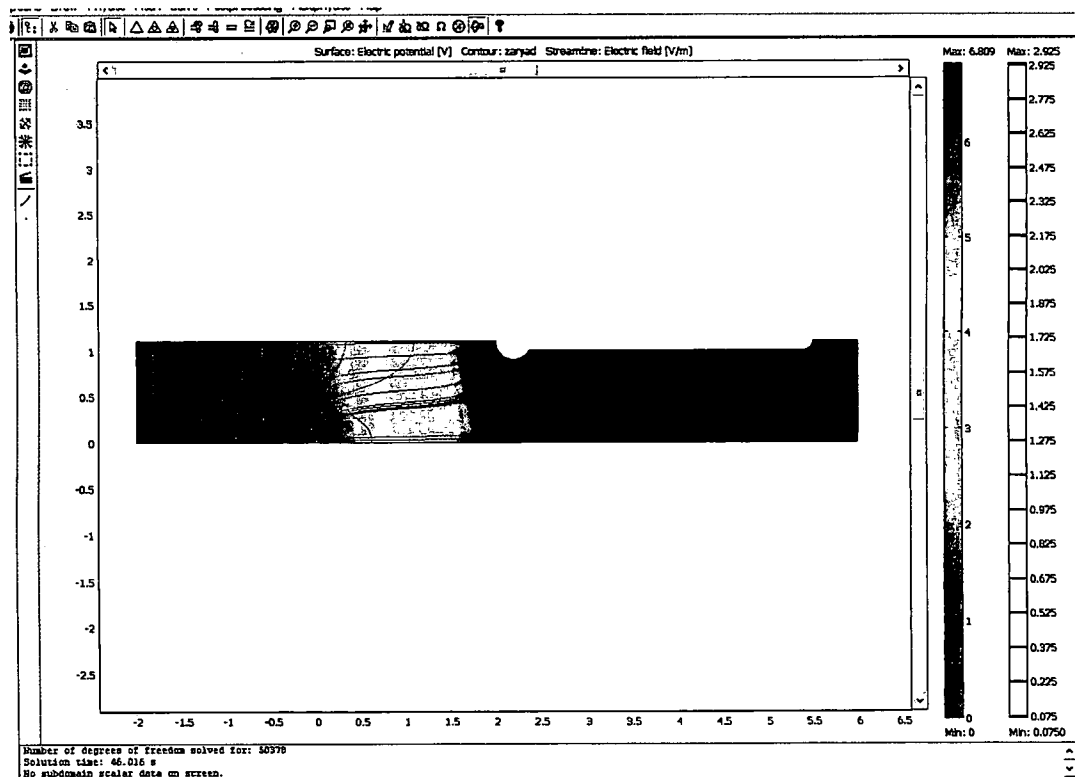


Figure 3.39 Electric field profiles for a single stage EHD pump at 80Volts.

2) Height of the channel:

The height of the channel is the main criterion in the analysis of the pump. The height of the pump determines the amount of the fluid that has to be propelled by emitter electrode. The electric field between the emitter and the collector electrode increases as the distance between them is decreasing, but at the same time the boundary layer and wall effects also influence the flow velocities. Figure 3.40 shows that the pressure decreases, when the height of the EHD channel increases. This can be weakening electric fields and charge density profiles. The velocity profile actually reaches peak around 110 microns. This is the height when the body columbic forces equal the viscous forces and above this height, the viscous forces dominate the flow dynamics and the flow rates and pressure.

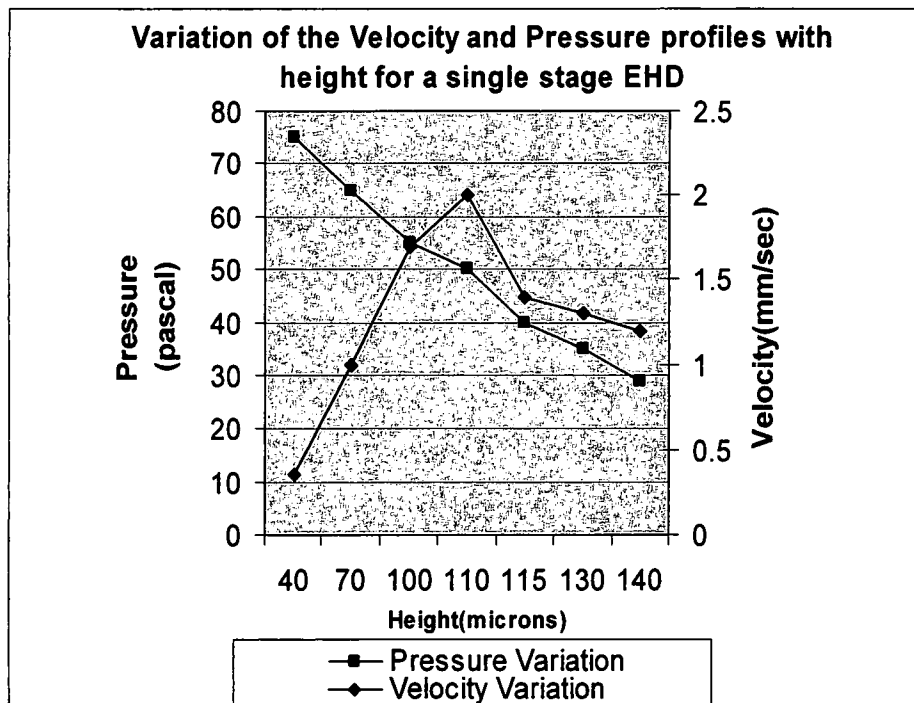


Figure 3.40 Variation of the velocity and pressure with the height of a single stage EHD pump.

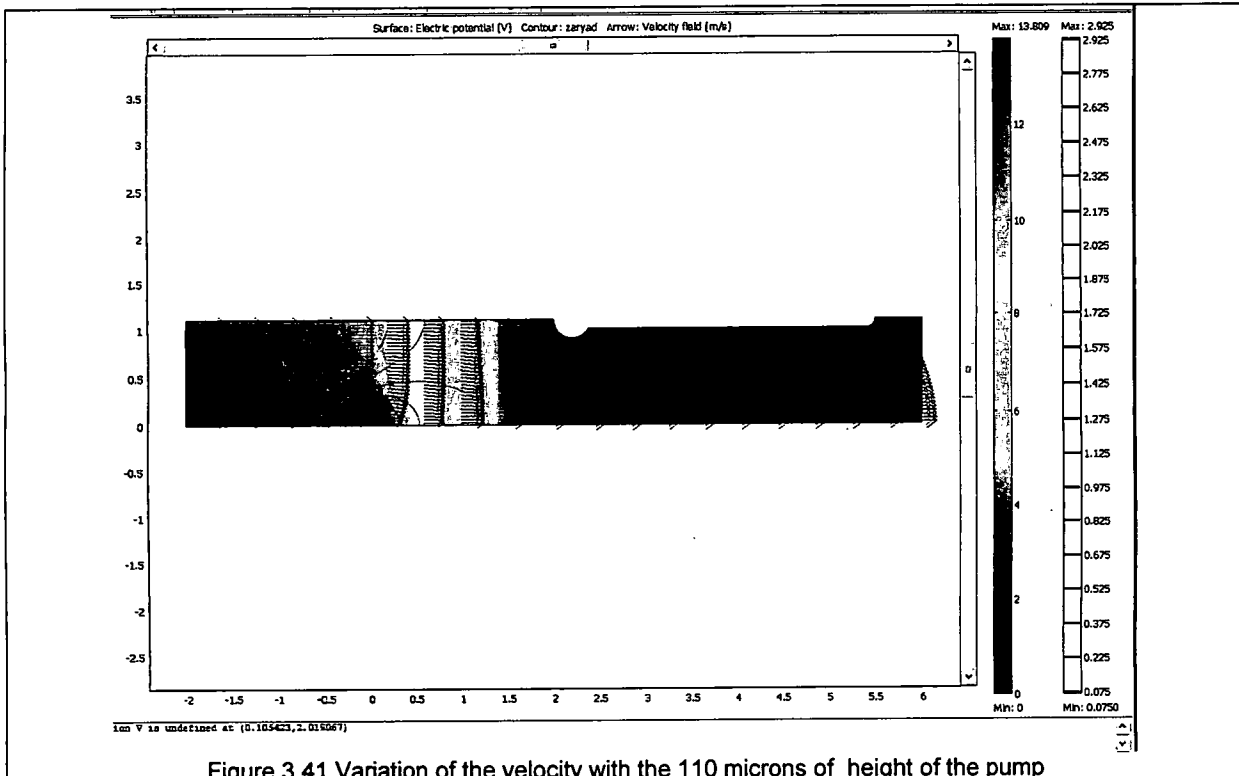


Figure 3.41 Variation of the velocity with the 110 microns of height of the pump

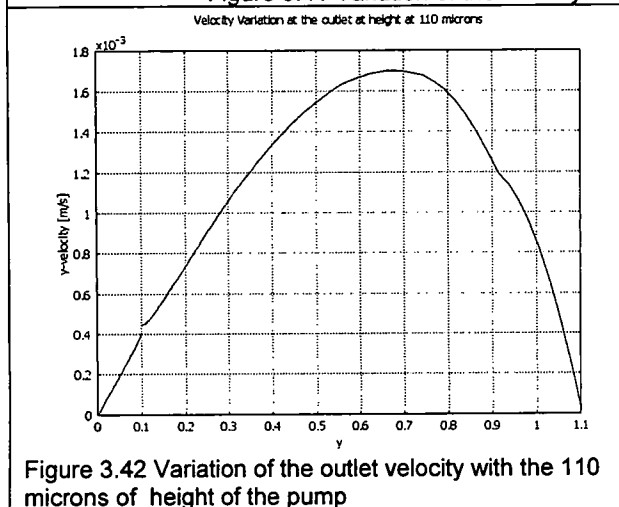


Figure 3.42 Variation of the outlet velocity with the 110 microns of height of the pump

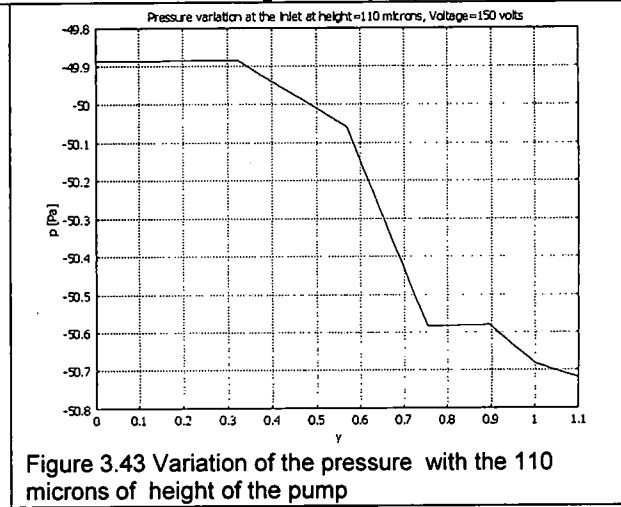


Figure 3.43 Variation of the pressure with the 110 microns of height of the pump

Following points are noticeable from the above Figures 3.44-3.45.

- 1) Figure 3.42 shows that the velocity profile of plug flow at outlet of the model domain at 110 microns of height and 150 volts applied to the emitter is above height of 100. The magnitude of the velocity is 1.8 mm/sec

- 2) Figure 3.43 shows that pressure profile at the outlet of the model and is about 50 pascals

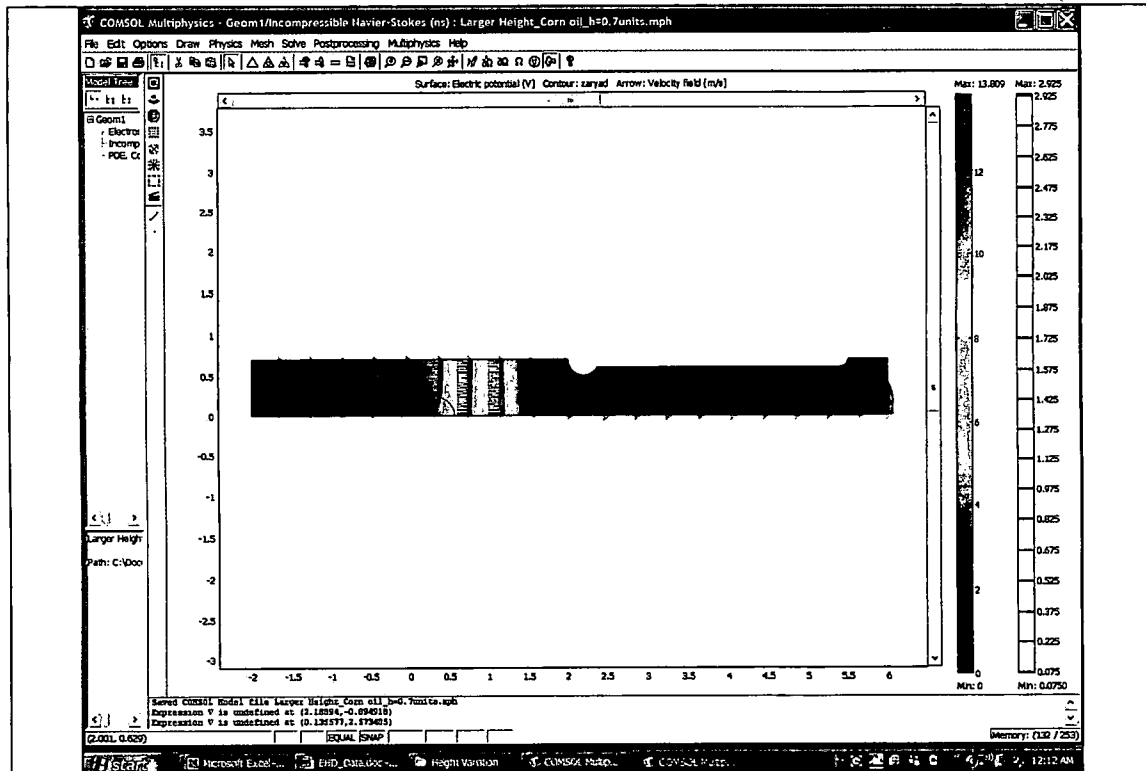


Figure 3.44 Variation of the velocity with the 70 microns of height of the pump

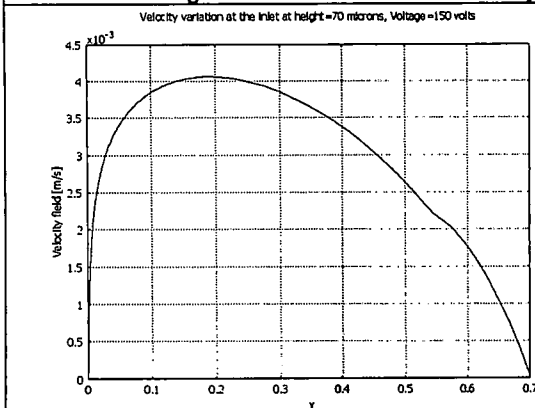


Figure 3.45 Variation of the velocity at the outlet with the 70 microns of height of the pump

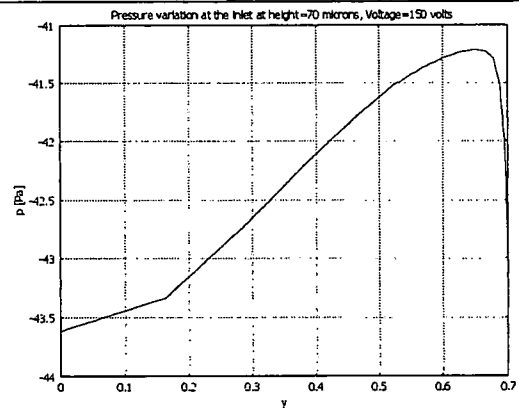


Figure 3.46 Variation of the pressure at the outlet with the 70 microns of height of the pump

Following points are noticeable from the above Figures 3.47-3.48.

- 3) Figure 3.45 shows that the velocity is the parabolic flow of about 0.45 mm/sec at the height of 70 microns, which is less than the base case of 100 microns.

- 4) Figure 3.46 shows that pressure profile at the inlet of the model is around 42 pascals.

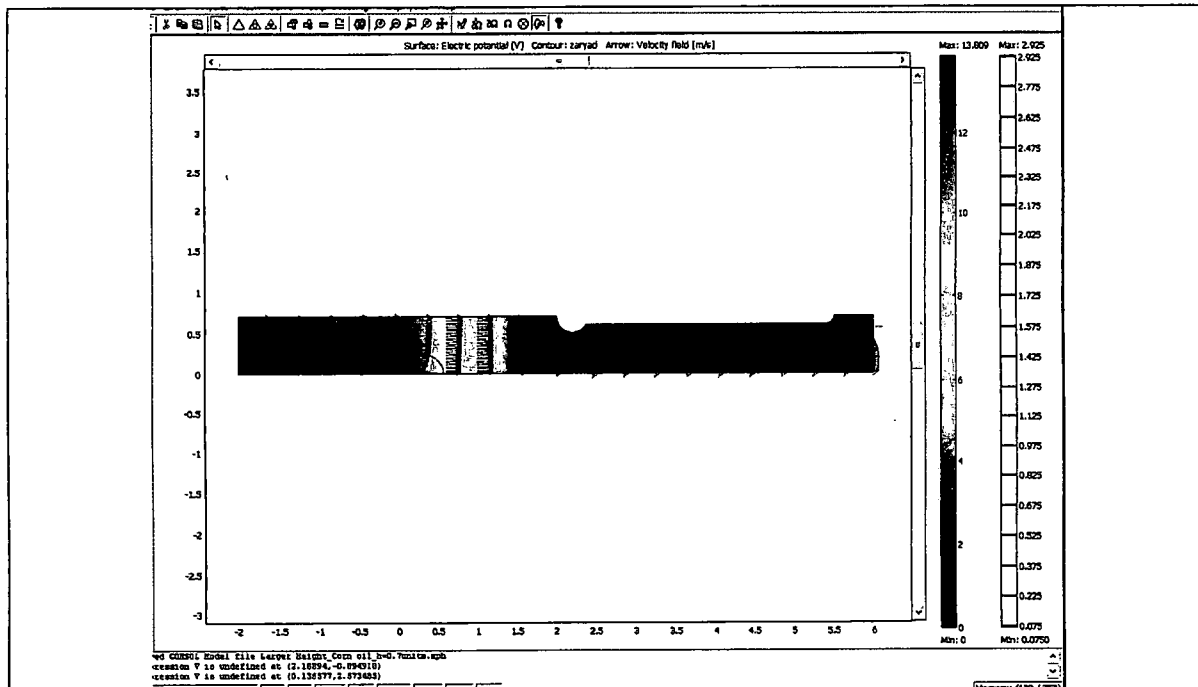


Figure 3.47 Variation of the velocity with the 40 microns of height of the pump

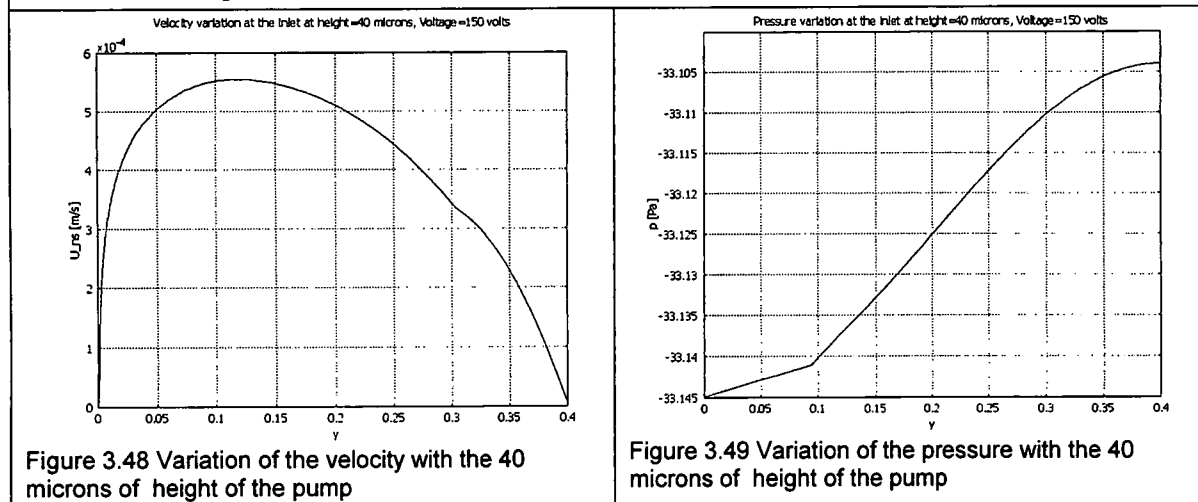


Figure 3.48 Variation of the velocity with the 40 microns of height of the pump

Figure 3.49 Variation of the pressure with the 40 microns of height of the pump

Following points are noticeable from the above Figures 3.48-3.49.

- 5) Figure 3.48 shows that the velocity of about 0.60 mm/sec at the height of 40 microns which is less than the base case of 100 microns.
- 6) Figure 3.49 shows that there is about 33 pascals of pressure at the inlet of the model domain.

3) Distance between the electrodes:

The distance between the electrodes is a critical criterion influencing electrohydrodynamics. The distance is increased from 5 microns to 20 microns and corresponding flow rates decrease from 2 mm/sec to 1 mm/sec in approximately parabolic way. The electric fields vary with the square of the distance between the electrodes. Flow rates vary in a square with the electric fields.

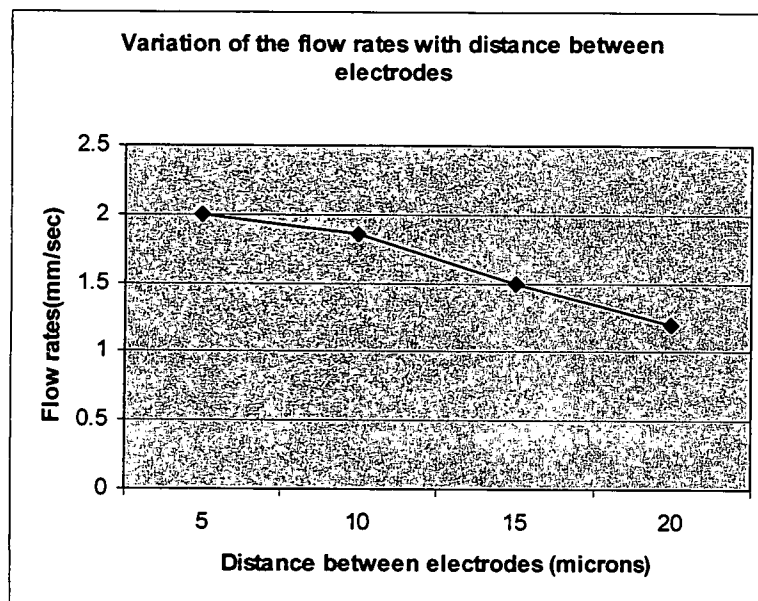


Figure 3.50 Variation of the velocity with the distance between the electrodes

3.7 Thermally Induced EHD Pumping

One of the important factors in EHD pumping is the placement and positioning of the electrodes. The central emitter electrode in ion drag EHD pumping is responsible for the generation of the momentum and is solely responsible for the velocity fields. If the electrode is placed at the bottom rather than at the center, there is no pumping involved and the inlet and outlet flows are identical as illustrated by modeling as shown in the Figure 3.51 below. This type of design

doesn't result in the overall cumulative axial force. The design of the electrode considered in the simulation of the design is Sergey Korpov's central emitter electrode and not the *parallel electrode design* from ANSYS®. The design of the electrode doesn't play a role in the induction pumping of the fluid. From the simulation standpoint, it was easier to place similar emitter electrode at the bottom rather designing a new rectangular electrode at the bottom and observing the electrohydrodynamics, as the design of the electrode doesn't matter. A schematic of the computational domain is shown below:

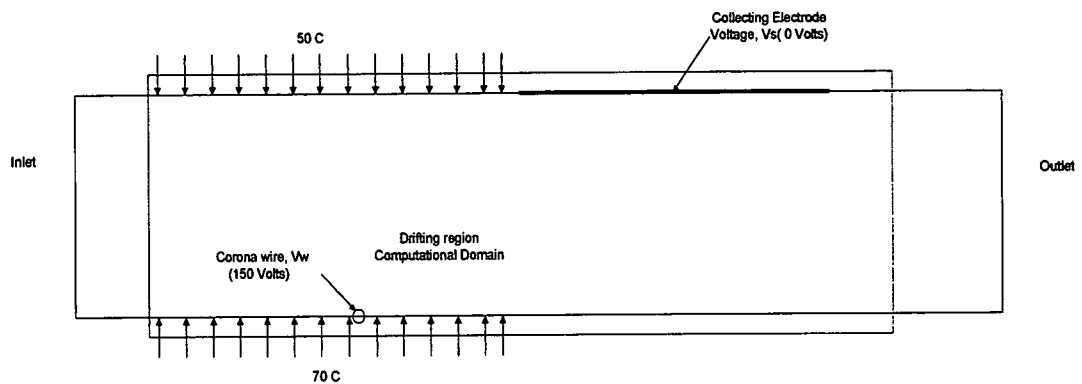


Figure 3.51 Schematic of the computational domain of the induced EHD pump with heat flux specified for temperature gradient.

To simulate the temperature induced EHD flows, electrostatics Gaussian equation (5), PDE charge equation (6), Navier Stokes equation (8) and Energy equation (12) and all the four equations are solved simultaneously with two way coupling for the velocity and pressure fields in the domain. Figure 3.52 shows the variation of the velocity along the distance of the pump and the charge distribution between the Sergey Korpov's electrodes without the application of temperature. In case of the temperature induced EHD, when the temperature differential by application of temperature of about 70C and 50C at the top and bottom respectively, perpendicular to the fluid flows. Figure 3.53 shows the

velocity variation profile along the distance of the pump, with temperature applied at the top and the bottom of the device.

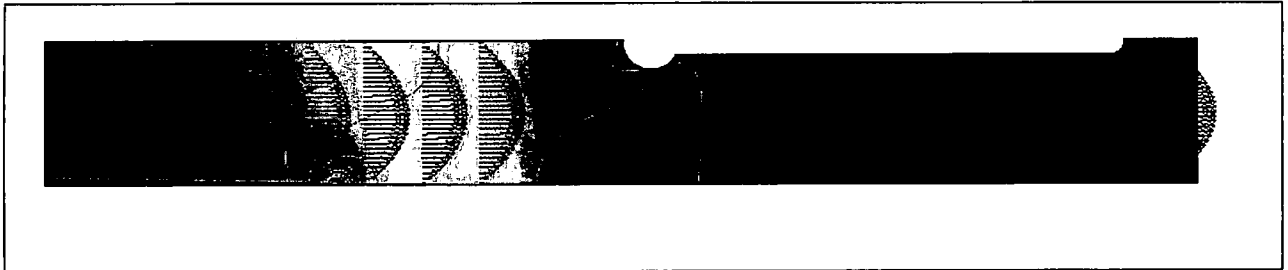


Figure 3.52 Velocity fields in COMSOL® for the voltage applied between the electrodes without the temperature fields.

The figure 3.53 shows the variation in temperature along height. Circulatory patterns evolve from the application of the electric fields and temperature fields and occur above the electrodes. The question arises as to what happens due to the presence of two electrodes. Two set of electrodes are designed and the results show that two circulatory patterns evolve on those electrodes and the velocity output from right outlet is 1 mm/sec.

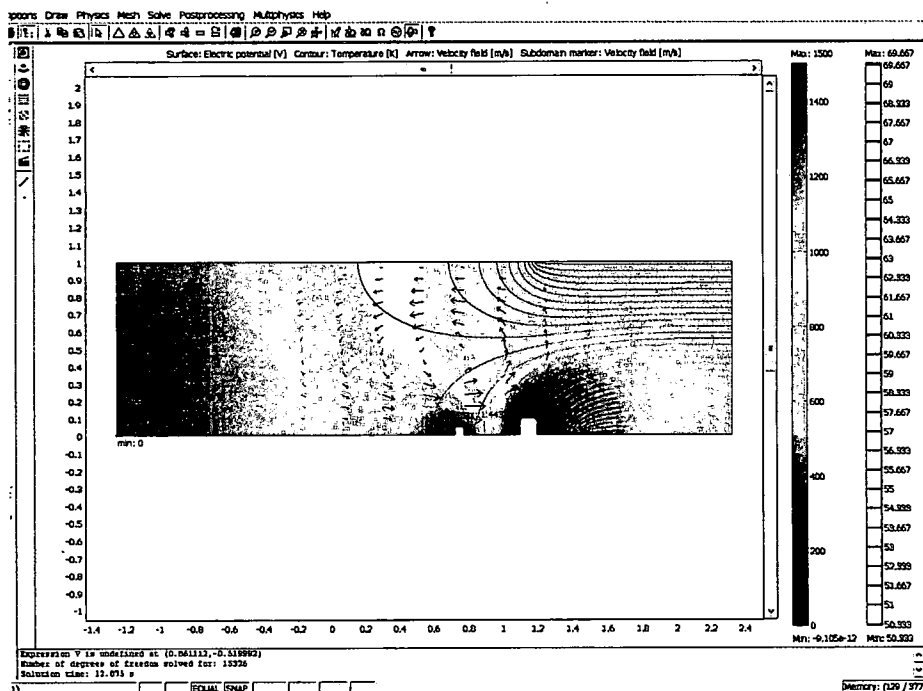


Figure 3.53 Velocity fields in COMSOL® for the voltage applied between the electrodes by applying temperature induced fields.

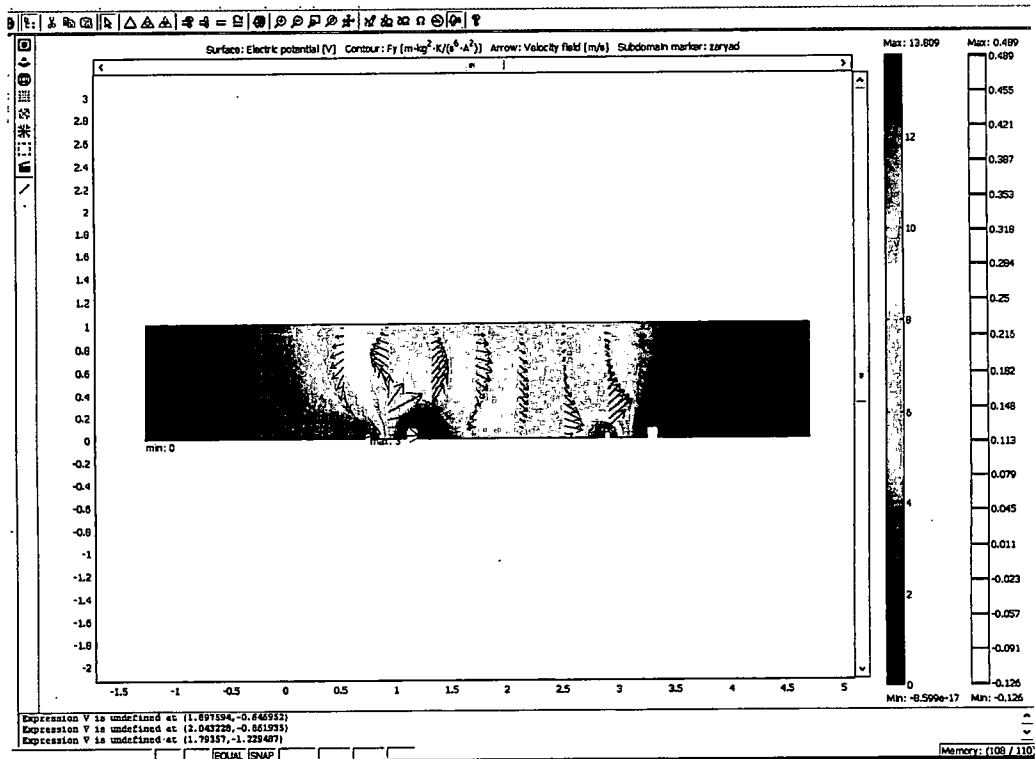


Figure 3.54 Velocity fields in COMSOL[®] for the voltage applied between the electrodes by applying temperature induced fields.

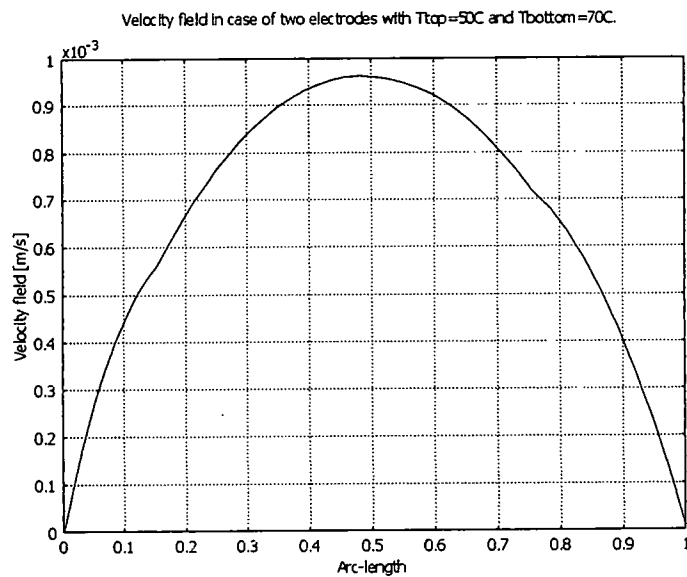


Figure 3.55 Velocity fields at the outlet in COMSOL[®] for by applying temperature of 50C and 70C at the top and bottom of the device.

3.8 Summary

The simulations on the thermally induced EHD simulations showed the effect of the temperature/heat flux on the electrohydrodynamic pumping. To the best of the author's knowledge, this is first thermally induced EHD simulation done in commercial software like COMSOL®, using regular design electrodes on the bottom on a micro level. Simulation of two phase pump of liquid-gas medium can also simulated but presents much more complex challenges on the computational domain. In case of temperature induced EHD, energy equation coupled with other equations presented definite challenges for the computational domain, as most computational domains were not converging either in static or transient cases. The only one simulated case in Figures 3.53-3.55 showed velocity profiles at the outlet to be 1 mm/sec.

The results of the velocity and pressure have been simulated for range of electric fields where the lower end would be at zero volts and the higher end would be at the electric breakdown strength of the fluid medium. The results near the electric breakdown strength should be considered as the actual phenomenon of dissociation and association of the atoms has not been considered in this analysis. The breakdown phenomenon is a complex phenomenon and is subject of study by itself, as the experimental or empirically data for the phenomenon is hardly available. This study only point towards the trends and micro domain example studies and doesn't constitute any bench mark for further experiments. For further experiments, a refreshing and more fulfilling study must be performed to look at the trends of the pressure and velocity fields. The ion drag study is a copyright of Sergey Korpov. This temperature application of 50C and 70C at the top and bottom sides, results in the variation of the electrical conductivity which

results in volumetric columbic forces in the semi-insulating dielectric and is included in the source term of the navier strokes equation and is solved using two-way coupling. However, the scaling implications like the formation of electric double layer and the boundary layer phenomenon have not been considered. The heat transfer coefficient also increases as the macro devices are scaled to micro level. These have resulted in micro cooling applications as well. These phenomena have to be considered in order to get a realistic view of the velocity and pressure fields and also benchmarked experimentally.

CHAPTER IV

4 Conclusion and future work

The asymmetric electrode configuration suggested by the Sayeed Yagoobi et al [58] and Sergey Korpov [56] is the most promising electrode pattern for high-voltage ion drag electrohydrodynamic pumping and low-voltage conduction electrohydrodynamic pumping.

The design of the electrodes is the key player in producing a flow in the Electrohydrodynamic. The electrodes define the voltage pattern and the electric field pattern between the electrodes and their position. This results in the resultant columbic force configuration being hugely dependent upon the electric field pattern. If the electrodes are placed such that the radial components of all forces acting on the fluid continuum are canceled, then it can result in a cumulative axial component. This axial columbic force component in the fluid continuum is responsible for the overall axial momentum of the fluid. In addition, electrode design structure also plays a crucial role and provides a holistic approach to induce further momentum in the fluid. Lot many challenges are faced on the fluid side due to impurities causing fluids to breakdown. From both the computational as well as the experimental work, it can be reasonably concluded that the conduction EHD pumping is the most suitable for the actuation as well as cooling applications.

In Ion Drag pumping, a very high voltage is applied to the electrodes. This results in deterioration of the surface of the electrodes where the ions are released from the surface, which eventually etches the surface. The high electric fields between the collector and the emitter results in the force on the ions, which in turn, exerts force on the fluid. The best configuration for producing a cumulative axial force would be a face to face emitter-collector configuration. This results in the strongest axial force with no radial component. This design can be modified to a more streamlined and better pointed design for more axial force, rather a circular emitter. Rather having a pointed emitter and pointed collector, EHD designers modified the design to a pointed emitter and a flat collector, where the flat collector embraces more electric field lines and produces more force.

In the conduction EHD pumping, the voltage applied between the collector and the emitter is very small compared to the ion drag pumping. The conduction pumping relies on the breakdown of the impurities by the process of the association and dissociation. This process develops axial force on the insulating oil. The configuration of the mesh and ring collector and the planar emitter helps in the association/dissociation of ions in the fluid.

In the induction electrohydrodynamic pumping, the electrode design can be a symmetric or asymmetric with respect to the actuator design. This type of pumping actually uses the differentials in the electrical conductivity between the fluids between the interfaces (or) volumetric heating in the device. This temperature differential along the radial direction results in the generation of charges in the varying amounts along the height. This non-uniform charge generation along the height results in the non uniform generation of the force. In fact this phenomenon is extremely useful in cases where the design is

symmetric. Hence, application of temperature/heat flux and two fluids are common strategies in pursuing induction electrohydrodynamic pumping. In short, Induction EHD pumping and Conduction EHD pumping can be realized as strategies in actuation and cooling technologies. A summary of the achievements is described below:

- *Computationally*, the basic physics of electrohydrodynamics is illustrated, where the Ion drag pump driven by central emitter and peripheral collector, a velocity of 1.8mm/sec at 150 volts could be achieved. A pressure differential of about 50 Pascals could be achieved.
- Positioning of the electrodes were researched computationally. It was discovered that the regular set of electrodes don't result in pumping of the dielectric medium. This jibes with common opinion among the EHD community that for a regular set of electrodes, there would be no velocity and pressure fields involved without the application of the temperature fields and/or the presence of two phases.
- Induced EHD pumping augmented by temperature gave some preliminary results that could not be verified experimentally. A pump with two electrodes with the dielectric medium was producing a velocity fields of 1mm/sec with a voltage of 120Volts, with temperature of 70C and 50C being applied at the top and bottom of the pump.

Some of the propositions listed below can be investigated, which either were not executed due to lack of sufficient time and /or funding. Before, embarking on the micro-electrohydrodynamics, few meso-pumps could be built to further understand the basics of the physics of the electrohydrodynamics. It is easier to build a meso pump than to build a micro pump and possibly benchmark other

published designs to educate and understand the intricacies of fabricating and packaging electrodes as well as the top part of the pump.

4.1 Computational Recommendations:

Induction EHD models augmented by the application of temperature should be evaluated more thoroughly for different temperature differentials. A temperature differential was applied by applying 50C and 70C was applied at the top and the bottom of the device, but it resulted in the circulations inside the pump which is noteworthy. These circulations could not be identified due to the convergence problems. More intensive studies of the actual temperature profiles could help understand the intricacies between the dependency of the fluid charge density profiles and applied temperature fields. A directionality could be adopted to benchmark the experimental work done in temperature induced EHD, like that of Melcher et al [6,7,8] and Seyed Yagoobi [14, 15,17,19] .

1. More transpositions of different electrode patterns and designs mentioned in the figures 2.4 and 2.5 should be investigated. The spacing between the electrodes, the height of the electrodes, and magnitude of voltage application should be should be varied to determine the optimized performance and characteristics of the device. The conduction EHD pumping first investigated by Seyed Yagoobi and Seong Jeong [58] should be investigated. The fundamental chemistry for the electrochemical reactions and still is an important arena which is worth investigating. Different insulating fluids possessing different electrical conductivities and dielectric constants could be investigated for the pressure developed and the fluid momentum.

2. Having investigated the parametric analysis of the device, a more robust design on a system level where the electrodes can be placed in series or parallel is worth solving.

4.2 Experimentation Recommendations:

A good experimental set-up alleviates most of the problems encountered during the operation and also gives accurate results.

- Fabrication of electrodes, and device packing:

1. Cleaner lift off processes in the clean room should be adopted for the construction of the electrodes. Particles sticking to the electrodes create mayhem for the electrohydrodynamic phenomenon. Some of the representative samples were tested and found shorted. These samples could be source of the errors in the fabrication processes. Few of the silicon substrates containing electrodes were tested open at first and later on tested shorted. These could be due to the presence of the particles either sticking to it peripherally or embedded in the electrodes in the enclosure box, in spite of repeated cleaning and flushing. For those ones which actually turned out faulty electrode configurations, one should inspect the concentration of the solvents, timing of etching and the purity of cleaning solvents.

2. Cleanness of upper glass part which covers the electrodes should be ensured by some sort of vacuum cleaning. Device packing of the top and bottom part to form a pump is also crucial for a good pumping performance. It has to be made sure that the electrodes don't get damaged by the placement of the glass top. In our case, transparent epoxy was chosen as the bonding medium. Anodic bonding can be a very good way of sealing two parts to shield the electrohydrodynamic domain from the outer environment.

However, its only drawback is the possibility of separating the top and bottom parts. In our case, separating the top part from bottom part resulted in the damaging the bus lines and the electrodes beyond repair. Hence the packing design is a very important of the experimental puzzle which has to be dealt so that the top and bottom can be opened and separated. One such design is illustrated by Amir Shoostari [59]. He designed an enclosure for a mesopump where the bottom part containing electrodes and the glass part can be replaceable. The top and the bottom parts are connected through a hinge, which makes them open. Similar enclosure can be designed and sealed well for the replacement of the different wafers containing electrodes and the top glass part. This should eliminate the contamination of the liquid.

- Working semi insulated dielectric liquid

One of the important criterion on which the electrohydrodynamics rests on is properties of the fluid. Crowley [11] and Seyed-Yagoobi [17, 18] prescribed a very comprehensive selection criterion for the selection of the fluids. They mentioned that high dielectric constant and low viscosity leads to low velocities and low conductivity and ion mobility could promote the high efficiency. Corn oil was chosen as the working fluid as it was the most accessible and most pure fluid. It also has excellent electrical properties, especially the electrical conductivity, with good heat transfer properties. So the fluid for the induction EHD pumping can be unsuitable for other EHD applications ion drag and conduction EHD pumping applications.

CHAPTER V

5 Appendix

A. Lessons Learnt (Micro pump Design and Fabrication)

5.1 Introduction

The micro pump design is the heuristic design for channeling electrohydrodynamics flows and optimized geometry for the electrode placement, high voltage application and pressure production with in the fluid in the actuator. The micro scaling offers the potential for application of low voltages on the electrodes, which is not possible on a macroscale or even on a mesoscale. Scaling actually results in avoiding some of the high voltage issues such as the size of generator required for generating high voltages, insulation of the device for high voltages. In fact, scaling provides the platform for pursuing the electrohydrodynamics high voltage research easily accessible by lowering the voltage.

5.2 Setbacks and challenges

The design of electrodes posed a major challenge to fabricate within the in-house manufacturing facilities. The electrodes were fabricated by using the laser machining and the distance between them was 100 microns and the length of the electrodes was about 1 cm. There were about 300 electrodes. This constituted the bottom part of the device.

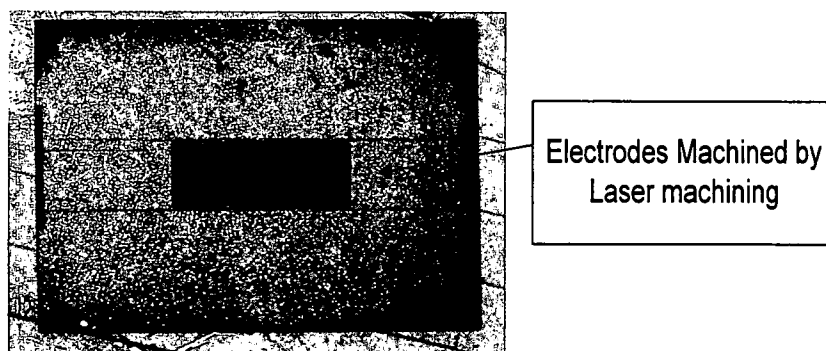


Figure 5.1 Laser machined electrodes on bottom substrate

The top part of the device was constructed by ultrasonic machining, further explanation of which is given below. A picture of the electrodes constructed by laser machining is shown in Figure 5.1. The Top part is a pocket, carved out of from the glass. This cavity is manufactured by means of Ultrasonic machining. The glass pocket communicates with the outside environment with the help of two holes which were drilled to install pipettes, which are connected to the fluid reservoirs. As the three phase electric field marches on the electrodes, the three phase electric phase drags the fluid around the electrodes and produces the pressure. The pocket is machined in such a manner that it can house 3000 metallic thin film electrodes on silicon wafer substrate, as shown in the Figure 5.2

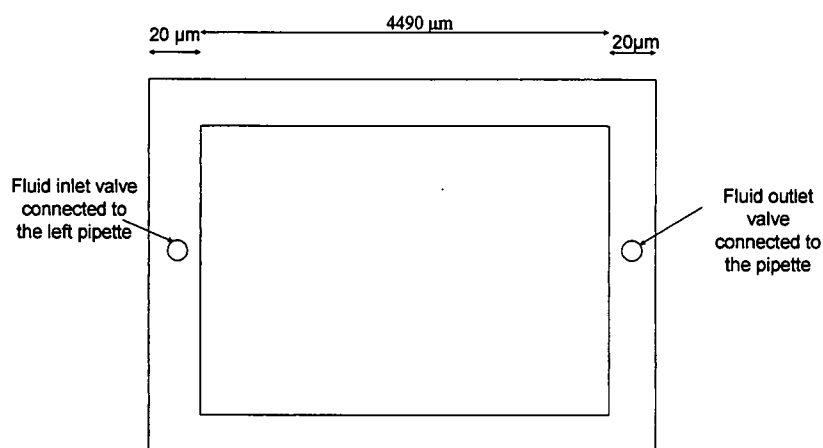


Figure 5.2 Ultrasonic machined glass top

When the top part is fixed to the bottom part, the bottom part of the electrodes came off along with the top part and could be a successful attempt to bond the top and the bottom parts. The picture of the damaged electrodes along with the broken top is shown in the Figure 5.3. This gave us lot of expertise in device packaging. The final design strategy was to construct the electrodes using lithography techniques for making the electrodes.

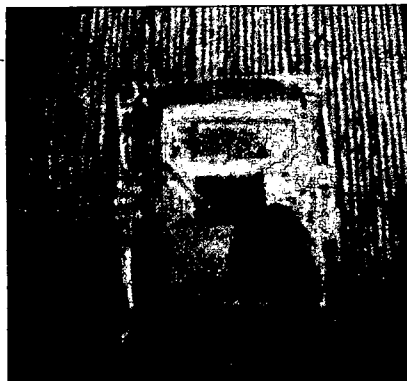


Figure 5.3 A picture of the top part connected to the pipettes along with the broken part.

5.3 Fabrication of the EHD actuator

The actuator housing is consisting of the top part and the base part. The base part is a silicon wafer with the electrodes and the top part is a glass plate and has a machined rectangular pocket in it. The top part is sealed to the bottom by means of a sealant, which in this case, is an epoxy adhesive. The sealant ensures that the actuator does not leak and holds the silicon substrate and the glass part together. They should be able to sustain the EHD induced stresses and should also be structurally integral. The end of the actuator is connected to two fluid reservoirs (pipettes) and a change in fluid pressure head in the pipettes indicates a pressure produced due to the electrohydrodynamic action of the fluid.

5.3.1 The Bottom part

The bottom part of the actuator consists of an array of electrodes, which are excited by means of a three-phase electric excitation traveling in a particular manner, as shown in the Figures 5.4. In the Figure 5.5, the electrode E_1 is the first electrode of the series of the electrodes connected to the first bus line #1. Similarly the electrodes E_2 and E_3 are the first electrodes of the series of electrodes connected to the bus lines #2 and bus line #3 respectively. A mildly insulating dielectric fluid is being assumed as fluid in the EHD actuator. The electrodes E_1 , E_2 , E_3 are excited by the respective three components of a three phase traveling voltaic field at a particular instant of time t_1 , as shown in the oval circle in the Figure 5.4. The voltaic field is applied in such a manner that one particular electrode is positively charged and its immediate consecutive electrode is negatively charged with respect to the former one, so that the positive ions from volume charge get streamlined to produce effective drag on the surrounding fluid. The electric field, which emanates from positively charged electrode and ends at a relatively negatively charged electrode, drives positively charged ions in a direction as indicated in the Figure 5.4. The electric field from a particular electrode to the consecutive electrode must be aligned in the same direction for an EHD actuator to effectively produce more electrohydrodynamic pressure. This is a core integral aspect of the working of an electrohydrodynamic actuator. The electrodes are manufactured by means of lift-off process. This method is suitable compared to other means of manufacturing the electrodes because of the adaptability and the precision of the process for micro-manufacturing the electrodes, which are of the order of few microns. The distance between the electrodes is 10 microns and the width of the electrodes is 5 microns. There are

three electrodes in each set and there are 3000 sets of such set of electrodes on the substrate. Primarily a CAD file, as shown in the Figure 5.7, is generated, which contains the design of the electrodes. A zoomed version of the electrodes is shown in the Figure 5.8. This CAD file is fed to the Electric Beam Machine (EBL) and is interpreted and micro machined on a silicon substrate or a chromium plated glass. This forms the Mask as shown in Figure 5.8. Then a separate silicon substrate <100> or glass considered. The 10 micron lines on the <100> silicon wafer is produced by the following process:

1. Wafer cleaning (typical RCA clean):

A solution of one part of Hydrogen Peroxide, one part of Ammonium Hydroxide and five parts of water is heated to 70 C for 15 minutes and rinsed with the solution. Then it is rinsed with DI water. Then it is cleaned with a solution of one part of Hydrofluoric acid and ten parts of water DI water rinse. Then, it is rinsed with a solution of one part of Hydrochloric acid and one part of Hydrogen Peroxide, five parts of water heated to 70 C for 15 minutes. Then it is DI rinsed and bowed dry with nitrogen.

2. Silicon Nitride Sputtering:

A silicon oxide layer is sputtered using Perkin-Elmer sputtering system with a 6" silicon target, sputter down, 600 W RF (13.56 MHz) power supply, Seybold turbo and roughing pumps. The chamber is base vacuumed at $4\text{e-}7$ torr and it is created by pumping overnight and 120 SCCM of UHP nitrogen is made to enter the chamber till the pressure is regulated to 7 m torr chamber pressure. A power of 250 watts RF is applied for 30 minute sputter time and approximately 3000 angstroms of Si_3N_4 refractive index 1.97 is sputtered.

3. Photolithography:

Shipley 1818 photoresist is spin coated using Karl Suss MJB3 mask aligner and Solitec spinner. A 351 developer having one part 351 developer and five parts of water is added. It is washed with Chlorobenzene. It is spun at spread speed of 500 rpm for 5 sec and spin speed of 5000 rpm for 30 sec., and then softbake 95 C for 30 minutes. Then it is soaked in Chlorobenzene for 90 seconds bake for 3 minutes at 95 C. The pattern is developed for one minute, rinse in DI water for one minute, and blow dry with nitrogen and inspected.

3. Metallization:

At a 2 angstroms/sec evaporation rate, approximately at pressure 20 mtorr, 3000 angstroms of Aluminum is deposited on the already spun pattern.

4. Lift-off:

Heat Mallinckrodt Baker PRS-3000 photoresist remover to 80 C, place substrate in solution and agitate until excess metal has lifted-off, rinse in 40 C acetone for one minute, rinse in DI water 1 minute, and blow dry with nitrogen.

7. Silicon Nitride Etching:

The silicon nitride is etched by using 9.6 SCCM of CF₄ and 0.5 SCCM of oxygen at 100 watts of RF power. Inspect for residual photo resist. If not completely removed, repeat the process

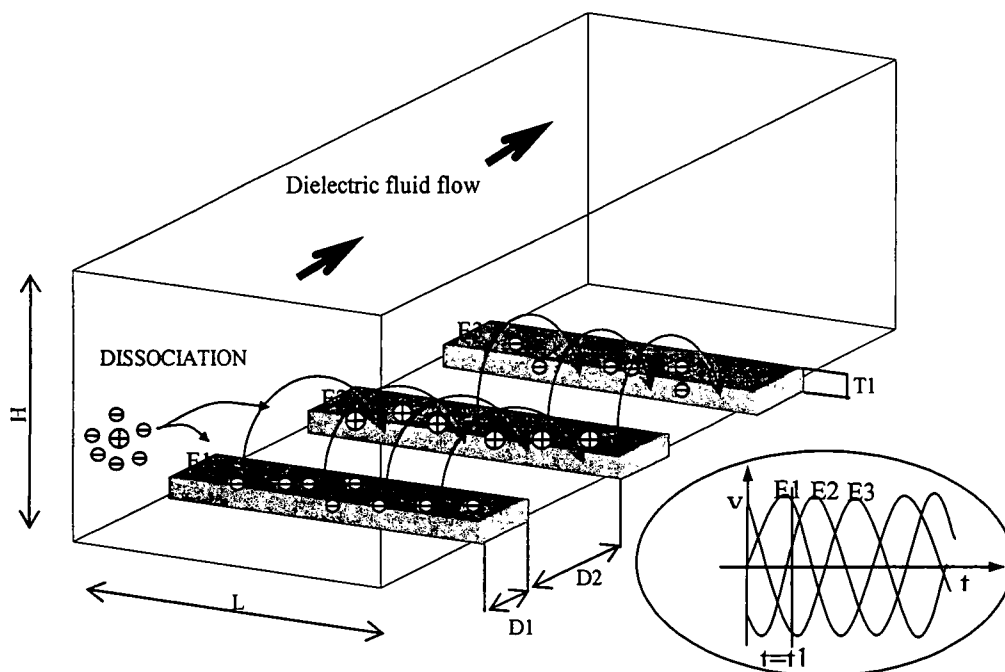


Figure 5.4 Schematic representation of the three dimensional actuator channels.

The whole pattern of the electrodes is covered with metal and subsequently is dipped in the acetone solution. The resultant design is the array of the metal electrodes along with all the three bus lines. Two innovative designs have been conceived for jumpers—copper wire jumpers, Figure 5.5 and the jumpers designed with the help of lithographic processes, Figure 5.6. In the former case, the jumpers connected to the second set of electrodes, are precisely hand soldered to the second bus line. In the latter pattern, the jumpers are made indigenously made with the help of lithographic processes, in the same way as that of electrodes. The construction of the jumpers in the second case is as follows. After the spraying the metal on the photoresist pattern of electrodes, the bus line #1 and bus line#3 are sprayed with an insulator coating, so that the jumpers don't contact them and arc. The jumpers are laid out skillfully and

precisely with the help of an aligner so that they align correctly with the second set of electrodes using the entire process of liftoff lithographic process. For laying of the jumpers on the substrate, the metallic electrodes are once again are sprayed with the insulator photo resist and baked in the same procedure as mentioned above. The image of the jumpers on the mask is correctly aligned using an aligner and the entire set up is exposed in the U-V chamber and is developed in the developer. The final design is the jumper designed with the lithographic process.

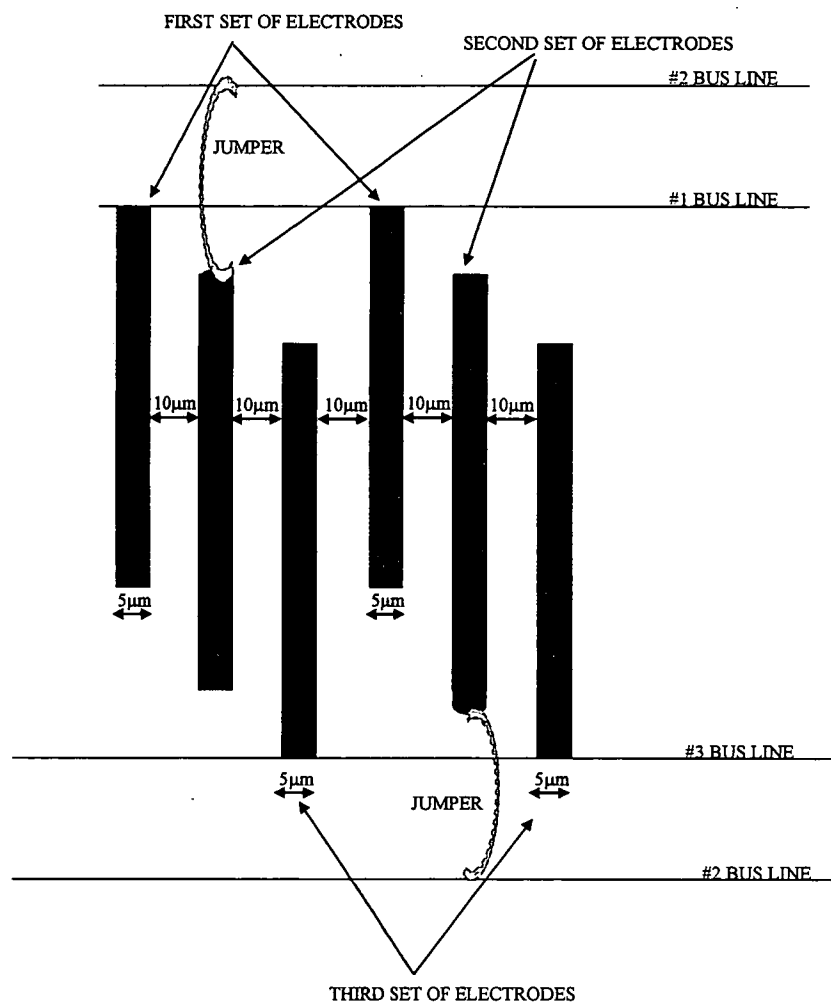


Figure 5.5 Schematic representation of the first set of design of electrodes on the top part.

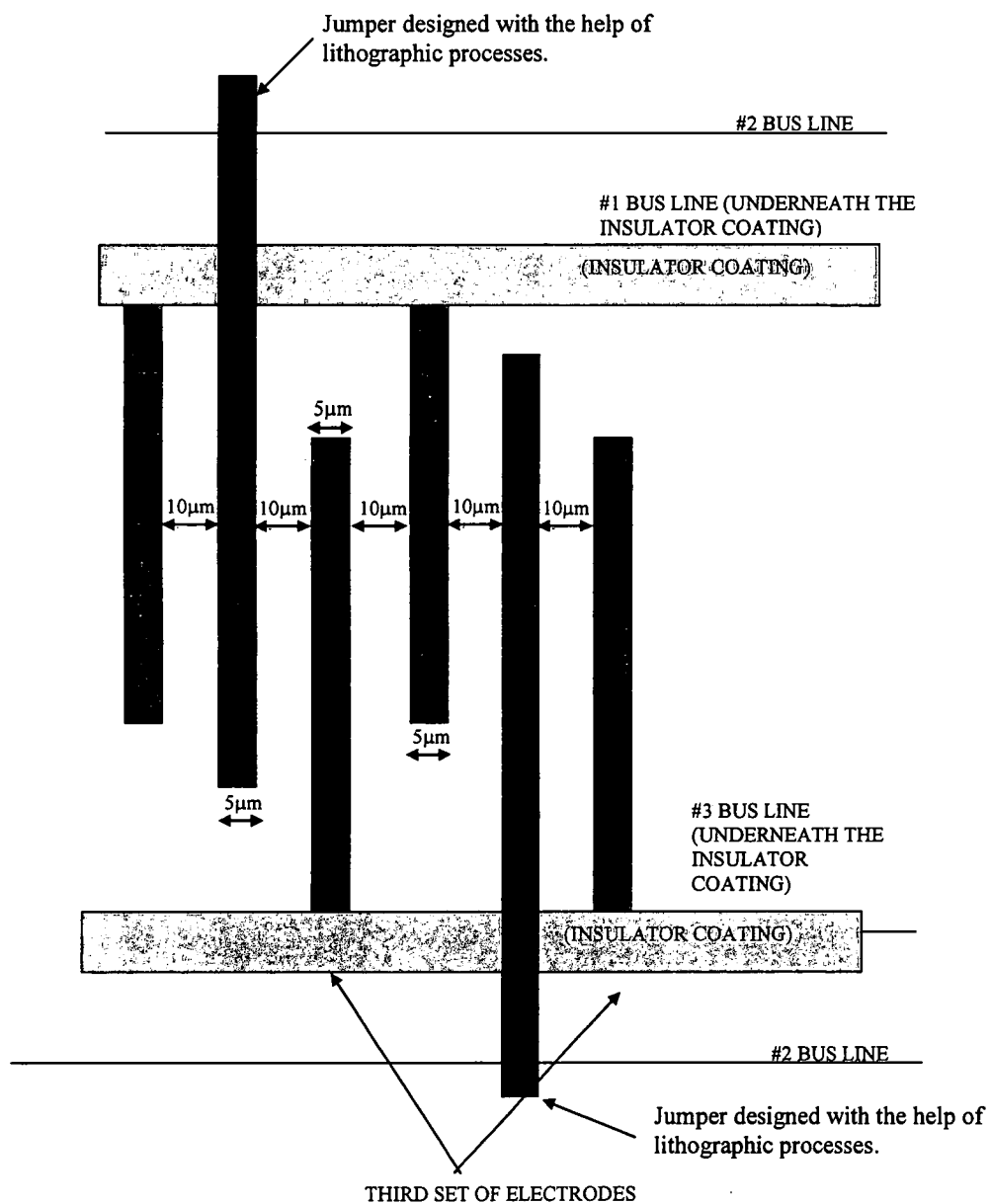


Figure 5.6 Schematic representation of the alternative set of design of electrodes on the top part of the actuator.

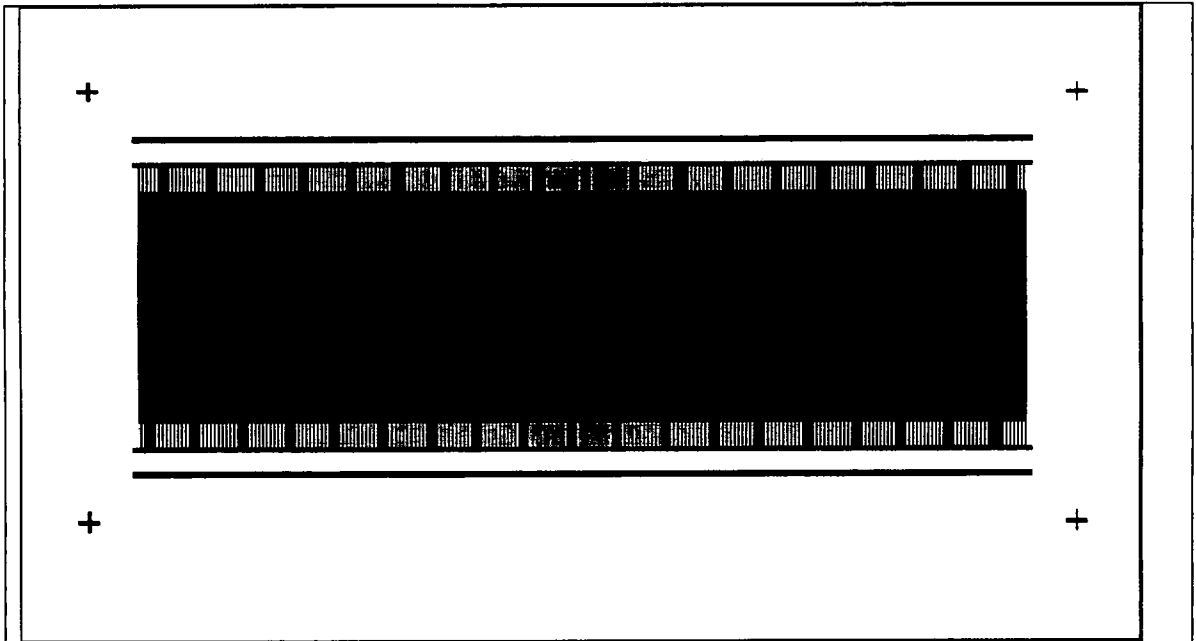


Figure 5.7 AUTOCAD® drawing of the electrodes of characteristic length of 5 microns.
(Note that the bus lines #1, #2 and #3 are visible and cross alignment marks are also clearly depicted at the four corners of the drawing).

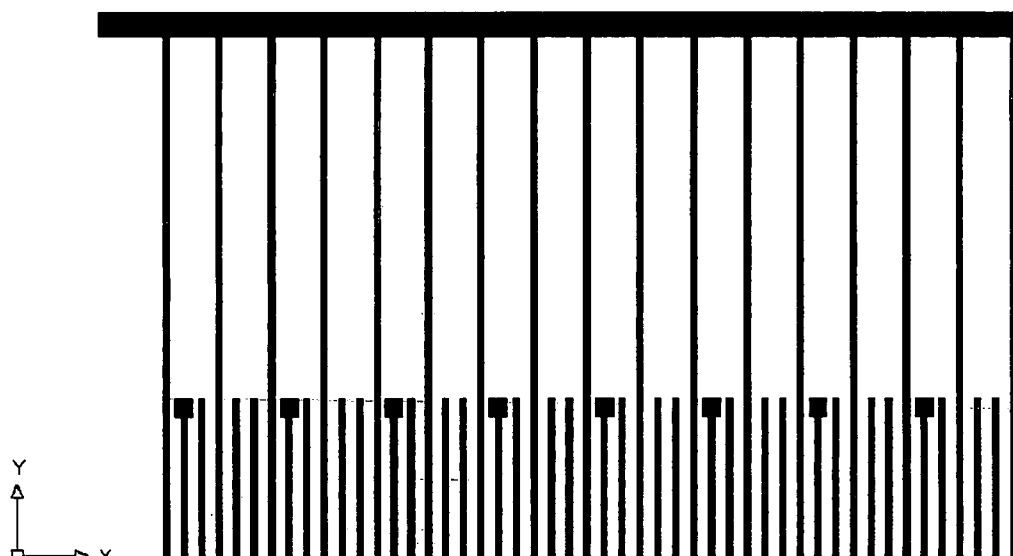


Figure 5.8 A zoomed area of top left corner of the figure 5.7 , depicting the electrodes with the the busline#1 and busline#2



Figure 5.9 An image of the electrodes, jumpers and the insulator block with alignment marks on the mask.

The following images, from Figures 5.10 to 5.13 are that of the silicon wafer and the electrodes laid out on it. The images also depict the buses for connection from the electrodes to the main bus lines

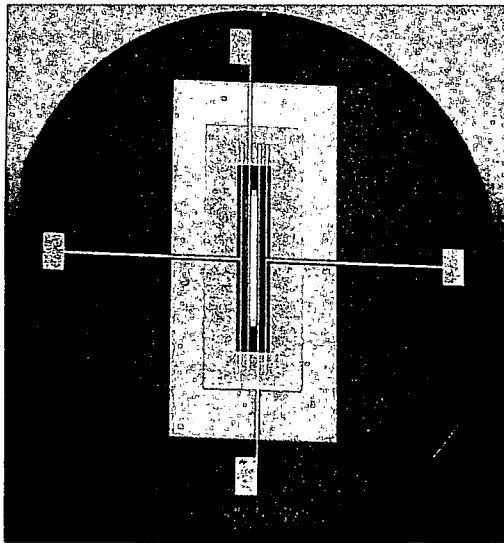


Figure 5.10 A picture of the jumpers along with electrodes

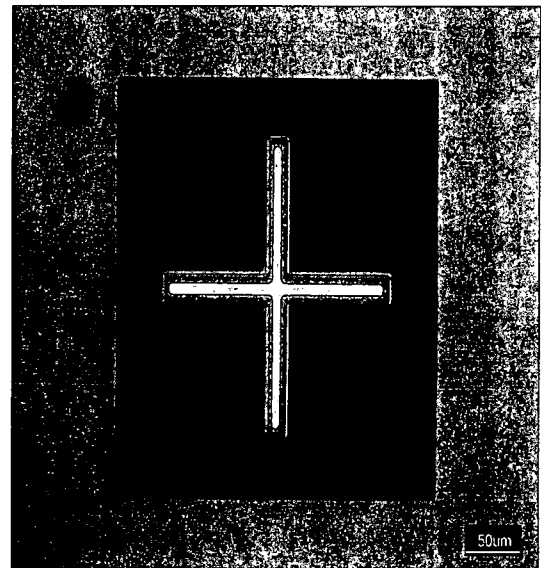


Figure 5.11 Alignment marks on the silicon electrodes

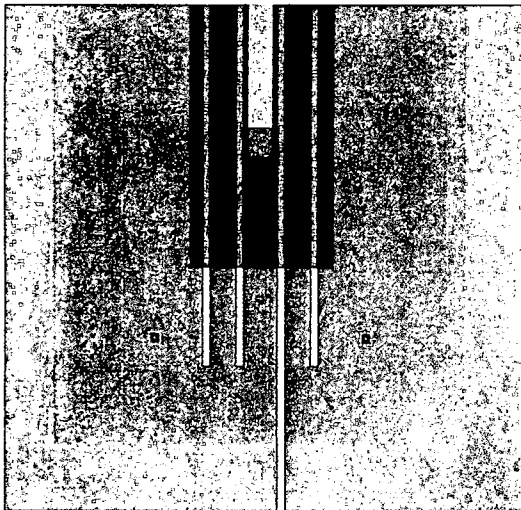


Figure 5.12 Picture of the bus lines along with the alignment marks

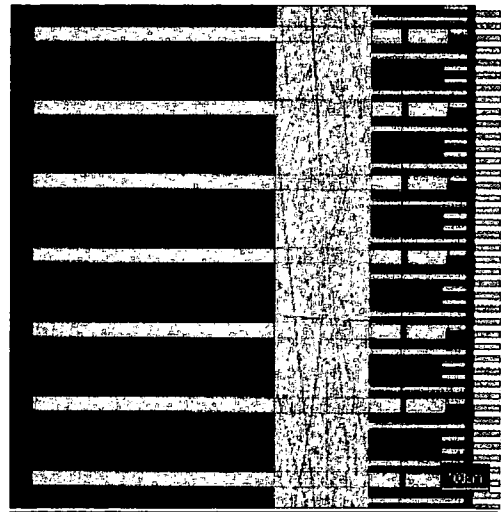


Figure 5.13 Jumpers along with the electrodes

The electrodes in the Figure 5.12 are connected to the electric bus lines and the area in brown is the insulating layer. The picture in Figure 5.13 is a sectional view of the jumper connections at a magnification of 100X. The electrodes are connected to the main bus lines through the jumpers. The horizontal electrodes (white colored lines) indicate the metallic electrodes. The jumpers actually pass over the electric bus lines and connect to the main electric bus line (which is not shown). The gray mark indicates the insulator photo resist

5.3.2 The Top part

The Top part is a pocket, carved out of from the glass. This cavity is manufactured by means of Ultrasonic machining. The glass pocket communicates with the outside environment with the help of two holes which were drilled to install pipettes, which are connected to the fluid reservoirs. As the three phase electric field marches on the electrodes, the three phase electric phase drags the fluid around the electrodes and produces the pressure. The pocket is machined in such a manner that it can house 3000 metallic thin film electrodes on silicon wafer substrate, as shown in the Figure 5.14. The width of the glass top is 4490 microns and the pipettes are attached at the ends. The liquids which can be used for the induction EHD pumping should have the electrical conductivity lying between 10^{-9} S/m to 10^{-11} S/m.

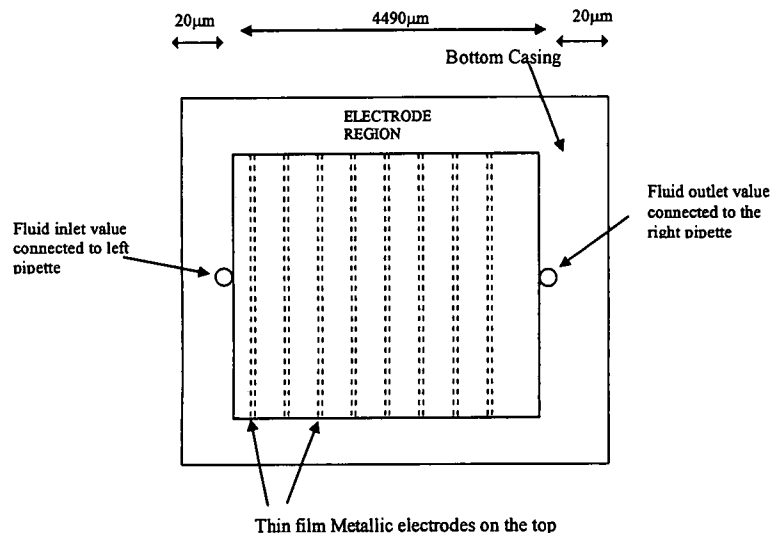


Figure 5.14 Schematic representation of the electrodes with the Glass cavity as seen from the top (the broken lines represent the electrodes).

5.4 The EHD Device

The top part being manufactured by using ultrasonic machining and the bottom part is manufacturing red by using liftoff lithography. These two parts are attached by carefully placing the cavity part of the glass part over the electrodes on the bottom substrate and properly bonding them by using epoxy. The pipettes are attached by placing the pipettes over the glass substrate, so the fluid can properly communicate between the two pipettes. Some of the device packaging pictures are shown below in Figures 5.15 and 5.16.



Figure 5.15 EHD pump along with the two pipettes attached with four wires.

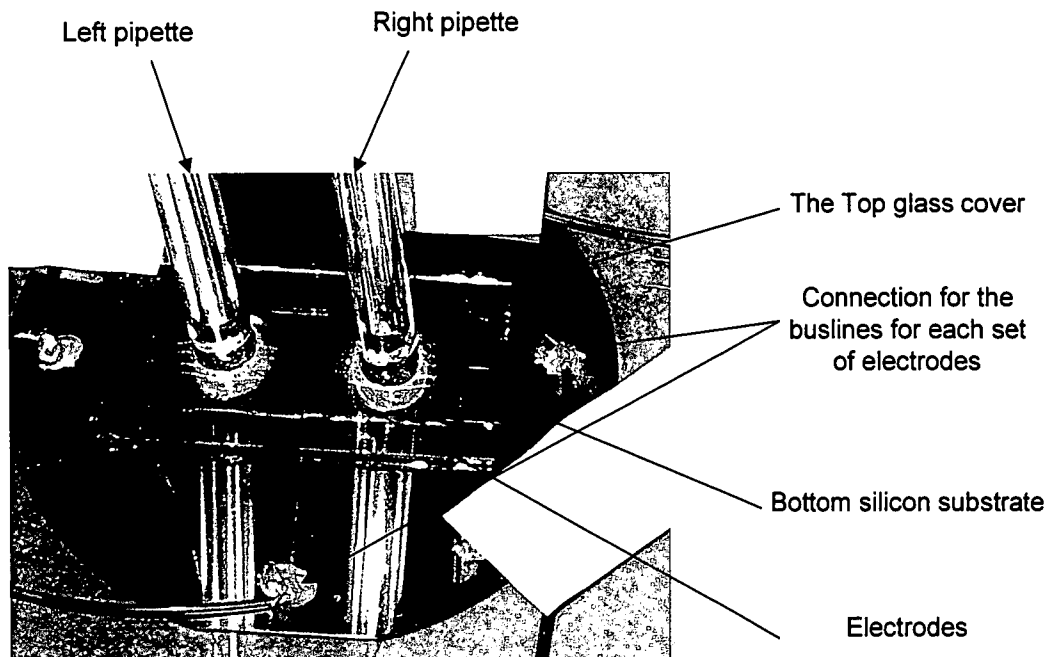


Figure 5.16 Close up view of EHD pump

5.5 Micro manufacturing Process Problems and Device packaging of the thin film electrodes

The manufacturing process of making these electrodes is initially conceived in-house micro manufacturing lab in an Ultra clean room facility, where there is negligible (almost zero) dust particulate density in the air and does not interfere with the micromanufacturing process. Atmost care has to taken in the laying of the electrodes in the nascent stage of the manufacturing, where the electrodes

are composed of the photo resist. The sputtering of the metallic materials on the photo resist and subsequent laying of the jumpers warrants more ultra cleaner environment. The entire manufacturing process is carried out using only use-and-throw products. In spite of all the strenuous efforts to make cleaner electrodes, the factors like dust density of the air of the clean room, frequent visits to the clean room, micro impurities present on the laboratory paraphernalia do adversely affect the manufacturing process and result in the damaged electrodes. Efforts are being made diligently to combat and eliminate these factors altogether. Two pictures, one of the damaged electrodes and the other of the undamaged electrodes are shown in the figures 5.17 and 5.18. We got acquainted with the method for laying of perfect rectangular electrodes, which is devoid of any defects present in the current micro manufacturing practices.

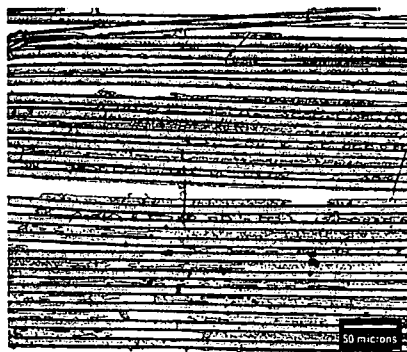


Figure 5.17 A picture of the completely damaged electrodes

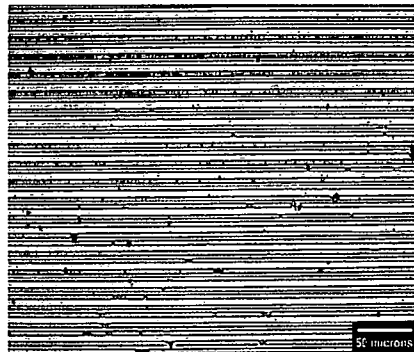


Figure 5.18 A picture of the near undamaged electrodes

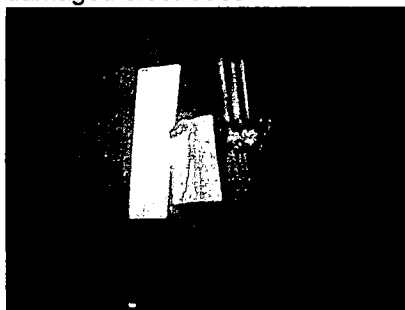


Figure 5.19 A picture of the top part connected connected to the pipettes



Figure 5.20 A picture of the top part pipettes along with the broken part.

The picture in Figure 5.17 is section of the damaged electrodes at a magnification of 50X. The picture is characterized by various defects like imperfectly aligned electrodes, broken electrodes, dust particles (seen as dark particles), torn ends. There are also thin strands of the photo resist cutting across the electrodes, which might have been due to the stray U.V exposure outside that of the U.V chamber in spite of having being considerable distance from it. The picture, as shown in figure 5.18, represents a major improvement over that in the Figure 5.17. The image is still characterized by various dust particles and certain unetched areas of electrodes (characterized by notches and pits at the sides of the electrodes) that are hard to remove, on upon which, we are currently working very hard. The dust particulate density is considerably improved in this image and the electrodes are also aligned perfectly without any spaces and breaks among them. The Figures 5.19 and 5.20 give, full view of the glass plate with the broken top, which is turn, connected to the one of the pipettes. This breakage occurred which the top part was being connected to the bottom glass plate. The other part of the glass plate is also shown near the top glass plate.

5.6 Experimentation for the EHD pumping

A toy camera is used in monitoring the level of the fluid and is calibrated by using alignment gauges, as shown in the Figure 5.21. The high voltage instrumentation is used for the high voltage source, as shown in Figure 5.22. A heat flux of 60 W/m^2 is applied at the bottom for the heat transfer to the corn oil. Corn oil is warmed enough for a very long period of time such that it attains equilibrium. High Voltage is applied to the electrodes when the heating has already been applied.

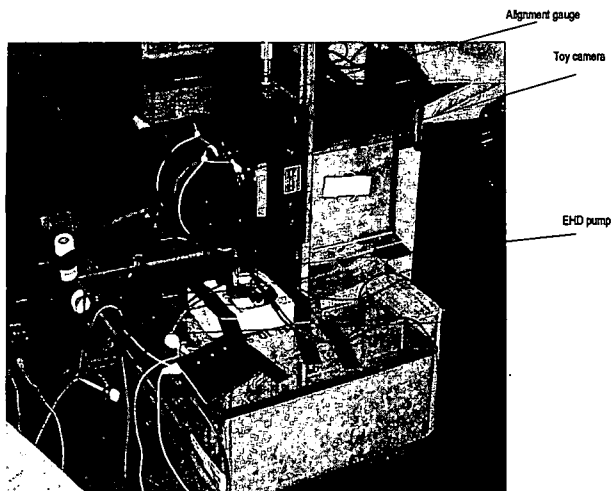


Figure 5.21 Picture of the Experimental setup

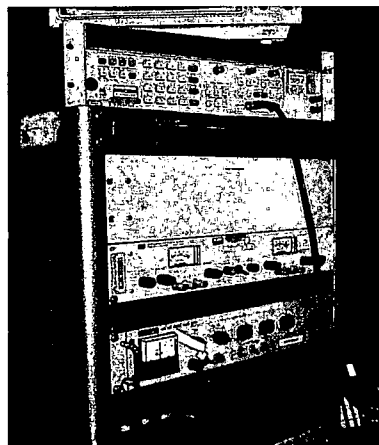


Figure 5.22 Picture of the High voltage panel with frequency counter

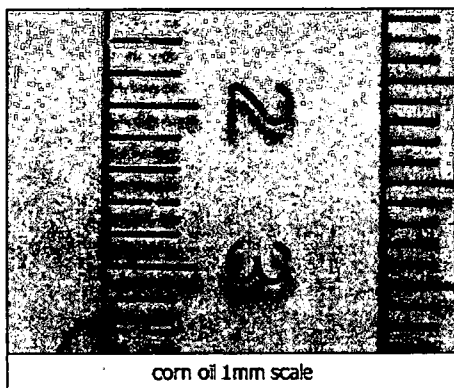


Figure 5.23 Picture of the scale signifying the millimetres for comparison.

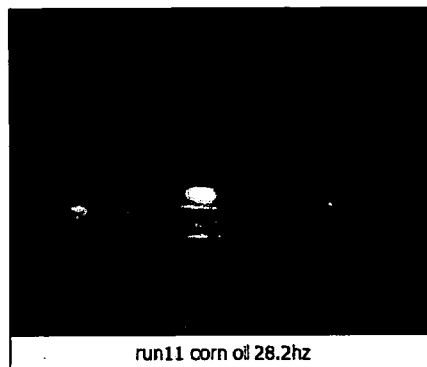


Figure 5.24 A photo of the zero level in the meniscus

The circuitry in the Tupperware, shown in Figure 5.25 is meant for generating a three phase voltage square supply, which is shifted by 120 phase angle. The plastic tupperware is used for insulating the circuitry and shielding the charges. There are three drivers which produce three phase supply, one of which is shown in the Figure 5.26. It is combination of the microprocessors, transistors and Opamps, which produces the three phase signal.

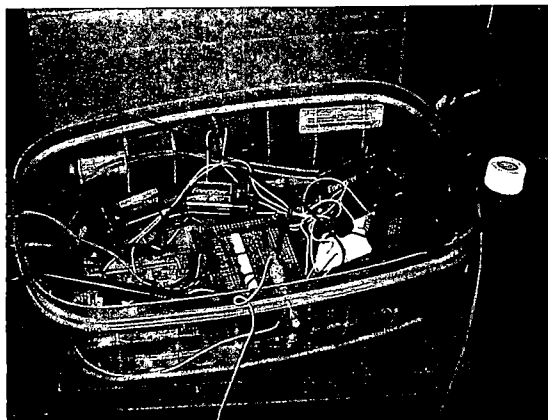


Figure 5.25 Picture of the electrical supply in the tupperware shown in the figure 5.24

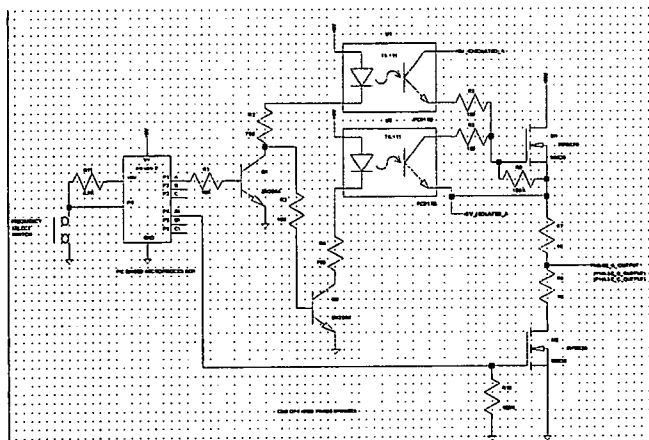


Figure 5.26 Schematic of the Circuit diagram for the one of the drivers for the Supply three phase supply in the tupperware shown in the figure 5.25

The working fluid is corn oil and has the following thermophysical values in Table

Table 5.1 Physical properties of corn oil

Physical properties of corn oil	
Liquid Density(kg/m ³)	900
Liquid Kinematic viscosity(N/m ² sec))	6.0E-02
Dielectric strength	~10e9V/m
Dielectric constant	3
Thermal conductivity(S/m)	5.00E-11
Mobility, (m ² /vsec)	3.30E-10
Diffusivity,	5.30E-03

An AC field is applied to three buses of electrodes connected to the voltages given below. The pumping height is shown below in the Table 5.2:

Table 5.2 Experimental values of Voltages applied and Height registered.

EHD Experimentation	
Voltage applied	Height registered(microns)
140 AC Volt @ 0.4Hz	0
140 AC Volt @ 0.53Hz	20
140 AC Volt @ 9.3Hz	40
140 AC Volt @ 12.9Hz	100
140 AC Volt @ 15.2Hz	300
140Volts @ 28.2Hz	600
140Volts @ 50Hz	250

There are *no* velocity and pressure fields registered, by applying high voltage to one electrode and grounding other electrode in the set of *parallel electrodes* in Induced EHD pumping *without* the application of temperature fields. This shows that there is consistency between the experimental data and the computational results for Induced EHD pumping without temperature application. This also confirms the experimental outcome where there is no temperature fields were applied.

When a differential heat flux was applied between the top and bottom of the device, little height raise was registered at different frequencies when a AC voltage was applied. There was no height registered when DC voltage was applied, while computationally it has been shown that there could be a height rise, when there was temperature of about 50C and 70C was applied at the top and bottom of the device. . As discussed in the literature section, it is shown computationally and experimentally, by applying differential temperature gradient to the actuator resulted in considerable velocity and pressure profiles for their electrode configurations. There is only little head at various frequencies except at 28.2 Hz where there was a blimp and a head of 600 microns was registered. For corn oil, this is equivalent to the pressure of 5.2 pascals. This data point was essentially repeated for four to five times to ensure repeatability. In essence, this proves that, for a *parallel design set of electrodes* computationally determined from the analysis in ANSYS®, there was no pumping observed computationally in COMSOL® when temperature fields were not applied. In other words, it proves that a temperature field needs to be applied to the top and bottom in case of Induction EHD pumping and agrees with popular notion of applying temperature fluxes and/or two phase flows, for a regular set of electrodes.

This discrepancy between the computational and experimental results in case of the application of both the temperature and voltage fields could be due to the myriad of reasons. There could have been the destruction of a few electrodes and bus lines, when the voltage was applied. There could have been particulates in corn oil, which could have shortened between the electrodes causing no resultant pumping. In fact, the structure of the electrodes and the glass top was observed by dissolving the transparent epoxy and the top and the bottom parts were separated. The post-experimental bottom silicon wafer showed damaged bus lines and the electrodes.

B. References

- [1] Stuetzer, O. M., "Ion Drag Pressure Generation," J. of Applied Physics, Vol. 30, 1959.
- [2]. Stuetzer, O. M. "Ion Drag Pumps," J. of Applied Physics, Vol. 31, pp. 136-146, 1960.
- [3]. Pickard, W. F., "Ion Drag Pumping I Theory," J. of Applied Physics, Vol. 34, 1963.
- [4]. Pickard, W. F., "Ion Drag Pumping II Experiment," J. of Applied Physics, Vol. 34, 1963.
- [5]. Sharbaugh, A. H., and Walker, G. W., "The design and Evaluation of an Ion Drag Dielectric Pump to Enhance Cooling in a Small Oil-Filled Transformer," IEEE-IAS Meeting, Mexico City, Oct. 19, 1983.15,
- [6]. Melcher, J. R., "Traveling-Wave Induced Electroconvection," Phys. Fluids, Vol. 9, pp. 1548- 1555, 1966.
- [7]. Melcher, J. R. and Firebaugh, M. S., "Traveling-Wave Bulk Electro Convection Induced Across a Temperature Gradient," Phys. Fluids, Vol. 10, pp. 1178-1185, 1967.
- [8]. Wong, J. R. and Melcher, J. R., "Thermally Induced Electroconvection," Phys. Fluids, Vol.12, pp. 2264-2269, 1969.
- [9]. Okapal, M. F., "Traveling-Wave Generation and Electrohydrodynamic pumping with a Single-Phase Voltage Supply," MS thesis, University Illinois, 1978.
- [10]. Krein, P. T ., " Analysis and Operation of an Electrohydrodynamic Pump Using a Single- Phase Voltage Supply," MS Thesis, University of Illinois, 1980.
- [11]. Crowley, J. M., "The efficiency of Electrohydrodynamic Pumps on Attraction Mode," J. of Electrostatics, Vol. 8, pp. 171-181, 1980.
- [12]. Kervin, D. J., "Three-Phase Variable Parameter Electrohydrodynamic Pumping," MS Thesis, University of Illinois, 1981.
- [13]. Kuo, B. "Flow Characteristics and Heat Transfer for Pressure and Electric Field Driven Laminar Flow with Temperature-Dependent," Ph.D. Dissertation,

University of Illinois, 1982.

- [14]. Seyed- Yagoobi, "Theoretical, Numerical, and Experimental Study of Electrohydrodynamic Pumping in Vertical Configuration," Ph.D. Dissertation, University of Illinois, 1984
- [15]. Seyed-Yagoobi, S. and Bohinsky, B. J., "Induction Electrohydrodynamic Pumping-Selecting an Optimum Working Fluid," Proceedings of the IEEE-IAS-1990 Annual Meeting, Seattle, pp. 795-801, Oct. 1990.
- [16]. Crowley, J. M., Wright, G., Chato, J. "Selecting a Working Fluid to Increase the Efficiency and Flow Rate of an EHD Pump," IEEE Transaction On Industry Application, Vol. 26, Jan. 1990
- [17]. Bryan, J. E. and Seyed- Y agoobi, J. "Experimental Investigation of Ion-Drag Pump in Vertical and Axisymmetric configuration," IEEE Trans. on Industry Applications, Vol. 28, No.2, March/ April 1992.
- [18]. Seyed- Yagoobi, J.; Margo, B. D.; Bryan, J. E., "Effect of frequency on heat transfer enhancement in temperature-induced electrohydrodynamic pumping," *IEEE Transactions on Dielectrics and Electrical Insulation* v 1 n 3 1994 p.468-473
- [19]. Bryan, J. E.; Seyed-Yagoobi, J., "Analysis of 2-dimensional flow field generated by a 1- electrode-pair ion-drag pump," *IEEE Transactions on Dielectrics and Electrical Insulation*, v 1 n 3 1994 p.459-467
- [20]. Barbini, G. and Coletti, G. "Influence of electrode geometry on ion-drag pump static pressure," *IEEE Transactions on Dielectrics and Electrical Insulation*. v 2, n 6. Dec 1995, p 1100-1105. IEEE, Piscataway, NJ.
- [21]. Coletti, G., Centurioni, L., and Barbini, G., "Contribution to the study of electrohydrodynamic ion drag pumps," *IEEE International Conference on Conduction & Breakdown in Dielectric Liquids. ICDL*. 1996, p 500-503. IEEE, Piscataway, NJ, USA.
- [22]. Bart, S. F., Tavrom, L. S., Mehregany, M. and Lang, J. H., 1990, "Microfabricated electrohydrodynamic pumps, Sensors and Actuators, A21-23, pp. 193-1970
- [23]. Richter, A., and Sandmaier, H., "An Electrohydrodynamic Micropump," Proc. Of IEEE MEMS, pp. 99-104, 1990.
- [24]. James R Melcher. and Millard S Firebaugh, "Traveling Wave Bulk electroconvection Induced across a temperature gradient," *The Physics of Fluids*, pp. 1178-1184, 1967.
- [25]. Choi, J. and Kim, Y., "Microelectrohydrodynamic Pump Driven by Traveling Electric Fields," Proc. of IEEE IAS, 1995, pp. 1480-1484.

- [26]. Francais, O., Dufour, I., and Sarraute, E., 1997, "Analytical Static modelling and optimization of electrostatic micropumps," *J. Micromech. Microeng.* Vol. 7, pp. 183-185.
- [27]. Bourouina, T., Bosseboeuf, A., and Grandschamp, J-P, 1997, "Design and simulation of an electrostatic micropump for drug-delivery applications, *J. Micromech. Microeng.*, Vol. 7, pp. 186-188
- [28]. Kashani, R. and Hallinan, K. "Electrohydrodynamic Actuation with Application to Active Vibration Control" *The Proceedings of 1999 SPIE International Symposium on Smart Structures and Materials* (book 3675), New Port Beach, CA, March 1999
- [29]. Hallinan, K. P., Bhagat, W. W., Kashaboina, B. and Kashani, R. "Electrohydrodynamic Augmentation of Heat Transport in Micro Heat Pipe Arrays" *Proceedings of the 1998 ASME Heat Transfer Division, Vol. 3 "Application of Heat Transfer in Engineering Systems and Education"* pp 165-171; *Int. Mechanical Engineering Conf. and Exhibition, Anaheim 1998*
- [30] J.M. Whitney, *Fatigue Characterization of Composite Materials*," AFWAL-TR-79-4111, Air Force Materials Laboratory, Oct. 1979.
- [31]. V.S. Avva et al, "Effect of Impact and Fatigue Loads on the strength of Graphite/Epoxy Composites," *Composite Materials: Testing and Design (Seventh Conference)*, ASTM STP 893.
- [32]. J.M. Whitney, Ed., ASTM, Philadelphia, 1996, pp. 196-206; H. T. Hahn et al, "Failure Characterization of a Graphite/Epoxy Laminate Through Proof Testing," *Composite Materials: Testing and Design (Sixth Conference)*, ASTM STP 787, I.M. Daniel, Ed., ASTM, Philadelphia, 1982, pp. 247-273
- [33]. R.A. Simonds et al, "Effects of Matrix Toughness on Fatigue Response of Graphite Fiber Composite Laminates," *Composite Materials: Fatigue and Fracture, Second Volume*, ASTM STP 1012, P.A. Lagace, Ed., ASTM, Philadelphia, 1989, pp. 5-18.
- [34]. Yu, Z., Pohlman, N. A., Hallinan, K. P. and Kashani, R., "Active Thermal Control of an Ion- Drag Pump Assisted Micro Heat Pipe," Accepted for publication in the *Proceedings of Heat Transfer of the 2000 ASME Int. Mechanical Engineering Conf. and Exhibition*, Nov. 5-10, 2000.
- [35]. Hallinan, K. P., Kashani, R., and Bartsch, M. "An Electostatically-Driven Phase Change Actuator for Vibration Control", *Proceedings of the ASME design Engineering Division*, 1996
- [36]. Kashani, R. "High Power Actuators in Intelligent Rotor Application," *Proceedings of the 1993 SPIE North American Conference on Smart Structures and Materials* , Albuquerque, NM, Feb. 1993.
- [37]. Little, E., Kashani, R. Kohler, J., and Morrison, F., "Tuning of an Electro-rheological Fluid-Based Helmholtz Resonator as Applied to Hydraulic Engine

Mounts," *Transportation Systems*, Kashani, R. Editor, the ASME Book #G00898, DSC- Vol 54, 1994, pp 43-51

[38]. Smith, Douglas R. Parekh, David E. Kibens, Valdis. Glezer, Ari. Thrust vectoring with hybrid synthetic jet actuators High Speed Jet Flows American Society of Mechanical Engineers, Fluids Engineering Division (Publication) FED. v 8 1997. ASME, New York, NY, USA

[39]. Kang, Sung, "Feasibility Study of New Concept EHD-driven Micro-Pumped Actuator", 1999, Ph.D. Dissertation, University of Dayton.

[40]. Flower, W. 'Understanding Hydraulic Mounts for Improved Vehicle Noise, Vibration, and Ride Qualities' SAE #85079:12.

[41]. Singh, R., 'Linear Analysis of Automotive Hydro-Mechanical Mounts' J. of Sound and Vibration, V.158, No.2, p.219

[42]. Bhagat, W. W., King, W. P., and Hallinan, K. P., 1997, "Electrohydrodynamic Enhancement of Heat Transport Capacity of a Micro Heat Pipe," presented at the 1997 International Heat Transfer Conference, Kanpur, India, Dec. 29-31.

[43]. Busch-Vishniac I J –The case for magnetically Driven Micro actuators – Sensors and Actuators A33, p.207, 1992

[45]. Jerman H – Electrically Activated ,Normally-closed Diaphragm Valves – Transducers '91, proceedings of the IEEE conference on solid-state Sensors and Actuators, San Francisco, CA , USA p.1045, 1991

[46]. Product literature for silicon Microvalves, Rad wood Microsystems, Menlo Park, CA, USA, C1993

[47]. Eshahi M, Shoji S Nakamo A- Normally Closed Microvalve and Micropump Fabricated on Silicon Wafer - Sensors and Actuators, Vol 20, nos 1 and 2, 1989

[48]. Ray C A Sloan, C L Johnson A D, Busch J B, Petty B R – A silicon based shape memory alloy Microvalve - Proceedings of the spring Materials Research Society Conference, San Francisco, CA, USA, 1992.

[49]. O.E.Ramadan and S.L.Soo, Physics of Fluids 12, 1943 (1969)

[50]. T.Yamamoto and H.R.Velkoff, J of Fluid Mech. 108, 1 (1981)

[51]. R.S.Sigmond, Proceedings of the 7th International Conferences on Gas Discharges and Their Applications (Peregrines, London, 1982), p.104

[52]. M.H.Leen and G A Domoto, J. Appl. Phys. 61, 3931(1987)

[53]. M.H.Leen and G A Domoto, IEEE Trans. Magn. 24, 262 (1982)

- [54]. G.A.Kallio and D.E.Stock, J. Fluid Mech. 240, 133 (1992)
- [55]. R.S.Sigmond, A.Goldman, and M.Goldman, Proceedings of the 7th International Conferences on Gas Discharges and Their Applications (Peregrines, London, 1982), p.330
- [56]. Sergy Korpov's and Igor Krichafovitch, Electrohydrodynamics flow modeling using FEMLAB.
- [57]. James G Feng, Electro hydrodynamic flow associated with unipolar charge current due to the corona discharge from a wire in a rectangular shield, Journal Of Allied Physics, Volume 86, Number 5.
- [58]. Seong-il Jeong, Jamal Seyed Yagoobi, "Experimental study of the electrohydrodynamic pumping through conduction phenomenon", Journal of electrostatics Number 56, 2002
- [59]. Amir Shoostari doctoral thesis, "Experimental and computational analysis of electrohydrodynamic mesopump for spot cooling applications", December 2004
- [60]. COMSOL[®] Multiphysics documentation, 2007, COMSOL[®] Inc.

R702034513